

AD-A101 169

SOUTHWEST RESEARCH INST SAN ANTONIO TEX  
ULTRASONIC TRANSDUCER PERFORMANCE REQUIREMENTS.(U)

JUN 81 H KWUN, G L BURKHARDT, C M TELLER

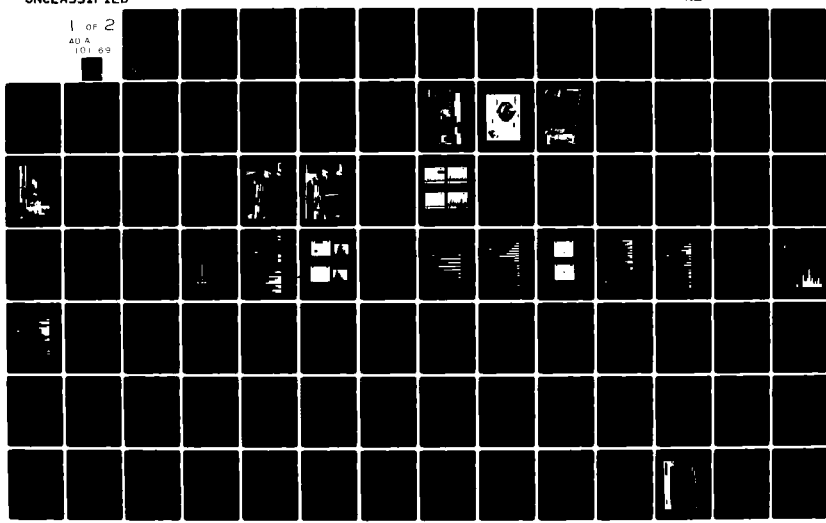
F/G 14/2

F41609-78-C-1823

NL

UNCLASSIFIED

1 OF 2  
404  
101 69



ADA101169

LEVEL 12

## ULTRASONIC TRANSDUCER PERFORMANCE REQUIREMENTS—PHASE II

### FINAL ENGINEERING REPORT

Contract No. F41608-78-C-1823  
SwRI Project No. 15-5468

June 1981

DTIC  
ELECTED  
S JUL 9 1981  
A

This document has been approved  
for public release and sale; its  
distribution is unlimited.

DTIC FILE COPY



SOUTHWEST RESEARCH INSTITUTE  
SAN ANTONIO

HOUSTON

SOUTHWEST RESEARCH INSTITUTE  
Post Office Drawer 28510, 6220 Culebra Road  
San Antonio, Texas 78284

# ULTRASONIC TRANSDUCER PERFORMANCE REQUIREMENTS - PHASE II

by

Hegeon Kwun  
Garry L. Burkhardt  
Cecil M. Teller

## FINAL ENGINEERING REPORT

Contract No. F41608-78-C-1823  
SwRI Project No. 15-5468

The investigation reported in this document was requested by the U.S. Air Force Nondestructive Analysis Branch, San Antonio Air Logistics Center/MMEI, Kelly Air Force Base, Texas 78241, under Government Contract No. F41608-78-C-1823; however, it does not necessarily bear the endorsement of the requesting agency.

October 1978 to June 1981

DTIC  
ELECTRONIC  
JUL 9 1981

A

Approved for public release; distribution unlimited.

Approved:

*John R. Barton*

John R. Barton, Vice President  
Instrumentation Research Division

*311369*  
81 8 08 011

## UNCLASSIFIED

SECURITY CLASSIFICATION OF THIS PAGE (When Data Entered)

REPORT DOCUMENTATION PAGE		READ INSTRUCTIONS BEFORE COMPLETING FORM
1. REPORT NUMBER	2. GOVT ACCESSION NO.	3. RECIPIENT'S CATALOG NUMBER
		AD-A101-169
4. TITLE (and Subtitle)	5. TYPE OF REPORT & PERIOD COVERED	
Ultrasonic Transducer Performance Requirements Phase II	Final Engineering Report October 1978- June 1981	
7. AUTHOR(s)	6. PERFORMING ORG. REPORT NUMBER	
Hegeon Kwun Gary L. Burkhardt Cecil M. Teller	SwRI Project No. 15-5468	
9. PERFORMING ORGANIZATION NAME AND ADDRESS	8. CONTRACT OR GRANT NUMBER(s)	
Southwest Research Institute 6220 Culebra Road San Antonio, Texas 78284	F41608-78-C-1823	
11. CONTROLLING OFFICE NAME AND ADDRESS	10. PROGRAM ELEMENT, PROJECT, TASK AREA & WORK UNIT NUMBERS	
U.F. Air Force Nondestructive Analysis Branch San Antonio, ALC/MMEI Kelly Air Force Base, Texas 78241		
14. MONITORING AGENCY NAME & ADDRESS(if different from Controlling Office)	12. REPORT DATE	
	June 1981	
	13. NUMBER OF PAGES	
	15. SECURITY CLASS. (of this report)	
	Unclassified	
	15a. DECLASSIFICATION DOWNGRADING SCHEDULE	
16. DISTRIBUTION STATEMENT (of this Report)		
Approved for public release; Distribution unlimited.		
17. DISTRIBUTION STATEMENT (of the abstract entered in Block 20, if different from Report)		
18. SUPPLEMENTARY NOTES		
19. KEY WORDS (Continue on reverse side if necessary and identify by block number)		
Nondestructive inspection, ultrasonic transducers, transducer characteristics, contact testing, flaw detection, correlation analysis, specifications, acceptance limits		
20. ABSTRACT (Continue on reverse side if necessary and identify by block number)		
Characteristic ultrasonic transducer parameters were measured for over one hundred sixty contact type ultrasonic transducers (of equivalent sizes) used by depot and field NDI shops in the Air Force. For each transducer a maximum of twenty-four parameters was obtained which included electrical impedance, rf-echo and frequency spectrum, beam characteristics, sensitivity, and signal-to-noise ratio parameters. Transducers were categorized into six groups according to their nominal frequency and beam angle (i.e. 5 MHz and 10 MHz; (over)		

UNCLASSIFIED

SECURITY CLASSIFICATION OF THIS PAGE(When Data Entered)

$0^\circ$ ,  $45^\circ$  and  $60^\circ$ ). Except for 10 MHz- $60^\circ$  transducers, thirty-two transducers were evaluated for each category. For measurement of the beam characteristic parameters of the contact transducers, a side-drilled hole block and an automated data acquisition system were developed. Three small fatigue cracks of different sizes were used for the measurement of flaw signal-to-noise ratios (which determine the flaw detectability of a transducer). Wide variations were observed in the characteristic parameters for individual ultrasonic transducers having the same name-plate size, frequency and angle. However, the average performance for all transducers evaluated in each category of transducers was found consistent with theory. In order to find the characteristic parameters which primarily determine the flaw detectability of a transducer, a linear correlation analysis between pairs of parameters was conducted for each transducer category. High correlation was obtained between the signal-to-noise ratios of the echoes from the fatigue cracks, and between the loop sensitivity and the flaw responses. Moderate correlation was obtained between the sensitivity and signal-to-noise ratios. It was found that the sensitivity does not primarily determine the flaw detectability of the transducer as long as electrical noises of the system are not larger than the background noises of the material to be inspected. Based on the results of this study, preliminary test methods and specifications (acceptance limits) for ultrasonic transducer performance parameters were developed.

UNCLASSIFIED

SECURITY CLASSIFICATION OF THIS PAGE(When Data Entered)

## FOREWORD

This project was sponsored by San Antonio Air Logistics Center, Kelly Air Force Base, Texas, under Contract No. F41608-78-C-1823. Technical direction was provided by Mr. B. W. Boisvert and Mr. Vernon Vitterbo, Air Force Nondestructive Analysis Branch, MMEI. The period of performance was October 1978 through June 1981. Southwest Research Institute, San Antonio, Texas, was the contractor. Dr. Cecil M. Teller was the Project Manager and Dr. Hegeon Kwun and Mr. Gary L. Burkhardt were the Project Engineers.

Appreciation goes to those who assisted with this project; Mr. T. C. Doss and Mr. D. R. Bouressa for measuring transducer parameters; Mr. A. Nagy and Mr. A. E. Nicholls for preparing the fatigue crack specimens; Mr. R. D. Williams, Mr. J. S. Brune, Mr. H. P. King for preparing the reference blocks; Mr. R. S. Birkelbach and Mr. A. S. Lozano for developing the computer programs; Mr. D. J. Krueger and Mr. A. Ramirez for preparing drawings; and Mrs. R. F. Hogue, Mrs. D. Granados and Ms. C. Flores in typing the final report.

The authors also wish to express their appreciation for the support and cooperation received from each participating Air Force and Air National Guard NDI activity without which the success of the project would not have been possible.

## ABSTRACT

Characteristic ultrasonic transducer parameters were measured for over one hundred sixty contact type ultrasonic transducers (of equivalent sizes) used by depot and field NDI shops in the Air Force. For each transducer a maximum of twenty-four parameters was obtained which included electrical impedance, rf-echo and frequency spectrum, beam characteristics, sensitivity, and signal-to-noise ratio parameters. Transducers were categorized into six groups according to their nominal frequency and beam angle (i.e. 5 MHz and 10 MHz; 0°, 45° and 60°). Except for 10 MHz-60° transducers, thirty-two transducers were evaluated for each category. For measurement of the beam characteristic parameters of the contact transducers, a side-drilled hole block and an automated data acquisition system were developed. Three small fatigue cracks of different sizes were used for the measurement of flaw signal-to-noise ratios (which determine the flaw detectability of a transducer). Wide variations were observed in the characteristic parameters for individual ultrasonic transducers having the same name-plate size, frequency and angle. However the average performance for all transducers evaluated in each category of transducers was found consistent with theory. In order to find the characteristic parameters which primarily determine the flaw detectability of a transducer, a linear correlation analysis between pairs of parameters was conducted for each transducer category. High correlation was obtained between the signal-to-noise ratio of an echo in a reference block and the flaw signal-to-noise ratios of the echoes from the fatigue cracks, and between the loop sensitivity and the flaw responses. Moderate correlation was obtained between the sensitivity and signal-to-noise ratios. It was found that the sensitivity does not primarily determine the flaw detectability of the transducer as long as electrical noises of the system are not larger than the background noises of the material to be inspected. Based on the results of this study, preliminary test methods and specifications (acceptance limits) for ultrasonic transducer performance parameters were developed.

TABLE OF CONTENTS

	<u>Page</u>
FOREWORD	ii
ABSTRACT	iii
TABLE OF CONTENTS	iv
LIST OF ILLUSTRATIONS	v
LIST OF TABLES	vii
 I. INTRODUCTION AND SUMMARY	 1
A. Background and Objectives	1
B. Summary of Progress and Findings	2
 II. EXPERIMENTAL PROCEDURES	 5
A. General	5
B. Measurements of Beam Characteristic Parameters	6
C. Measurement of Electrical Impedance, Rf-Echo and Frequency Spectrum Parameters	13
D. Measurements of Loop Sensitivity, Flaw Response and Signal-to-Noise Ratio Parameters	15
 III. EXPERIMENTAL RESULTS AND DISCUSSION	 25
A. Beam Characteristic Parameters	25
B. Electrical Impedance, Rf-Echo and Frequency Spectrum Parameters	33
C. Loop Sensitivity, Flaw Response and Signal-to-Noise Ratio Parameters	37
 IV. CORRELATION ANALYSIS	 50
A. Linear Correlation - Background	50
B. Results and Discussion	56
 V. CONCLUSIONS AND RECOMMENDATIONS	 61
A. Conclusions	61
B. Recommendations	63
 REFERENCES	 64
APPENDIX A. LIST OF PARTICIPATING AIR FORCE BASES	66
APPENDIX B. DEFINITION OF ULTRASONIC TRANSDUCER PERFORMANCE PARAMETERS	68
APPENDIX C. TABLES OF DATA OBTAINED FOR ULTRASONIC TRANSDUCER PERFORMANCE PARAMETERS	72
APPENDIX D. PREPARATION OF FATIGUE CRACK SPECIMENS	83
APPENDIX E. TABLES OF LINEAR CORRELATION COEFFICIENTS	86
APPENDIX F. PRELIMINARY TEST METHODS AND SPECIFICATIONS (ACCEPTANCE LIMITS) FOR ULTRASONIC TRANSDUCER PERFORMANCE PARAMETERS	99

LIST OF ILLUSTRATIONS

<u>Figure</u>		<u>Page</u>
1	Side-Drilled Hole Block	8
2	Block Diagram of Computer Automated Transducer Beam Evaluation System	9
3	Experimental Arrangement for Measuring Beam Parameters	10
4	Four-Wire Spring Suspension Mechanism	11
5	Experimental Arrangement for Scanning Side-Drilled Hole Block	12
6	Semi-Circle Block	14
7	Block Diagram for Measuring Rf-Echo and Spectrum Parameters	16
8	Experimental Arrangement for Rf-Echo, Frequency Spectrum, and Loop Sensitivity Measurements	17
9	Block Diagram for Loop Sensitivity Measurements	18
10	Transducer Positions for Flaw Response Measurements	20
11	Experimental Arrangement for Flaw Response Measurements (for Angle Beam Transducers)	21
12	Experimental Arrangement for Flaw Response Measurements (for Straight Beam Transducers)	22
13	Photos of Reflectoscope® Video Output of Crack Signals and Noise Signals Displayed on Oscilloscope	24
14	Typical Beam Profiles (Obtained with a 5 MHz-45° Transducer)	26
15	Typical Beam Profiles (Obtained with a 10 MHz-45° Transducer)	27
16	Distance-Amplitude Curve Obtained from Data in Figure 14	28
17	Distance-Amplitude Curve Obtained from Data in Figure 15	29
18	Number of Transducers vs. Beam Angle Measured in Aluminum (for Angle Beam Transducers)	34
19	Number of Transducers vs. Beam Angle (for Straight Beam Transducers)	35
20	Examples of Rf-Echo and Corresponding Frequency Spectrum	36

LIST OF ILLUSTRATIONS (Cont'd.)

<u>Figure</u>		<u>Page</u>
21	Number of Transducers vs. Center Frequency (for 5 MHz Transducers)	38
22	Number of Transducers vs. Center Frequency (for 10 MHz Transducers)	39
23	Two Types of Initial Excitation Pulse	40
24	Number of Transducers vs. Loop Sensitivity Ratio (for 5 MHz Transducers)	41
25	Number of Transducers vs. Loop Sensitivity Ratio (for 10 MHz Transducers)	42
26	Number of Transducers vs. Signal-to-Noise Ratio (for 5 MHz Transducers)	44
27	Number of Transducers vs. Signal-to-Noise Ratio (for 10 MHz Transducers)	45
28	Examples of Scatter Diagrams for Data Having High and Moderate Positive Correlation Coefficients	51
29	Examples of Scatter Diagrams for Data Having Low Positive and Negative Correlation Coefficients	52
30	Examples of Scatter Diagrams for Data Having Moderate and High Negative Correlation Coefficients	53
B-1	Frequency Spectrum Parameters Determination	69
D-1	Fatigue Crack Fracture Surface	84
D-2	Crack Surface Length vs. Number of Stress Cycles	85
F-1	Examples of Probe Wedge Misalignment	102
F-2	IIW Block - Type 1	102
F-3	Block for Measuring Beam Angle of Straight Beam Transducer	104
F-4	Beam Misalignment (Skew Angle)	106
F-5	Skew Angle Measurement	106
F-6	Center Frequency Measurement (Example)	109
F-7	Rf-Pulse Length Measurement (Example)	109
F-8	Dead-Zone Measurement	112

LIST OF TABLES

Table		
I      Average Values of Far Field Ratio (FFR), Beam Divergence Angle (BDA), and Experimental Beam Width (EBW)	31	
II     Average Values of Signal-to-Noise Ratio Parameters	46	
III    Average Amplitude Ratios Between Reflected Echoes	48	
IV    Confidence Limits of Linear Correlation Coefficient R for Thirty-Two Samples	55	
V    Probability of Random Correlation for Thirty-Two Samples with an Experimental Correlation Coefficient of Value R	56	
C-I   Ultrasonic Transducer Parameter Data for 5 MHz-0° Transducers	73	
C-II   Ultrasonic Transducer Parameter Data for 5 MHz-45° Transducers	75	
C-III   Ultrasonic Transducer Parameter Data for 5 MHz-60° Transducers	77	
C-IV   Ultrasonic Transducer Parameter Data for 10 MHz-0° Transducers	79	
C-V   Ultrasonic Transducer Parameter Data for 10 MHz-45° Transducers	81	
E-I   Linear Correlation Coefficients for 5 MHz-0° Transducers	87	
E-II   Linear Correlation Coefficients for 5 MHz-45° Transducers	89	
E-III   Linear Correlation Coefficients for 5 MHz-60° Transducers	91	
E-IV   Linear Correlation Coefficients for 10 MHz-0° Transducers	93	
E-V   Linear Correlation Coefficients for 10 MHz-45° Transducers	95	
E-VI   Average Linear Correlation Coefficients Among Beam, Electrical Impedance, Rf-Echo, and Frequency Spectrum Parameters	97	
E-VII   Average Linear Correlation Coefficients Between Beam, Electrical Impedance, Rf-Echo, and Frequency Spectrum Parameters and Sensitivity and Signal-to-Noise Ratio Parameters	98	

## I. INTRODUCTION AND SUMMARY

### A. Background and Objectives

Ultrasonic nondestructive inspection (NDI) is one of the most widely used methods for inspecting materials and structures for defects. This is primarily due to the capability of ultrasonics to detect and locate small internal and surface flaws or discontinuities. Furthermore, ultrasonics is capable of providing valuable information on the characteristics of defects, e.g. type, size, and orientation. This information is vital in determining the integrity and serviceability of structural parts or components.

The use of ultrasonic NDI in the Air Force on critical aircraft components has been steadily increasing over the years. However, the flaw detectability of ultrasonic systems is much lower<sup>1</sup> than either perceived or expected, not to mention their capability to characterize flaws. Also, the results of ultrasonic NDI have demonstrated wide variation from application-to-application and even from day-to-day on the same application. The lack of reproducible and uniform test results has thus resulted in poor reliability and often loss of confidence in ultrasonic inspections. Some of the difficulties can be attributed to the varying degree of an inspector's skill as well as the differences in the performance of electronic instruments employed. Another major source of the variations which is rather peculiar to the ultrasonics, lies in the variability of the performance of ultrasonic transducers. Ultrasonic transducers used by Air Force field and depot NDI shops are commercial, off-the-shelf, expendable items procured by Defense General Supply Agency. A wide variety of ultrasonic transducers is commercially available in varying configurations and operating parameters, but it has been known that even two supposedly identical transducers (i.e. same name-plate size, frequency, etc.) obtained from the same manufacturer may have very different<sup>2</sup> performance characteristics. Therefore, there is a great need for establishing a standard which would allow control of transducer performance characteristics and thus eventually lead to uniform and improved ultrasonic NDI results.

A number of ultrasonic performance parameters are directly measurable, e.g. beam angle, frequency, and sensitivity. By controlling these measurable parameters, variation in the performance of ultrasonic transducers can be reduced. However, controlling all the measurable parameters would be very costly and thus economically unjustifiable. Furthermore, only few among these measurable parameters may be primarily responsible for the flaw detectability and ultimately the characterization capability of a transducer. Therefore, there is a practical need for investigating the relationship between measurable characteristic parameters and the flaw detectability/characterization capability of ultrasonic transducers. Such an investigation will provide a practical basis for selecting parameters which should be controlled in order to achieve high reliability and uniformity of ultrasonic NDI.

Accordingly, the objectives of the present project were established a) to generate engineering data relating the measurable transducer parameters to flaw detectability, b) to develop a preliminary procurement document with realistic performance requirements based upon measurable parameters, and c)

to recommend test methods for these parameters. The present project included straight and angle beam 5 MHz and 10 MHz transducers having piezoelectric element of 6.35 mm (0.25 in.) diameter or square routinely used in Air Force field and depot NDI shops.

#### B. Summary of Progress and Findings

This project is an extension of previous work<sup>2</sup> (Contract No. F41608-77-C-1381, SWRI Project No. 15-5024, titled "Engineering Services to Determine Acceptance Limits of Ultrasonic Transducers for Nondestructive Inspection", Final Engineering Report, June, 1978). In that project (Phase I), twenty-three longitudinal beam contact transducers of various frequencies and sizes were evaluated primarily by immersion testing, and linear correlation analyses of seventeen measurable characteristic parameters were conducted.

Initially, the present project (Phase II) was aimed at performing the same measurements and linear correlation analyses of parameters as those conducted in Phase I, but with both longitudinal wave (straight beam) and shear wave (angle beam) transducers used in the contact mode. Accordingly, for the measurements of beam profile as well as the near-to-far field transition distance of contacting transducers a side-drilled hole test block was developed. An automated data acquisition system and the necessary computer program for the data analysis were also developed. Subsequently, data were acquired on fourteen longitudinal wave transducers and twenty-three shear wave transducers, and linear correlation analyses of the parameters were conducted. High correlation was found between the loop sensitivity ratio and the flaw responses from EDM (Electric Discharge Machined) notches, side-drilled holes, and fatigue cracks. However, it was found difficult to assign tolerances to the parameters, partly because of the relatively low confidence limits on the results of the statistical correlation analyses and partly because of the mixing of several different types and sizes of transducers in the analyses. Also, it was determined that the effect of extended field-service upon the performance characteristics of the transducers (which was one of the initial objectives of this project) could not be determined because of the lack of information on the initial performance characteristics as well as the length of time and conditions of the field-service.

This project was therefore re-structured to cover six groups of transducers (different frequencies and angles) with approximately thirty transducers in each group. This would enhance the confidence of the correlation analyses and reduce unnecessary variations of parameters due to the mixing of several different types of transducers. In anticipation that more highly correlated transducer parameters would become evident as the threshold of sensitivity is approached, three specimens with reasonably small size fatigue cracks were also prepared.

For each transducer category (5 MHz-0°, 5 MHz-45°, 5 MHz-60°, 10 MHz-0°, and 10 MHz-45°), thirty-two transducers were evaluated. Almost all the transducers evaluated in this project were obtained from various Air Force and Air National Guard NDI shops (more than forty shops around the United States) at which they had been put into inspection service. The results of this latter part of the project constitute this final report.

A total of twenty-four parameters were measured for each transducer. Results of the measurements and the linear correlation analyses of the parameters showed that:

- 1) There is a wide variation in the values of each characteristic parameter for nominally identical transducers,
- 2) The relationship between the average values of loop sensitivity and flaw responses is consistent with that theoretically expected,
- 3) On the average, 5 MHz-60° transducers were found to be inferior to 5 MHz-45° transducers in detecting fatigue cracks (which are grown normal to the surface) because of the energy loss due to mode conversion of the 60° shear waves upon reflections from the right angled edge formed by the crack,
- 4) Straight beam longitudinal transducers can not reliably detect small surface fatigue cracks because of the interference effects from the surface of the part near the fatigue crack,
- 5) High correlations (correlation coefficient greater than 0.7) were shown to exist between the loop sensitivity and the flaw responses; between the signal-to-noise ratios from cracks and a large surface reflector; between the spectral band width and the number of rf cycles in the pulse; and between the peak frequency and the center frequency,
- 6) Moderate correlations (correlation coefficients between 0.7 and 0.4) were found between the center frequency (or peak frequency) and the spectral band width (or the number of rf cycles in the pulse), between the sensitivity parameters (loop sensitivity or flaw responses) and the signal-to-noise ratios,
- 7) Low correlations (correlation coefficient less than 0.4) were found among the rest of the pairs of parameters.

Since flaw detection capability is directly proportional to the flaw signal-to-noise ratio, the signal-to-noise ratio is the most important performance parameter of a transducer where detectability alone is of concern. The moderate correlation between the sensitivity and signal-to-noise ratio parameters reflects the fact that as long as the sensitivity of the system is adequate, i.e. the system electrical noise is smaller than the background noise from the transducer and the material being inspected, sensitivity does not significantly influence flaw detection. The high correlations between the loop sensitivity and flaw responses, and between the signal-to-noise ratio of the echo from the reference block and the flaw signal-to-noise ratios suggest that minimum detectable flaw size can be estimated from a DGS (Distance-Gain-Sizing) diagram.<sup>3</sup> This can be accomplished by measuring the signal-to-noise ratio of an echo from a corner or the back surface of the material being inspected.

Based on the results of this project, a preliminary document on the test methods and specifications (acceptance limits) for ultrasonic transducer

performance parameters was developed (see Appendix F). This specification is primarily intended for procurement of ultrasonic transducers for the Air Force depot and field level use.

## II. EXPERIMENTAL PROCEDURES

### A. General

Characteristic parameters were acquired from a total of one hundred sixty three transducers. These transducers were divided into six different categories based on the nameplate frequency and beam angle. A breakdown of the number of transducers evaluated in each category in this study is as follows:

<u>Freq. (MHz)</u>	<u>Beam Angle (degrees)</u>	<u>No. Evaluated</u>
5	0	32
5	45	32
5	60	32
10	0	32
10	45	32
10	60	3

All transducers had piezoelectric elements of approximately equivalent sizes [either 6.35 mm (0.25 in.) diameter for circular element or 6.35 mm (0.25 in.) side for square element]. The transducers were designed for use in a contacting mode on essentially flat surfaces through a thin layer of couplant (typically SAE 10W to 40W motor oil<sup>4</sup>). The transducers with zero degree beam angle were longitudinal wave transducers, while the other transducers were shear wave transducers. The angle beam of the shear wave transducers is generated by mode conversion of longitudinal waves using an appropriate wedge or shoe (typically an acrylic resin plastic). More detailed descriptions on the construction of a typical transducer may be found in the references.<sup>2,4</sup>

Among these transducers, one hundred and forty-seven were obtained from various NDI shops in the Air Force and Air National Guard where they had been put into actual inspection service. (The rest of the transducers were directly purchased from manufacturers.) More than forty depot or field level NDI shops participated in the program furnishing the necessary in-service transducers (a list of participating Air Force bases is given in Appendix A).

A total of twenty-four parameters were selected for the characterization of a transducer. These parameters were divided into three groups: 1) electrical impedance, rf-echo and frequency spectrum parameters, 2) beam characteristic parameters, and 3) sensitivity, and signal-to-noise ratio parameters.

#### 1. Electrical impedance, rf-echo and frequency spectrum parameters include:

- a) Impedance (IMP)
- b) Impedance Angle (IPA)
- c) Damping (DMP)
- d) Peak Frequency (PF)
- e) Center Frequency (CF)

- f) Band Width Ratio (BWR)
- g) Spectrum Symmetry Ratio (SSR)
- h) Spectrum Inflection Ratio (SIR)

2. Beam Characteristic Parameters include:

- a) Far Field Ratio (FFR)
- b) Experimental Beam Angle (EBA)
- c) Beam Divergence Angle (BDA)
- d) Beam Symmetry Ratio (BSR)
- e) Beam Inflection Ratio (BIR)
- f) Experimental Beam Width (EBW)
- g) Skew Angle (SA)

3. Sensitivity and signal-to-noise ratio parameters include:

- a) Loop Sensitivity Ratio (LSR)
- b) Side Drilled Hole Response (SDH)
- c) Flaw Response Ratio from fatigue cracks #1, #2, and #3 (FR1, FR2, FR3)
- d) Signal-to-Noise Ratio (SNR)
- e) Flaw Signal-to-Noise Ratio of fatigue crack #1, #2, and #3 (FN1, FN2, FN3).

The definition of each parameter is given in Appendix B.

Detailed descriptions of the measurement methods of these parameters are given in the following sections. For the sake of convenience, measurement methods of beam characteristic parameters are described in Section II-B; electrical impedance, rf-echo and frequency spectrum parameters in Section II-C, and finally, sensitivity and signal-to-noise ratio parameters in Section II-D. Throughout this project, an Automation Industries S-80 Reflectoscope® with a PR-2 pulser/receiver module was used for the pulser. Unless otherwise stated, this module was also used for the receiver. Control settings of the pulser were kept fixed throughout the measurements in order to minimize any effects of the variation in the electrical characteristics of the pulser on the performance of a transducer. Investigation of interactions between the transducers and different pulser/receivers and their effects on the transducer performance was beyond the scope of the project.

In Appendix C, all the data obtained in the parametric measurements are listed except those for the 10 MHz-60° transducers. Because of the unavailability of a sufficient number of 10 MHz-60° transducers, the linear correlation analyses of the characteristic parameters for these transducers were excluded from the project.

**B. Measurements of Beam Characteristic Parameters**

Measurements of transducer beam characteristics were obtained using a system in which the transducer (operating in a pulse-echo mode) was scanned past a series of side-drilled holes at different depths in an aluminum block

(Fig. 1). The response of the transducer as a function of position with respect to each side-drilled hole was recorded and processed using a computerized data acquisition system as shown in the block diagram in Fig. 2. As the transducer was scanned by a motor drive, its position was determined by a precision shaft angle encoder and an associated pulse counter, and this information was monitored by a computer. The transducer response to each hole as a function of position was measured by a gated peak detector in combination with an analog-to-digital converter and was stored on magnetic tape by a computer. Figure 3 shows the actual experimental arrangement of the apparatus.

The side-drilled hole block (Fig. 1) consisted of a 15.5 mm (0.610 in.) thick machined plate of 7075 T651 aluminum. Fifteen side-drilled holes reamed to a diameter of 1.59 mm (0.0625 in.), were placed through the block at depths from the top surface varying from 1.59 mm (0.0625 in.) to 127 mm (5.000 in.) to the hole center. Horizontal spacing of the holes is 12.7 mm (0.500 in.) which was sufficient to eliminate interference of echoes from adjacent holes on the transducer response. A shallow "well" was machined on the top of the side-drilled hole block to hold a thin film of light machine oil which was used as a couplant.

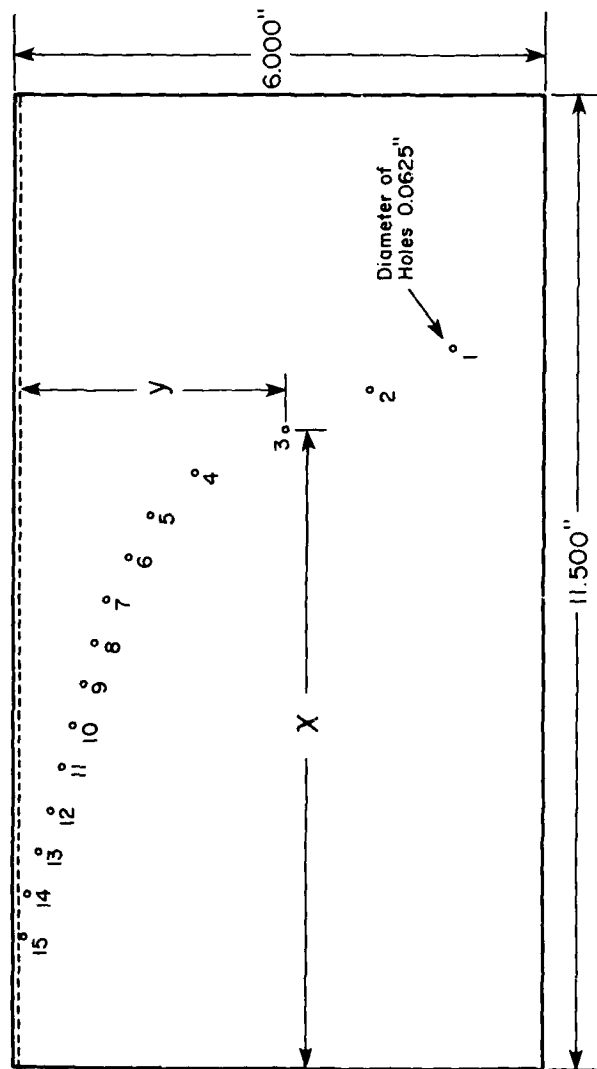
In order to assure consistent transducer alignment and coupling, a four-wire cantilever spring suspension mechanism (Fig. 4) was utilized to provide a constant downward force on the transducer. This mounting system allows angular, side-to-side compliance and maintains uniform contact of the transducer with the standard even if the bottom surface of the transducer is not square with the transducer housing. In addition, a pivot in the probe mount allows compliance in the fore-and-aft direction. A plastic holder was fabricated for each type of transducer case, and the transducer was inserted into the holder with only the bottom portion of the transducer protruding. This entire assembly was held in the mounting mechanism.

The scanning mechanism (Fig. 5) for the transducers consisted of a precision slide assembly and lead screw which was motor driven to scan the transducer suspension mechanism along the length of the side-drilled hole standard. An incremental shaft angle encoder was also driven by the lead screw and provided a resolution of 0.025 mm (0.001 in.) of transducer position. A counter was constructed to convert the output pulses from the encoder to a transducer position measurement which were displayed on a digital LED readout. A binary coded decimal (BCD) position output was supplied to the computer.

Ultrasonic instrumentation (Fig. 3) consisted of an Automation Industries S-80 Reflectoscope® with a PR-2 pulser/receiver module, a DAG-1 distance amplitude data module, and an optional peak detector circuit. Gain of the PR-2 module was adjusted for each transducer to obtain a response of approximately 80% of full scale on the Reflectoscope® display from the largest echo obtained from any of the side-drilled holes. The gain setting was recorded for later use in the computer calculations of the echo amplitude.

Each gain setting of the receiver was calibrated prior to the measurements. The calibration was accomplished by the use of monochromatic rf waves of 5 and 10 MHz generated by a signal generator (Hewlett Packard, Model 606A),

No. SDH	X (in.)	Y (in.)
1	8.5	5.0
2	8.0	4.0
3	7.5	3.0
4	7.0	2.0
5	6.5	1.5
6	6.0	1.25
7	5.5	1.0
8	5.0	0.875
9	4.5	0.750
10	4.0	0.625
11	3.5	0.5
12	3.0	0.375
13	2.5	0.25
14	2.0	0.125
15	1.5	0.062



NOTE: ALL DIMENSIONS IN INCHES (1 in. = 25.4 mm)

FIGURE 1. SUGGESTED HOLE BLOCK

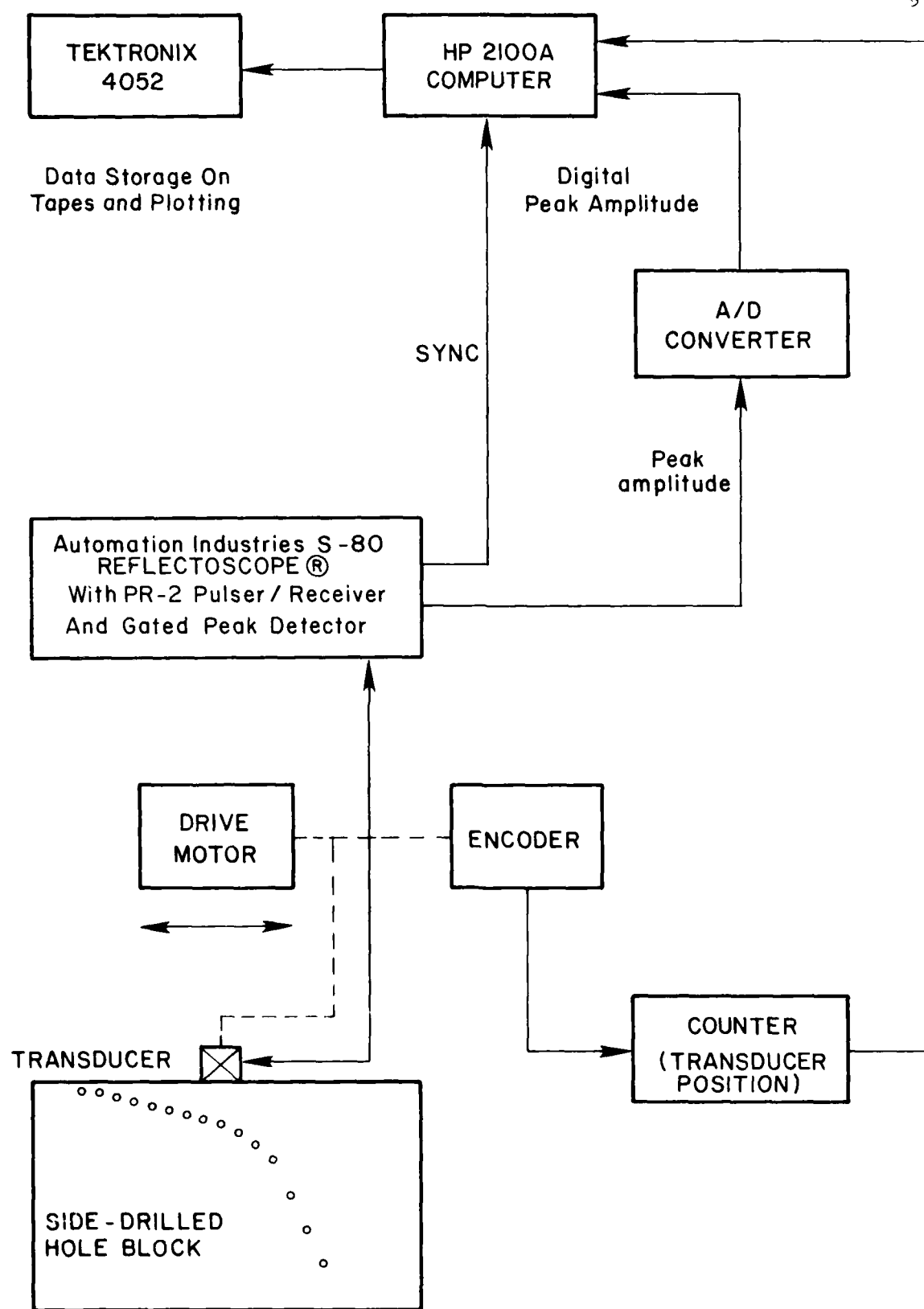


FIGURE 2. BLOCK DIAGRAM FOR COMPUTER AUTOMATED TRANSDUCER BEAM EVALUATION SYSTEM

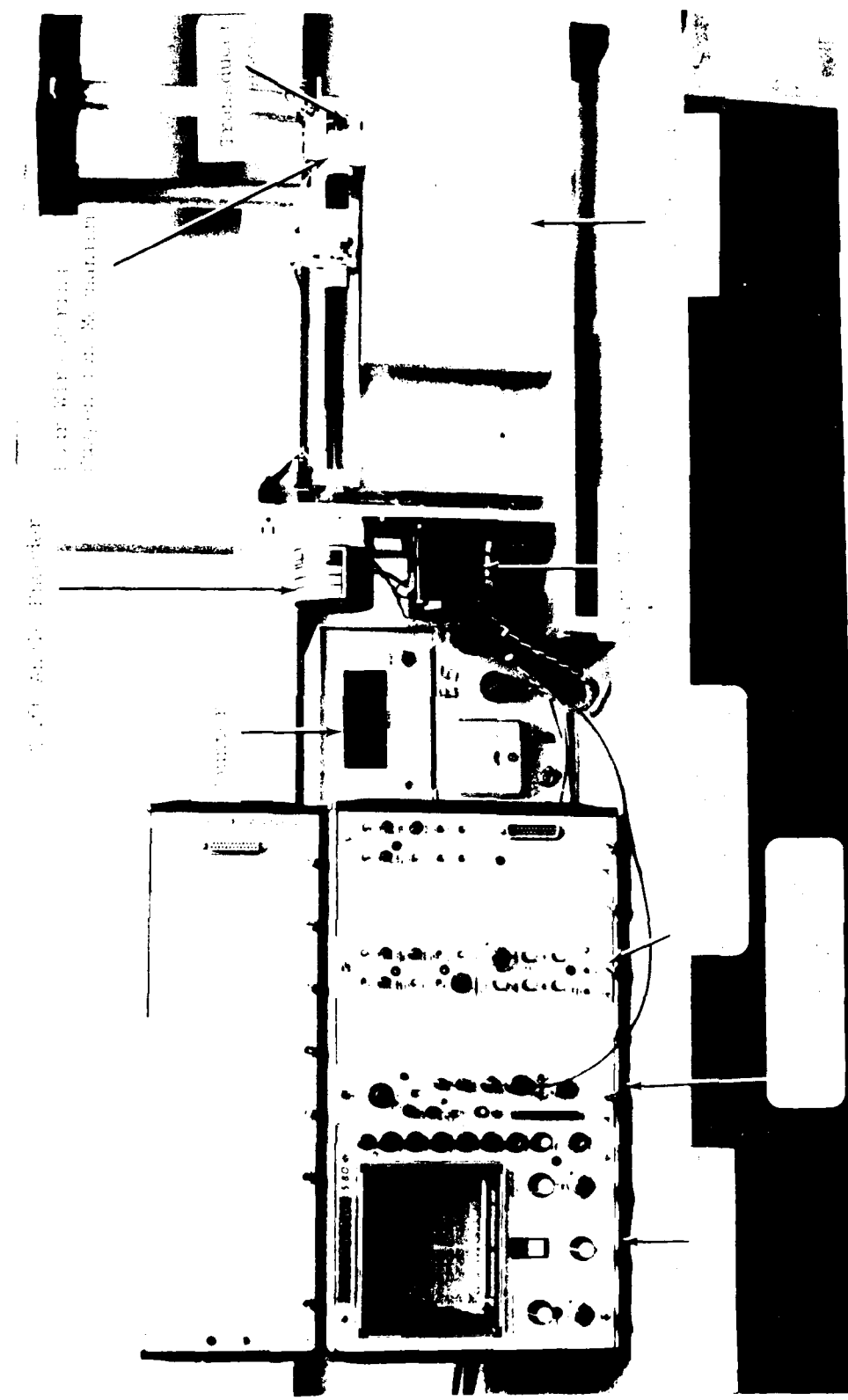


FIGURE 3. EXPERIMENTAL ARRANGEMENT FOR MEASURING BEAM PARAMETERS

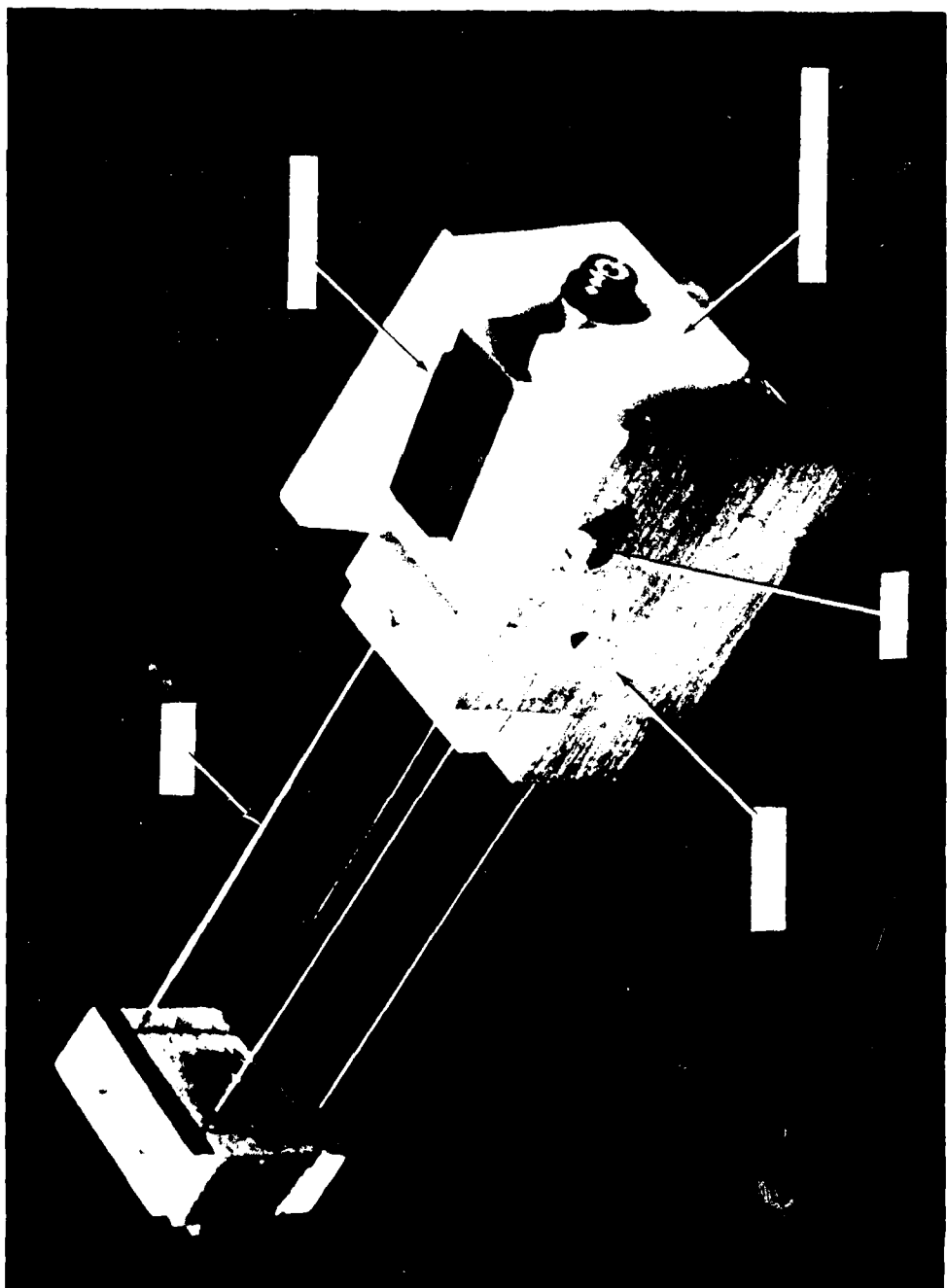


FIGURE 4. A PRECISION MECHANISM

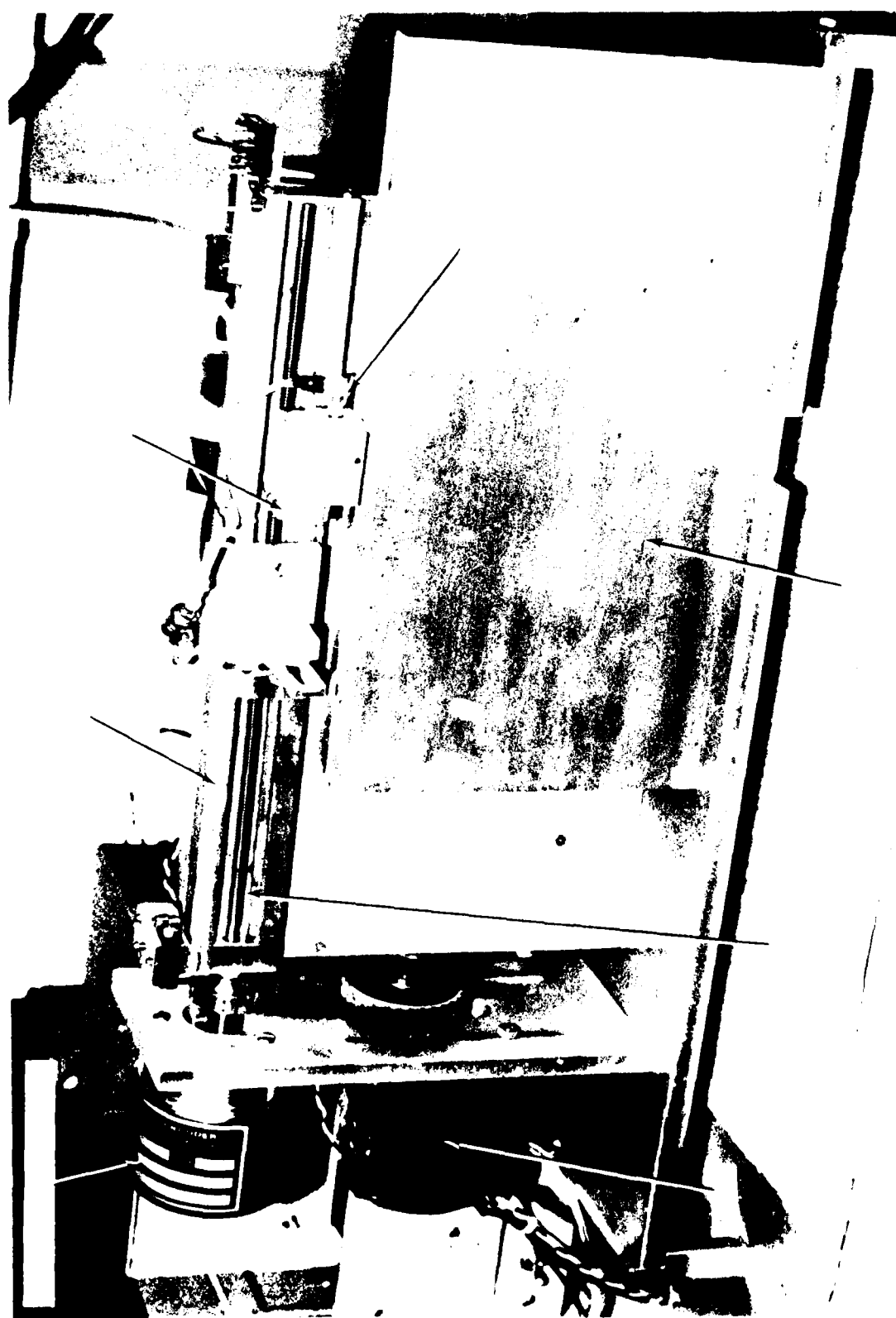


FIGURE 1. LUMINESCENCE IMAGE OF MAN IN DARK SUIT AND TIE

respectively. At a given gain setting, an rf signal was fed into the receiver and the peak-to-peak voltage of the rf signal was measured which was needed to produce a 1 volt video output on the Reflectoscope® (the PR-2 receiver was set to the corresponding frequency). The actual amplification factor of each gain setting was thus determined by dividing the video output voltage by the required input voltage of the rf signal. (In this calculation of the actual echo signal amplitude, no attempts were made to correct for the frequency dependence of the receiver gain or to take into account the effect of the spectrum content of the echo).

The gate in the DAG-1 module was set to include only the transducer responses from the side-drilled holes and not the initial excitation pulse. The peak detector circuit detects the maximum amplitude of the received echo in the gate and holds that value at a constant output level until the amplitude is measured by the analog-to-digital converter. The peak detector is then reset for the next echo.

The computer system consisted of a Hewlett-Packard 2100A minicomputer which was used for data acquisition and a Tektronix 4052 computer with graphics capability for storage, plotting and analysis of the data. The transducer position information was obtained directly from the digital BCD output of the shaft angle encoder counter. Signal amplitude was measured with an analog-to-digital converter with a resolution of one part in 512 over the signal voltage range measured. A typical data set consisted of a transducer scan distance of 24.13 cm (9.5 in.) with discrete measurements of the transducer response at 950 positions spaced 0.25 mm (0.010 in.) apart. These data were transferred to the Tektronix 4052 for storage on magnetic tape cassettes. Data analysis was performed using a BASIC language program run on the Tektronix 4052.

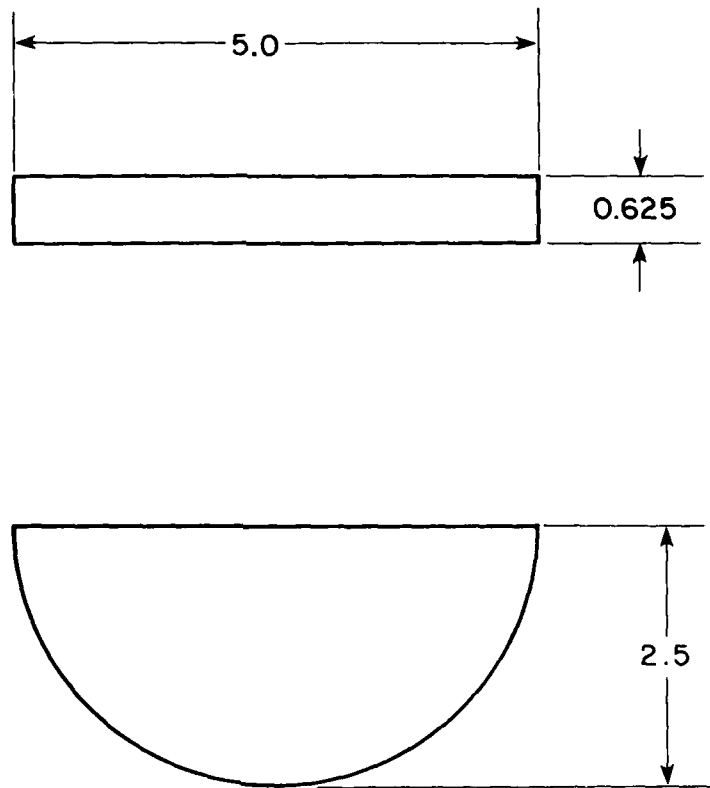
Measurements of the beam angle and skew angle of angle beam shear transducers were made with an aluminum IIW-2 reference block (see Fig. F-2 in Appendix F). The beam angle was obtained by maximizing the echo returned from the 50 mm (2 in.) diameter hole in the IIW-2 block. The skew angle was obtained by maximizing the echo from the corner (see Fig. F-5 in Appendix F) of the IIW-2 block.

The beam angles of straight beam longitudinal transducers were deduced from the analysis of the data obtained from scanning the side-drilled hole block.

#### C. Measurement of Electrical Impedance, Rf-Echo and Frequency Spectrum Parameters

The magnitude and phase angle of the transducer electrical impedance were measured by a vector impedance meter (Hewlett Packard Model 4815A) at the nominal transducer center frequency.

For the measurements of rf-echo and frequency spectrum parameters, the first returned echo in a semi-circle block shown in Fig. 6 was used. The semi-circle block was fabricated from 1.59 cm (0.625 in.) thick 7075-T651



All dimensions in inches (1 in. = 25.4 mm)

FIGURE 6. SEMI-CIRCLE BLOCK

aluminum plate. The radius of the block was 6.35 cm (2.5 in.). This block was adopted for these measurements because of the following reasons. First, it provides a reasonably large cylindrical concave reflecting surface. Since an echo from a flat bottom hole or a notch may be influenced<sup>5-7</sup> by diffraction from the sharp-edges of these reflectors, they are not suitable for the measurement of rf-echo and frequency spectrum parameters of a probe. Second, it provides a reflected echo at a fixed distance from the beam exit point of a probe, regardless of probe's beam angle. An echo from a side-drilled hole of a given size may be used; however, the result thus obtained may be influenced<sup>8,9</sup> by the variation in the path length for different beam angles as well as the hole size. Third, it provides a consistent and uniform measurement for both straight and angle beam probes.

Figure 7 shows the block diagram of the instrumentation for these measurements. A transducer, placed on the center of the semi-circle block, was excited by a pulse generated by the Reflectoscope®. To ensure repeatable alignment and coupling, the semi-circle block was clamped to the side-drilled hole block and the four-wire spring suspension mechanism was used (see Fig. 8). The reflected echo from the curved surface of the semi-circle block was received and amplified by a separate wide band receiver (Aerotech Laboratories, Ultrasonic Transducer Analyzer, Model UTA-3). This echo signal was then displayed on an oscilloscope (Tektronix, Model 5440). The position of the transducer was subsequently adjusted until a maximum echo signal was obtained. The step-less gate signal of the UTA-3 was also displayed on the oscilloscope. The position and width of the step-less gate were adjusted such that the gate covered the first and last instant at which the amplitude of the rf echo reached approximately 10% (-20 dB) of its maximum amplitude. This gated portion of the rf echo was fed into a spectrum analyzer (Hewlett Packard 141T Spectrum Analyzer System, with plug-in, Model 8553B and 8552B) which then displayed the corresponding frequency spectrum of the rf echo.

#### D. Measurement of Loop Sensitivity, Flaw Response and Signal-to-Noise Ratio of Parameters

Measurement of loop sensitivity was made with the semi-circle block described in Section II-C (Figs. 6 and 8). The position of a transducer was adjusted so that the first returned echo from the radius of the block was maximized. To avoid influence of the receiver characteristics, the signal amplitude of the echo was measured before it entered the PR-2 receiver section of the Reflectoscope®. This was done by putting a "T" connector and a 10X oscilloscope probe at the pulser output (or equivalently receiver input). The rf signals of both the initial excitation pulse and the reflected echo were then displayed on an oscilloscope (Tektronix, Model 5440). A block diagram of the measurement is shown in Fig. 9. The loop sensitivity ratio (LSR) of each transducer was calculated from the equation  $LSR = 20 \log_{10} (A_e/A_i)$  where  $A_e$  and  $A_i$  are the peak-to-peak amplitude of the echo signal and the initial excitation pulse, respectively.

While maintaining the same set-up, the signal-to-noise ratio (SNR) of the first returned echo from the radius of the semi-circle block was measured. Measurements were made as follows: a) the echo height was set at a predetermined

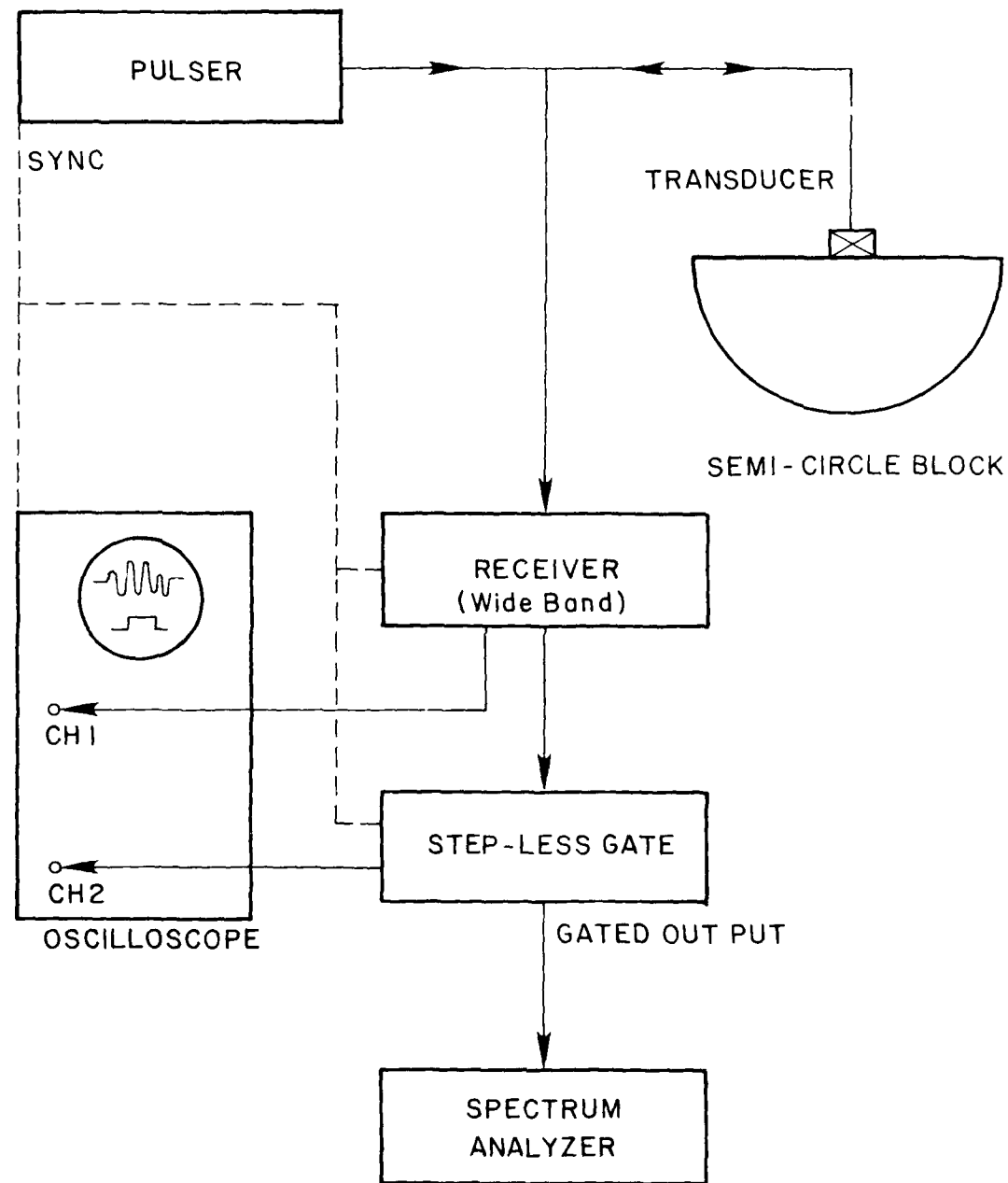


FIGURE 7. BLACK DIAGRAM FOR MEASURING RF-ECHO AND SPECTRUM PARAMETERS

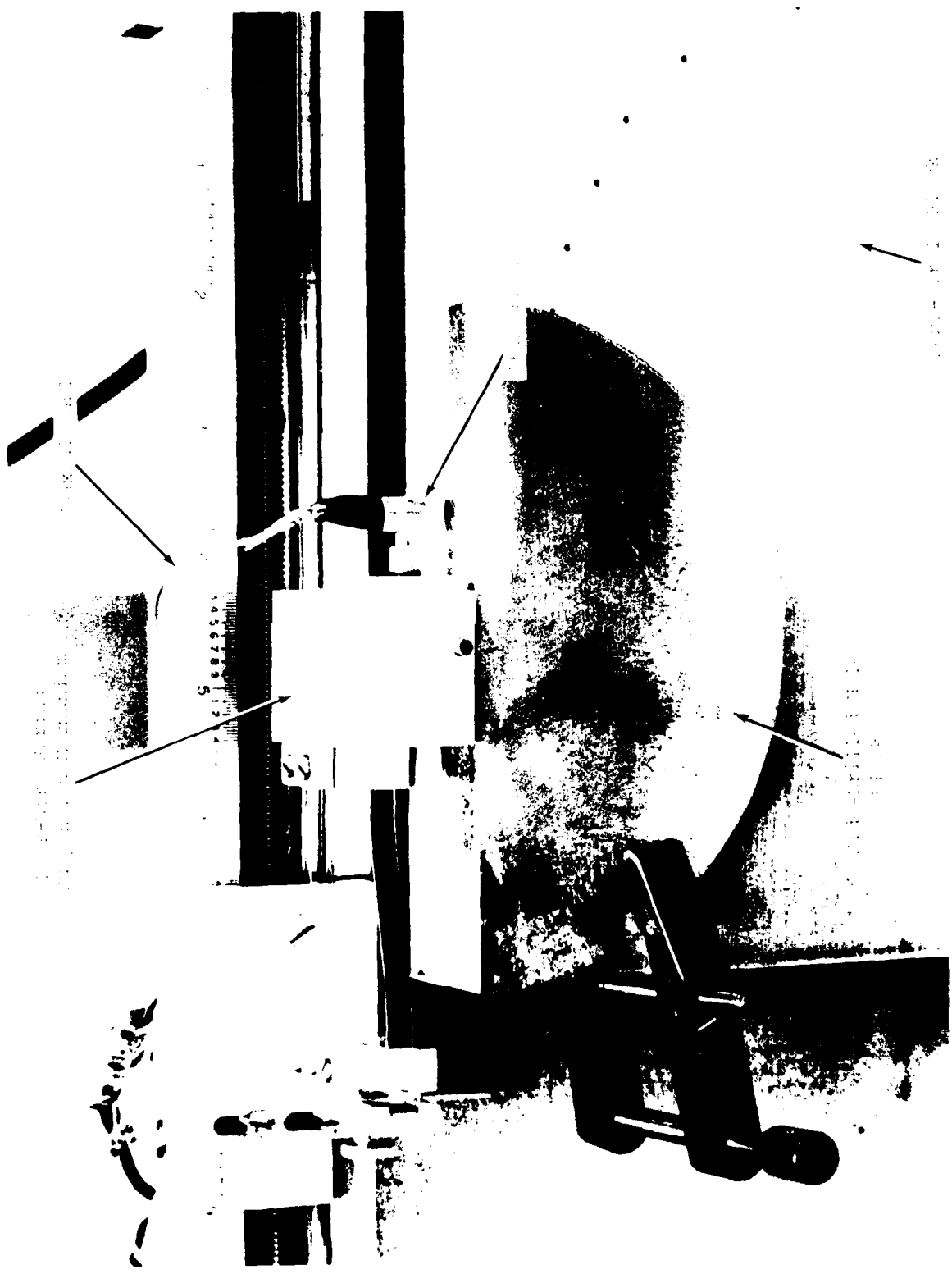


FIGURE 3. EXPERIMENTAL ARRANGEMENT FOR RF-ECCHO, FREQUENCY SPECTRUM AND ECP SENSITIVITY MEASUREMENTS

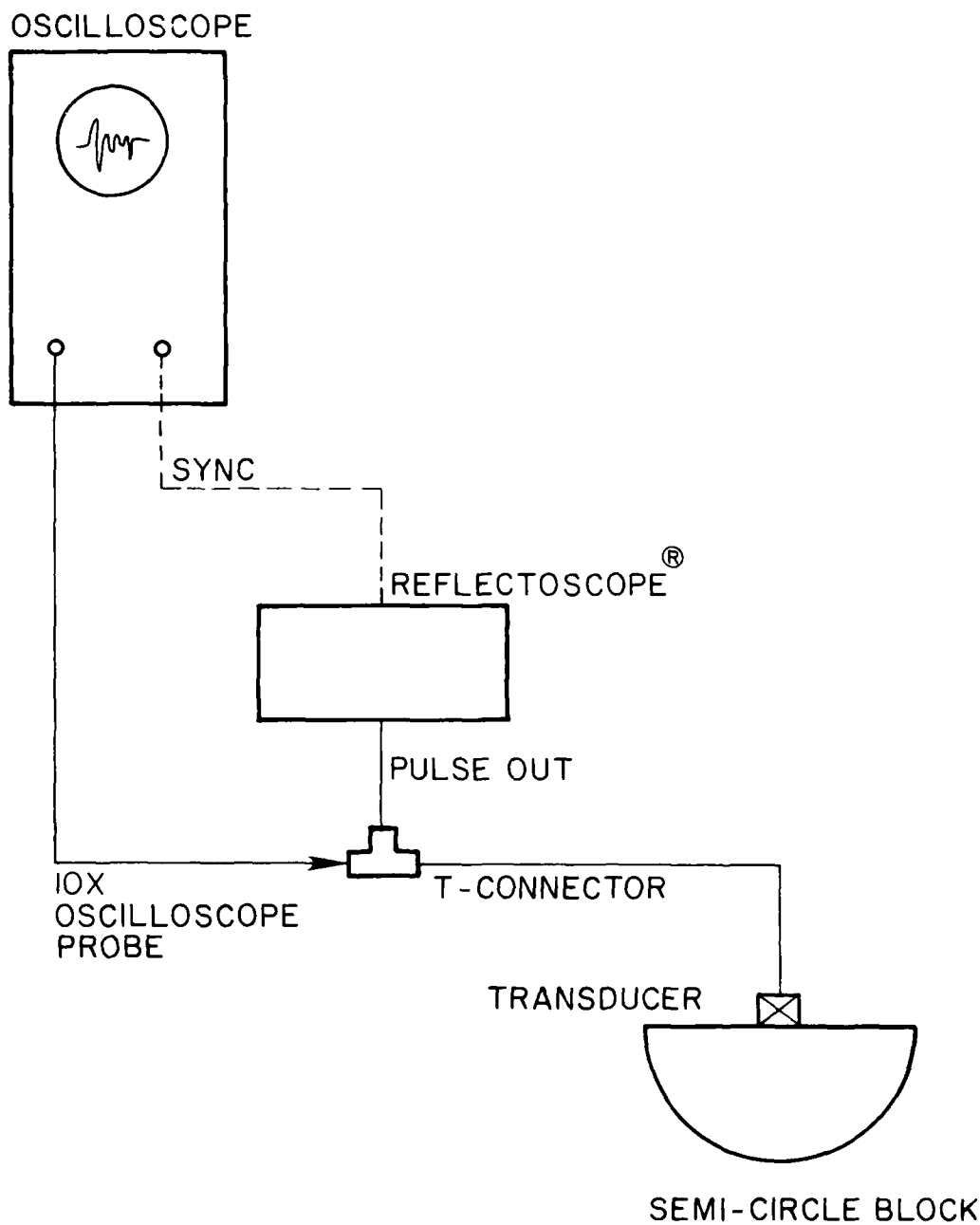


FIGURE 9. BLOCK DIAGRAM FOR LOOP SENSITIVITY MEASUREMENTS

value, typically 50% of full scale of the Reflectoscope® display, by adjusting the receiver gain and the gain was read in dB, and b) the receiver gain was increased until the noise level was at the same predetermined value and the gain was read in dB. SNR is the difference between these two gain readings.

For the measurement of the flaw response and flaw signal-to-noise ratios of transducers, three fatigue crack specimens made from 7075-T651 aluminum were used. The specimens contained fatigue cracks of surface length 1.27 mm (0.05 in.), 2.54 mm (0.10 in.) and 3.81 mm (0.15 in.), respectively. The surface length-to-depth ratios were estimated to be approximately 4 to 1 for the cracks of 1.27 mm (0.05 in.) and 2.54 mm (0.10 in.) surface length, and 2 to 1 for the crack of 3.81 mm (0.15 in.) surface length. (For the fatigue crack specimen preparation and the estimation of the surface length-to-depth ratios, refer to Appendix D.) The reason for using these small size fatigue cracks in the flaw response and flaw signal-to-noise ratio measurements was that the responses from these flaws would approach or reach the threshold of sensitivity or detectability of each transducer. As the detectability threshold is approached, it was anticipated that the relation between transducer parameters and the flaw detectability would be more evident and practical assignment of tolerances would be possible on those parameters highly correlated with the flaw signal-to-noise ratios.

Since flaw detectability is proportional to the magnitude of the flaw signal-to-noise ratio, the measure of the flaw detectability of a transducer can be essentially represented by the flaw signal-to-noise ratio.

Figure 10 illustrates the placement of transducers for flaw response and flaw signal-to-noise ratio measurements. Angle beam shear wave transducers were placed on the face of the specimen where the fatigue crack is located. The crack echo was obtained at one skip distance (Fig. 10-a) which was typically about 36.8 mm (1.45 in.) for 45° shear wave transducers (rated in steel) and 45.7 mm (1.80 in.) for 60° shear wave transducers (rated in steel). Straight beam longitudinal wave transducers were placed on the end of the specimen (Fig. 10-b). In this case, the distance to the crack was approximately 52.3 mm (2.06 in.).

To ensure consistent and repeatable measurements, fatigue crack specimens as well as transducers were placed in a fixture clamped to the side-drilled hole block and the same transducer suspension system was used. Actual arrangement of the measurement is shown in Figs. 11 and 12.

To measure the flaw responses and flaw signal-to-noise ratios, the position of a transducer was adjusted laterally or longitudinally until the crack echo on the Reflectoscope® was maximized. Next, the gain of the PR-2 receiver of the Reflectoscope® was adjusted so that the crack echo reached a predetermined level, typically 50% of full scale. In addition, the video output voltage of the crack echo was measured with an oscilloscope. Both the receiver gain and video output voltage of the crack echo were recorded and later used to calculate the actual crack signal amplitude. Finally, the receiver gain was raised until the noise reached the same predetermined level. The flaw signal-to-noise ratio is the increase in gain measured in dB.

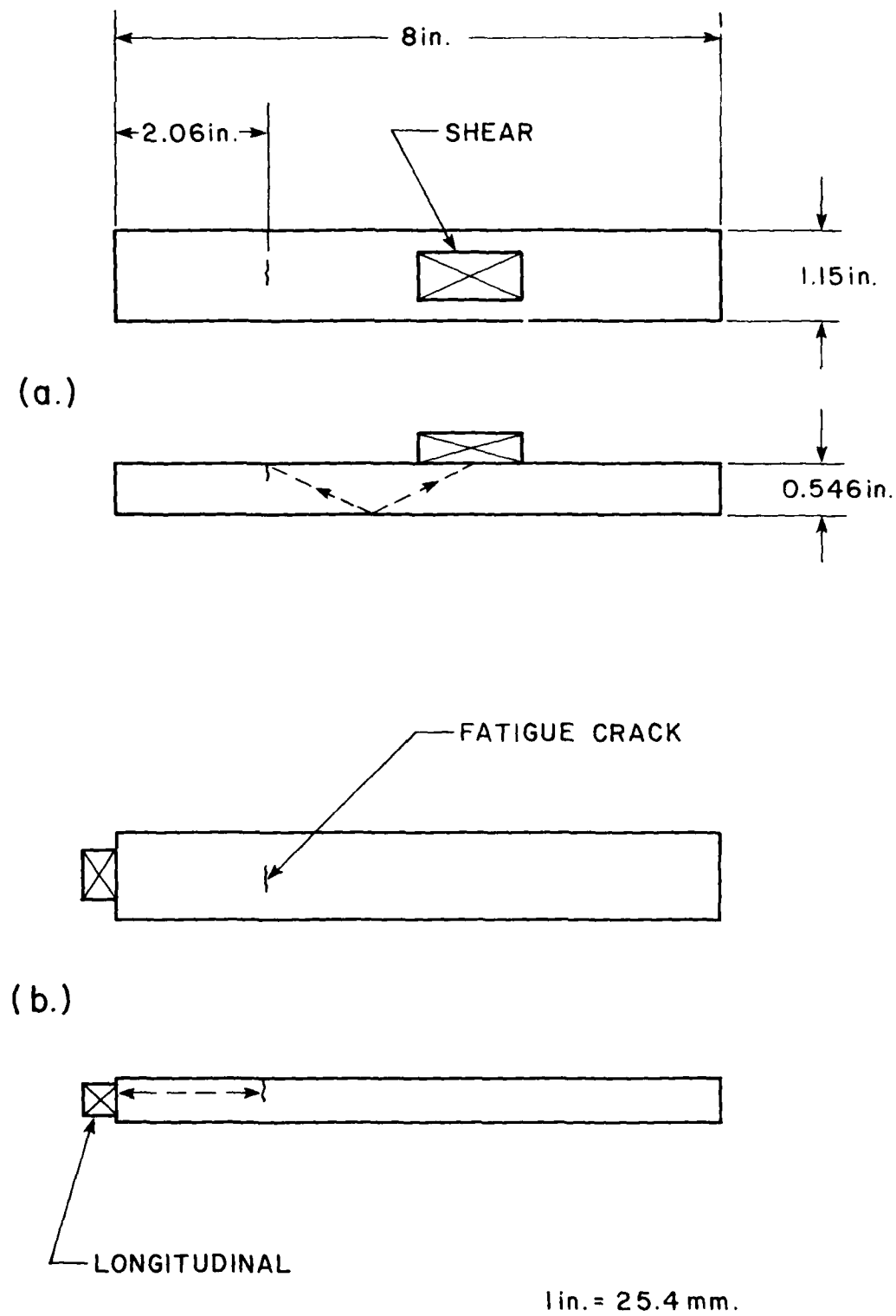


FIGURE 10. TRANSDUCER POSITIONS FOR FLAW RESPONSE MEASUREMENTS

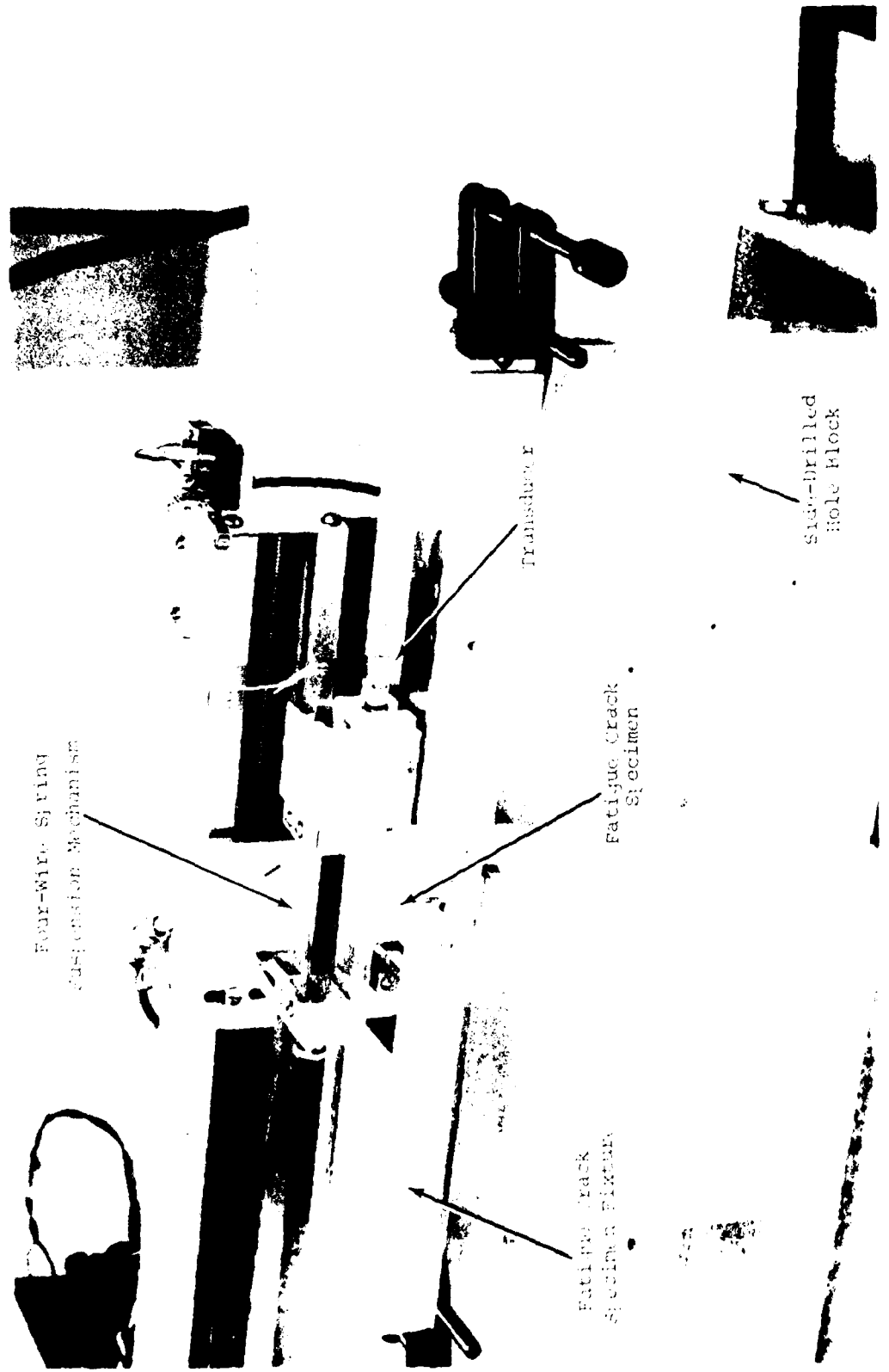


FIGURE 11. EXPERIMENTAL ARRANGEMENT FOR FLAW RESPONSE MEASUREMENTS (FOR ANGLE BEAM TRANSDUCERS)

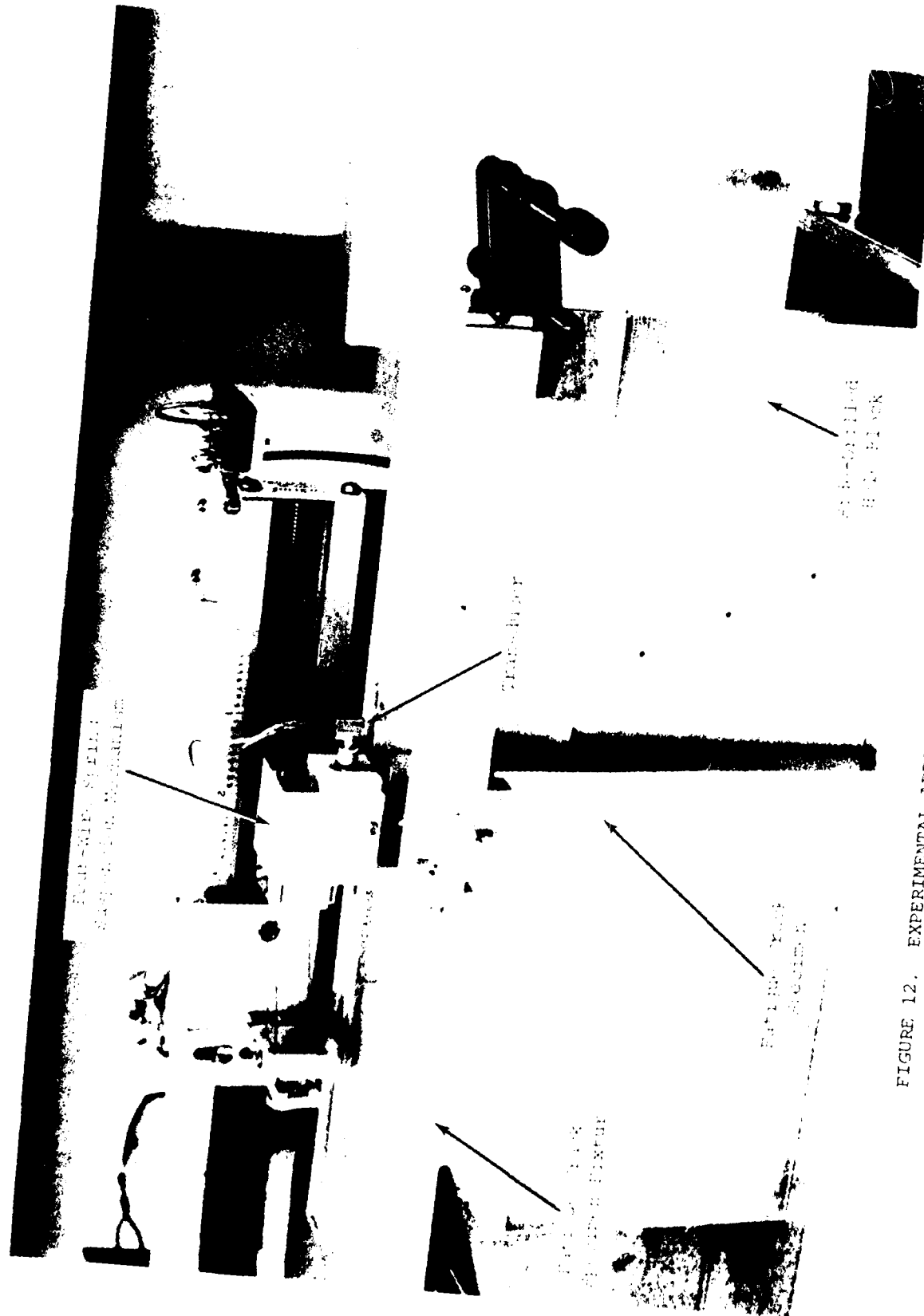


FIGURE 12. EXPERIMENTAL ARRANGEMENT FOR FLAW RESPONSE MEASUREMENT  
(FOR STRAIGHT BEAM TRANSDUCERS)

Figure 13 shows the measurement of flaw signal-to-noise ratios observed on the oscilloscope. In this figure, a) and c) show the initial excitation pulse and the crack echo (approximately 29 sec. from the initial excitation pulse) obtained from fatigue crack specimens #1 and #3, respectively. (The fatigue crack specimens were numbered in order of increasing surface crack length.) In b) and d) of Fig. 13, the background noise level was set to the initial crack signal level in a) and c), respectively, by increasing the receiver gain. In this measurement of signal-to-noise ratio, the internal noise peaks (such as the one shown in Fig. 13 at approximately 7.5 sec from the initial excitation pulse) were not taken into account. However, it is obvious that detection of small flaw signals is very difficult if they occur close to the internal noise signals.

The flaw response ratios (FR1, FR2, and FR3) of the flaw echo from the three fatigue cracks were calculated by using

$$FR_j = 20 \log_{10} (A_{Fj}/A_i), \quad j = 1, 2, 3$$

where  $A_{Fj}$  is the amplitude of the echo from the  $j^{\text{th}}$  crack. The  $A_{Fj}$  was calculated from the recorded video output voltage of the crack echo and the receiver gain of the Reflectoscope®.

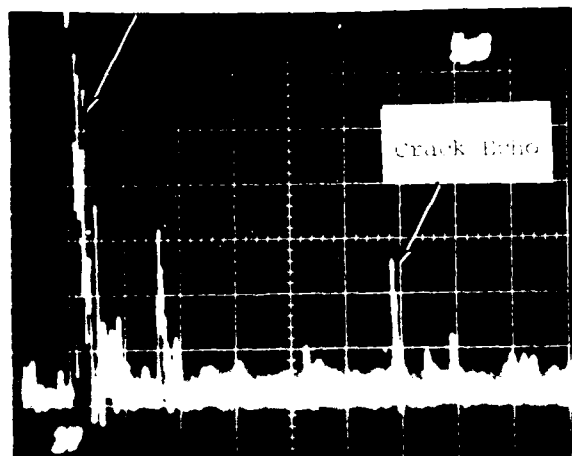
Likewise, the response from a side-drilled hole was calculated from

$$SDH = 20 \log_{10} (A_{SDH}/A_i)$$

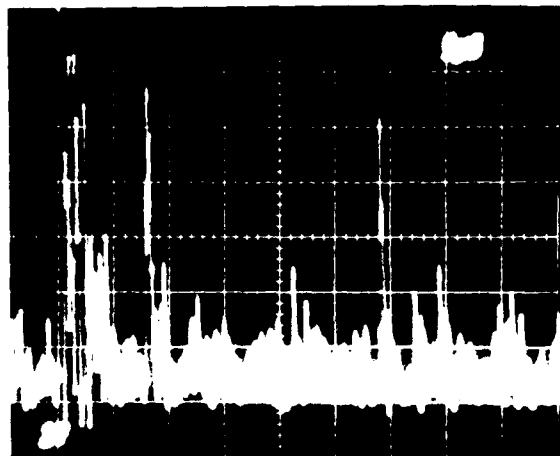
where  $A_{SDH}$  is the amplitude at the last maximum in the distance-amplitude curve described in Section II-B.

The video output voltage from the Reflectoscope® became saturated as the input signal exceeded the linear dynamic range of the receiver (in this case, approximately 1 volt). Since on many occasions, the amplitude of the first returned echo in the semi-circle block exceeded this linear dynamic range, apparently smaller signal-to-noise ratios were obtained. This apparent reduction in the SNR was corrected by adding the amplitude ratio (in dB) between the actual signal amplitude measured with the oscilloscope (using a 10X probe) and the apparent input signal amplitude calculated by using the video output voltage and the receiver gain.

Initial Excitation  
Pulse

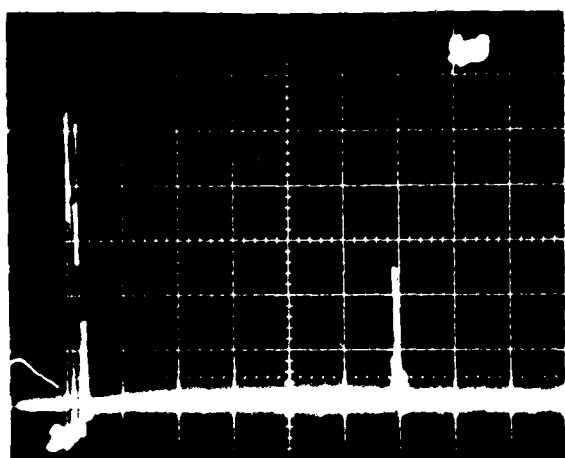


a) Crack Signal from Specimen #1

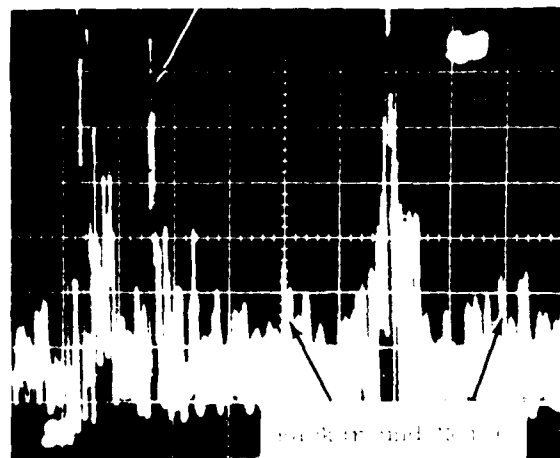


b) Noise Signals from Specimen #1  
(increased gain)

Internal Noise



c) Crack Signal from Specimen #3



d) Noise Signals from Specimen #3  
(increased gain)

FIGURE 13. PHOTOGRAPH OF ELECTROSCOPE VIDEO OUTPUT. PLACE CURSOR AND MOVE CURSOR DIALECTIC DISPLAYED ON CRT DISPLAY SCREEN.

### III. EXPERIMENTAL RESULTS AND DISCUSSION

#### A. Beam Characteristic Parameters

Transducer beam characteristics were obtained by measuring the transducer response as a function of position as it was scanned past side-drilled holes at different depths in the side-drilled hole block. Typical beam profiles are shown in Figs. 14 and 15. Figure 14 was obtained with a 5 MHz-45° transducer and Fig. 15 with a 10 MHz-45° transducer. Each peak in the figures is the response to one side-drilled hole, and the hole depths decrease from left to right in the plot. Amplitudes of the response were calculated by dividing the gated video output of the Reflectoscope® by the receiver gain. This calculation was performed on a computer (Tektronix 4052).

Transducer beam angles were calculated by first determining the scan position corresponding to the peak amplitude of each beam profile and identifying the associated side-drilled hole. Then, using a geometric model of the side-drilled hole block (Fig. 1) and the relative spacing between adjacent beam profile peaks, the angle of the beam was determined for each side-drilled hole response. An average beam angle was calculated from the individual measurements from holes with a path length beyond the far field maximum. Measurements within the near field were not included in the average since the near field beam profile may contain several peaks, and the beam angle determined from the position of the transducer at which the echo amplitude is highest can be erroneous.

Using the average beam angle, the path length to each side-drilled hole was calculated. The peak amplitude from the beam profile from each hole was plotted as a function of path length to obtain a distance-amplitude curve as shown in Figs. 16 and 17. The path length to the side-drilled hole which gave the last maximum amplitude response (arrows in Figs. 16 and 17) in the distance-amplitude curve was taken as the near-to-far field transition distance of the probe. [Nominal near-to-far field transition positions are also indicated in Figs. 16 and 17 which were calculated by using the equation  $(D^2 - \lambda^2)/(4\lambda)$ , where  $D$  is the nominal diameter of the piezoelectric element and  $\lambda$  is the wave length of the sound at the nominal frequency.] By using the beam profile at the near-to-far field transition distance (indicated by the arrows in Figs. 14 and 15), -6 dB Experimental Beam Width (EBW), Beam Symmetry Ratio (BSR) and Beam Inflection Ratio (BIR) were determined.

Another parameter, Beam Divergence Angle (BDA), was determined at the distance where nominal theoretical -6 dB beam width reaches 80% of the diameter of the circular piezo-electric element. Beam divergence angle for the -6 dB beam width is given by  $\theta_D = \sin^{-1}(0.7 \sqrt{D})$  for a monochromatic and continuous sound wave generated by an ideal piston sound generator where  $D$  is the diameter of the circular piezoelectric element and  $\lambda$  is the wave length of the sound in the medium. In this case, the -6 dB beam width reaches 80% of the piston diameter at a distance of approximately 2.3 [ $D^2/(4\lambda)$ ]. Since a sound beam does not diverge<sup>10</sup> until well beyond the near-to-far field transition distance, measurement of BDA should be made in the far field region. The BDA was obtained in this project by interpolating the BDA values determined from the beam profiles (Figs. 14 and 15) near the distance of 2.3 [ $D^2/(4\lambda)$ ]. Note that the angular resolution of a transducer is determined by BDA.

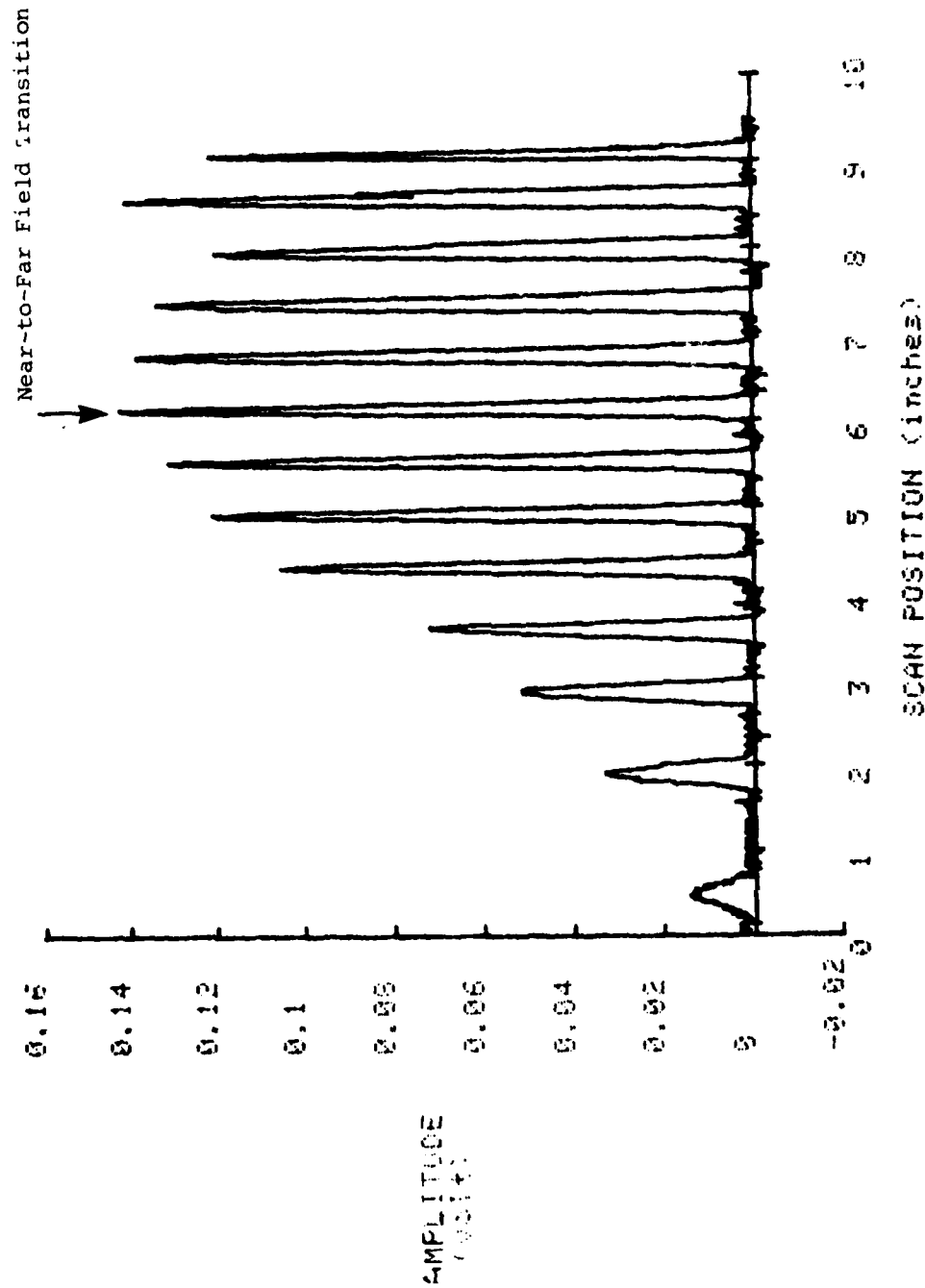


FIGURE 14. TYPICAL BEAM PROFILES (OBTAINED WITH A 3MHz-45° TRANSDUCER)

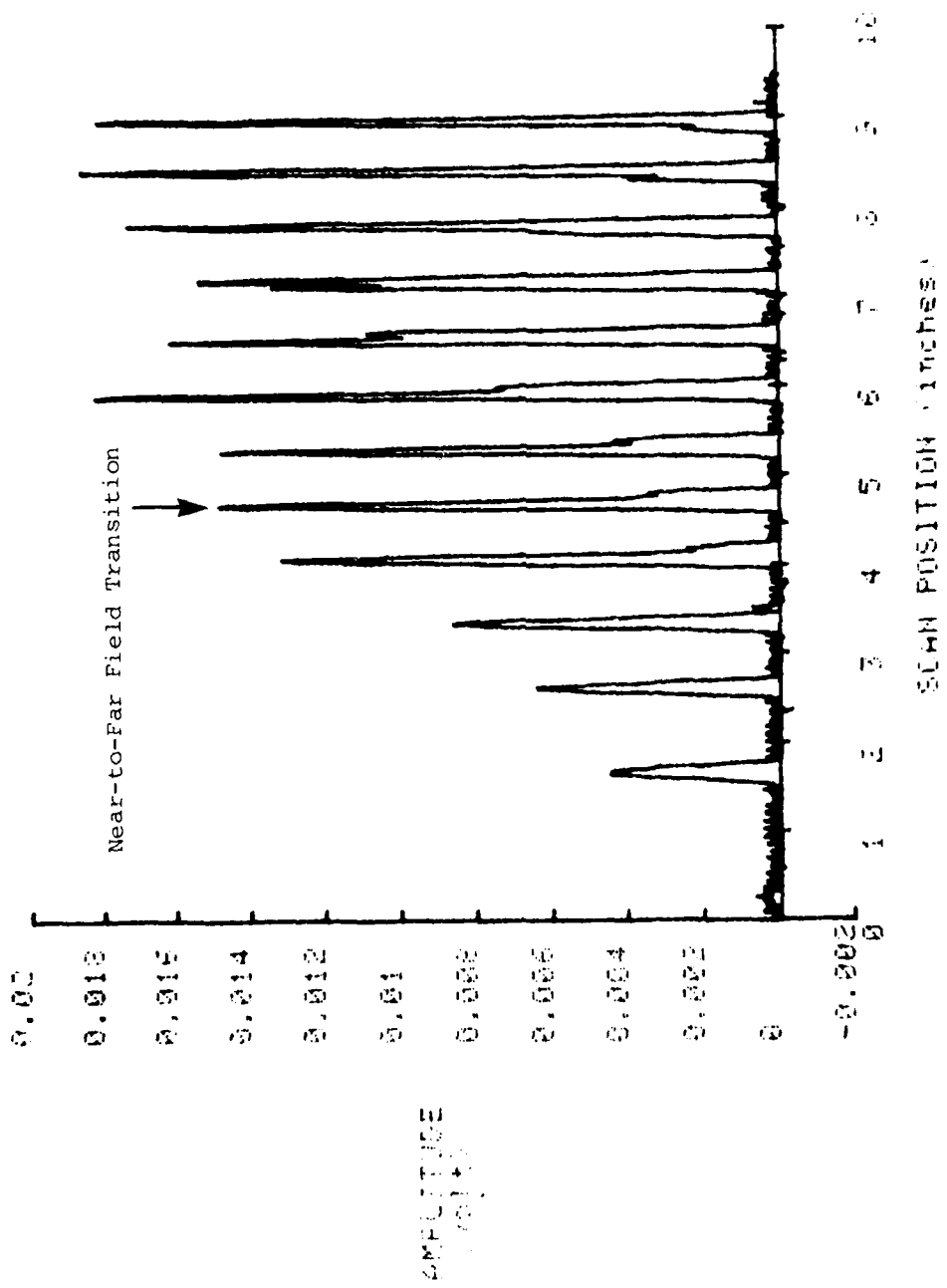


FIGURE 1. TYPICAL PULSE WITH GEMMAG (TRANSDUCER POSITION WITH GEMMAG)

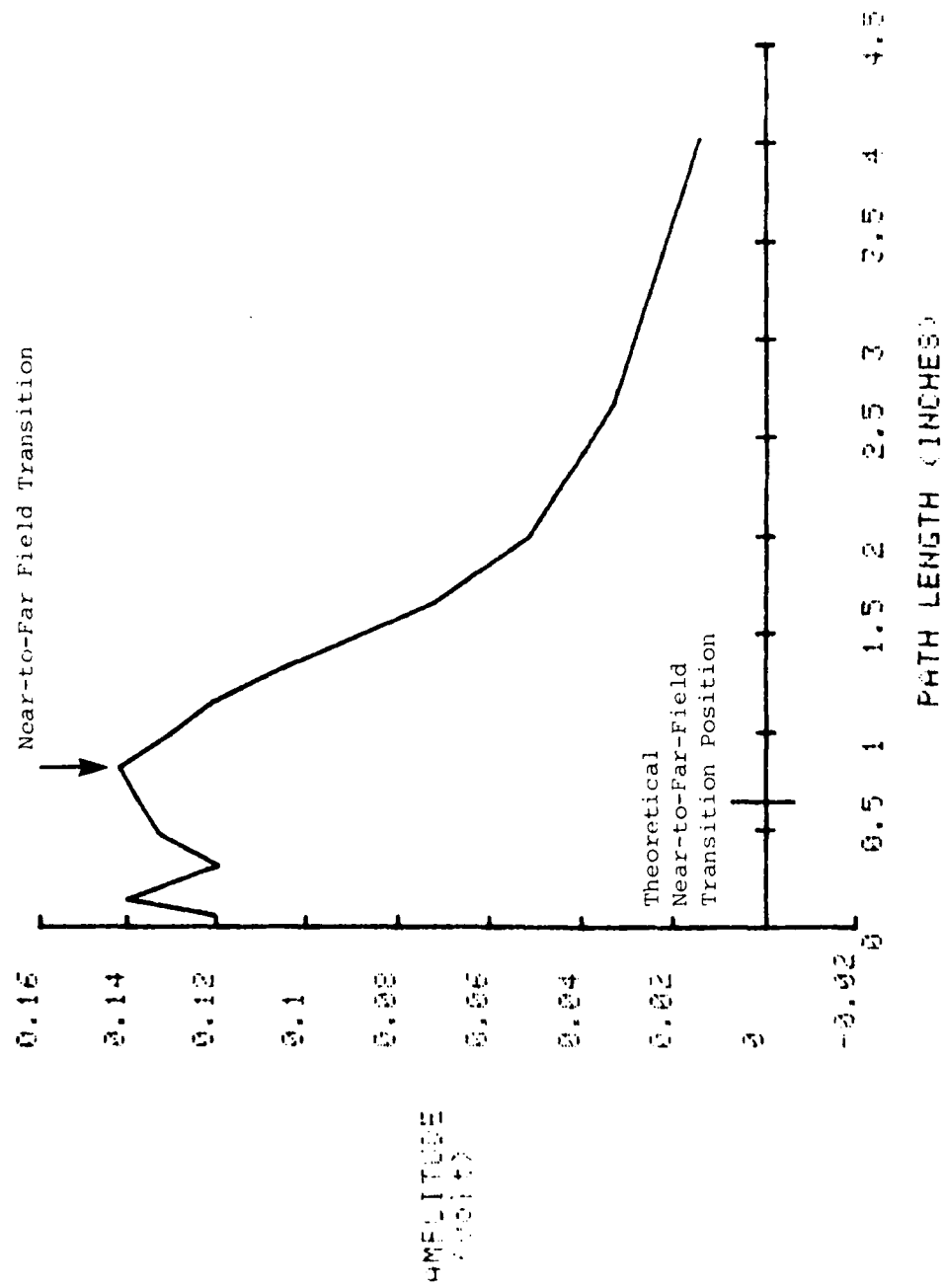


FIGURE 16. DIRECTIVITY-LENGTH CURVE OBTAINED FROM DATA IN FIGURE 14.

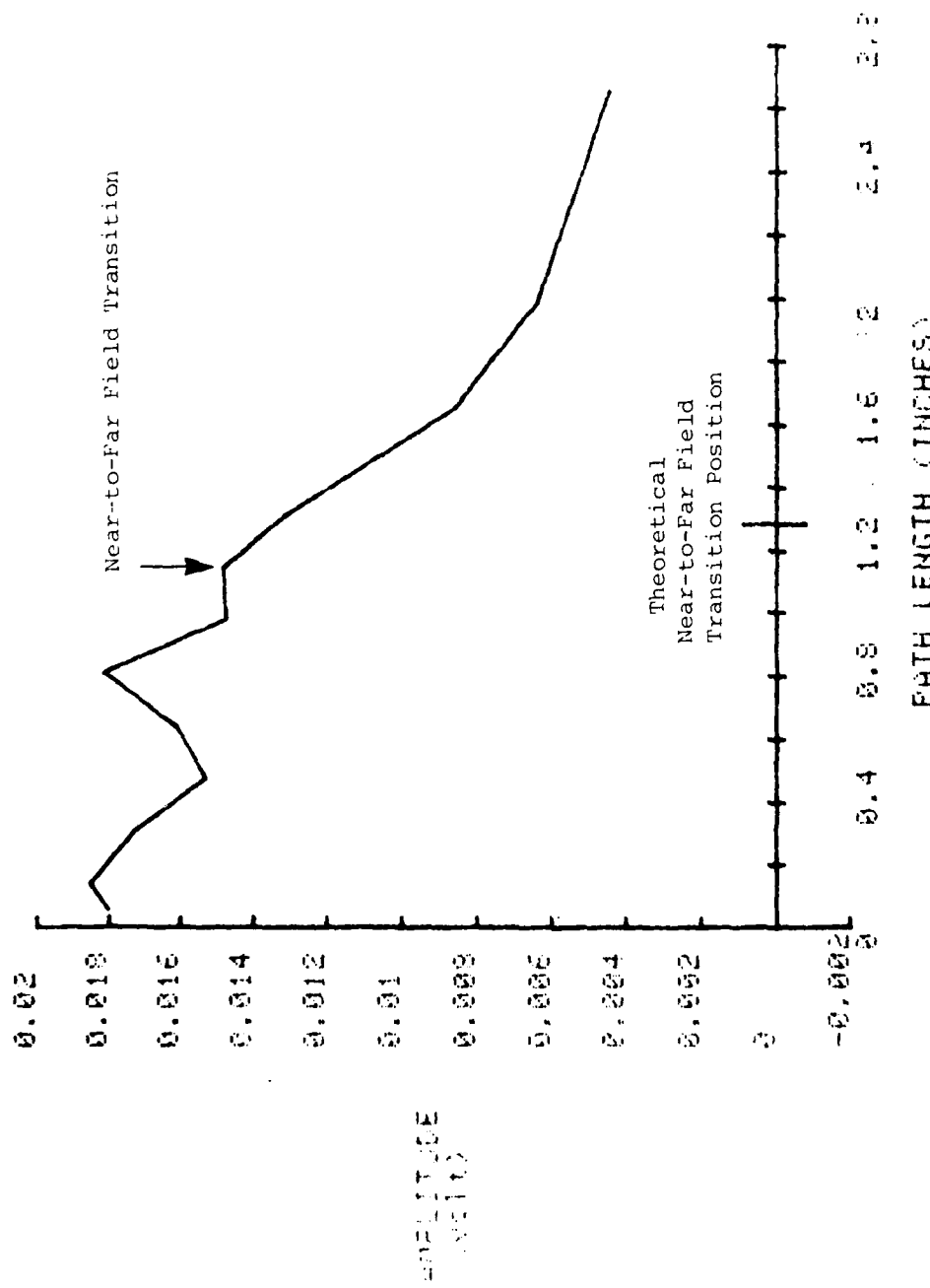


FIGURE 17. DISTANCE AMPLITUDE CURVE, OBTAINED FROM DATA IN FIGURE 15.

The beam profile as well as the distance amplitude curve obtained in the present measurements should be distinguished from those obtained in the Phase I experiments.<sup>2</sup> In Phase I, the transducers were immersed in water and a steel ball reflector was used to measure the profile of the beam as well as the variation of the sound amplitude along the center axis of the transducer. Since cylindrical reflectors (side-drilled holes) were used in the present measurements, the measured amplitude was essentially the average sound strength over a certain cross-sectional area of the beam rather than the sound strength at a point. As is well known, manufacturing a block which contains a well defined spherical reflector for use with contact transducers is quite difficult, but can be accomplished through the use of a diffusion bonding technique<sup>11</sup>. Even though the true beam profile cannot be measured with a cylindrical reflector, the simplicity in preparing a side-drilled hole block makes it a very attractive alternative. Furthermore, as evidenced in Figs. 14 to 17, the side-drilled hole reflectors are able to show the general features of the beam profile as well as the amplitude-distance curve. For these reasons, the use of the amplitude response from the side-drilled hole reflector is the most practical and convenient way of measuring and specifying the beam characteristics of contacting transducers.

The average values for Far Field Ratio (FFR), Beam Divergence Angle (BDA), and Experimental Beam Width (EBW) obtained in the measurements are shown in Table I. Note that FFR and BDA in Table I are respectively the normalized values of the near-to-far field transition distance and the beam divergence angle against the corresponding nominal theoretical values. This normalization was for the purpose of the comparison between the different categories of the transducers.

Many theoretical and experimental studies<sup>12-17</sup> have reported on the sound field of a pulsed piston radiator. It has been shown that the details of the beam profile as well as the distance dependence of the sound field vary with, among other things, the shape of the pulse and the number of rf cycles in the pulse. For pulsed radiation, there is less variation of the sound in the near field of the radiator than for the case of continuous radiation. It has been shown theoretically<sup>12</sup> that as the radiating pulse becomes narrower (equivalently as the spectrum band width of the pulse becomes wider), a) the near-to-far field transition point occurs farther from the radiator, and b) in the far field region, the sound amplitude along the center axis of the radiator decreases more rapidly. The reported beam characteristics<sup>17</sup> of the pulsed sound wave measured with an immersion transducer and a microprobe hydrophone showed that the sound amplitude along the center axis of the transducer did decrease more rapidly than that for the case of the continuous sound wave in the far field region. However, contrary to theory, the near-to-far field transition point was found to occur closer to the transducer. The results of a preliminary experiment conducted by the authors with the side-drilled hole block agree with the above experimental results reported. This discrepancy between the theory and experiment remains to be studied.

It should be noted that for the case of pulsed radiation, no simple relations exist between the center frequency of the pulse and the near-to-far field transition distance or the beam divergence angle.

TABLE I. AVERAGE VALUES OF FAR FIELD RATIO (FFR),  
BEAM DIVERGENCE ANGLE (BDA), AND EXPERIMENTAL BEAM WIDTH (EBW)

	FFR	BDA	EBW (inches)
5 MHz - 0°	1.54 ± 0.32	0.88 ± 0.18	0.142 ± 0.045
	1.14 ± 0.28	0.70 ± 0.07	0.127 ± 0.011
	0.77 ± 0.18	0.92 ± 0.10	0.148 ± 0.027
10 MHz - 0°	1.10 ± 0.27	0.83 ± 0.16	0.117 ± 0.020
	0.99 ± 0.19	0.76 ± 0.15	0.124 ± 0.030

Despite the wide variation in the center frequency and the number of rf cycles in the pulse [which is designated as Damping (DMP) in this report], the average values of FFR measured in the present work are not much different from unity for the case of 5 MHz-45°, 10 MHz-0°, and 10 MHz-45° transducers. The 5 MHz-0° transducers have considerably higher FFR. This may be caused by the influence<sup>18</sup> of the lateral wall of the side-drilled hole block. Because of beam spread, indirect reflections take place from the side wall and from the edge between the side-drilled hole and the lateral boundary [5 MHz-0° transducers have the widest beam spread among the categories of transducers investigated in this study. Recall that the beam divergence angle is given by  $\sin^{-1}(0.7\lambda/D)$  for -6 dB beam width.] The interference between these indirectly reflected waves and directly reflected wave from the side-drilled hole may cause a maximum echo amplitude to occur at a farther distance from the transducer.<sup>18</sup> Note that the 5 MHz-0° transducers have a moderate positive linear correlation coefficient (0.51, Table E-I-1, Appendix E) between FFR and BDA. On the contrary, the other categories of transducers have moderate to low negative linear correlation coefficients between FFR and BDA (Tables E-II-1, E-III-1, E-IV-1 and E-V-1, Appendix E), which may be expected since the near-to-far field transition distance is roughly proportional to the inverse of the beam divergence angle according to the simple theoretical expressions. Another possible cause for the high FFR of the 5 MHz-0° transducers may be the uncertainty of the position of the last maximum point in the distance amplitude curve. This uncertainty is due to the fact that the path lengths to the side-drilled holes are in discrete increments, and if the true maximum occurs between these increments then the actual distance to the maximum cannot be resolved. Since 5 MHz-0° transducers have the smallest value of the nominal theoretical near-to-far field transition distance among the categories of transducers investigated, the systematic error is the largest (approximately 0.41) due to the position uncertainty of approximately 3.18 mm (0.125 in.). in this case. (This could be clarified by increasing the number of side-drilled holes in the block and spacing them at closer increments.)

The relatively smaller value of FFR for 5 MHz-60° transducers could be due to the following reason. The cross section (in a plane normal to the propagation direction) of the 60° angle beam is elliptical (or rectangular depending on whether the piezoelectric element is circular or square, respectively), since the beam is contracted upon refraction along the direction parallel to the plane of refraction. In this case, the near-to-far field transition distance becomes shorter<sup>15</sup> than that of the circular (or square) radiator. (Note that the eccentricity of the 45° angle beam is much smaller than that of the 60° angle beam.)

The average values of BDA measured in the present work are smaller than the nominal theoretical beam divergence angle. This is consistent with what is expected for the pulsed radiation<sup>16</sup>. The larger value of BDA for 5 MHz-60° transducers also could be expected<sup>15</sup> due to the elliptical (or rectangular) cross-sectional beam.

The average value of EBW is roughly half the size of the piezoelectric element which is consistent with theoretical calculations.<sup>16,19</sup>

The distribution of the number of transducers of nominally the same beam angle is shown in Figs. 18 and 19 as a function of beam angle measured on an aluminum IIW-2 block. Note that transducers designed for a 45° beam angle in steel will have a 42.4° beam angle in aluminum. Likewise, those with a 60° angle in steel will have a 55.7° angle in aluminum. Approximately 70% of the 5 MHz-60° transducers investigated had beam angles within 2° of the nominal value. For the other categories of transducers investigated approximately 85% of the transducers had beam angles within 2° of the nominal values.

For the skew angle of the shear wave transducers, approximately 80% of the transducers investigated had a skew angle of 2° or less. It was not unusual for a transducer whose plastic wedge was noticeably unparallel to the case of the transducer, to have a relatively large skew angle.

#### B. Electrical Impedance, Rf-Echo and Frequency Spectrum Parameters

Figure 20 shows two examples of rf-echo and step-less gate signals displayed on an oscilloscope as well as the corresponding frequency spectra displayed on a spectrum analyzer. In the figure, a) and b) were obtained from nominally 5 and 10 MHz transducers, respectively. Damping (DMP) was determined from the displayed rf-echo on the oscilloscope. Note that DMP is roughly proportional to the length of the rf-echo which determines the depth resolution of a transducer.

From the frequency spectra, the respective upper and lower frequencies at which the spectrum amplitude decreases to 50% (-6 dB), 25% (-12 dB), and 10% (-20 dB) of its maximum amplitude were determined. By using the values of the upper and lower frequencies at -6 dB, -12 dB, and -20 dB, Center Frequency (CF), Band Width Ratio (BWR), and Spectrum Symmetry Ratio (SSR) were calculated as defined in Appendix B. In determining the frequencies at -6 dB, -12 dB, and -20 dB, the following rules were used: a) the upper and lower values of the frequencies at -20 dB were taken at the first points away from the maximum where the spectrum amplitude decreases to 10% of the maximum amplitude, b) the upper and lower values of frequencies at -6 dB and -12 dB were taken at the last points away from the maximum, but within the -20 dB frequency range, where the spectrum amplitude decreases to 50% and 25%, respectively, of the maximum amplitude.

The values of the rf-echo and frequency spectrum parameters as well as the electrical impedance of the transducers are listed in Appendix C.

Electrical impedance measured at the nominal frequency of the transducers ranged from several ohms to a few thousand ohms. Approximately 66% of the transducers investigated had electrical impedance of less than 100 ohms, 2% larger than 500 ohms, and the rest between 100 and 500 ohms. Impedance phase angles ranged from minus 90° to plus 90°. (The sign of the phase angle has a close relation with the general shape of the initial excitation pulse - see Section III-C). Approximately 31% of the transducers investigated had negative impedance angles, and approximately 31% of the transducers had impedance phase angles within  $\pm 45^\circ$ .

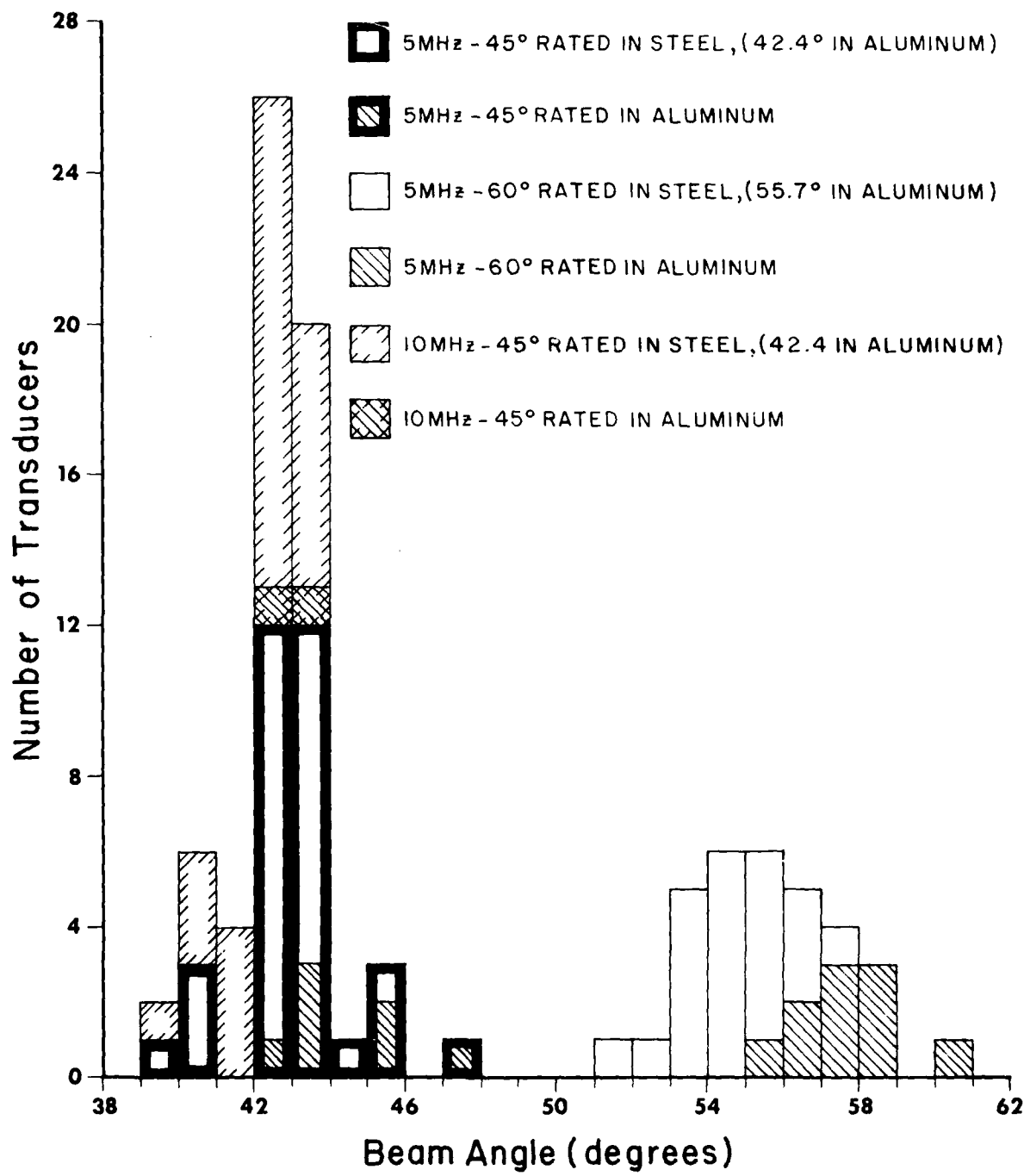


FIGURE 18. NUMBER OF TRANSDUCERS VS. BEAM ANGLE MEASURED IN ALUMINUM  
(FOR ANGLE BEAM STEERER E)

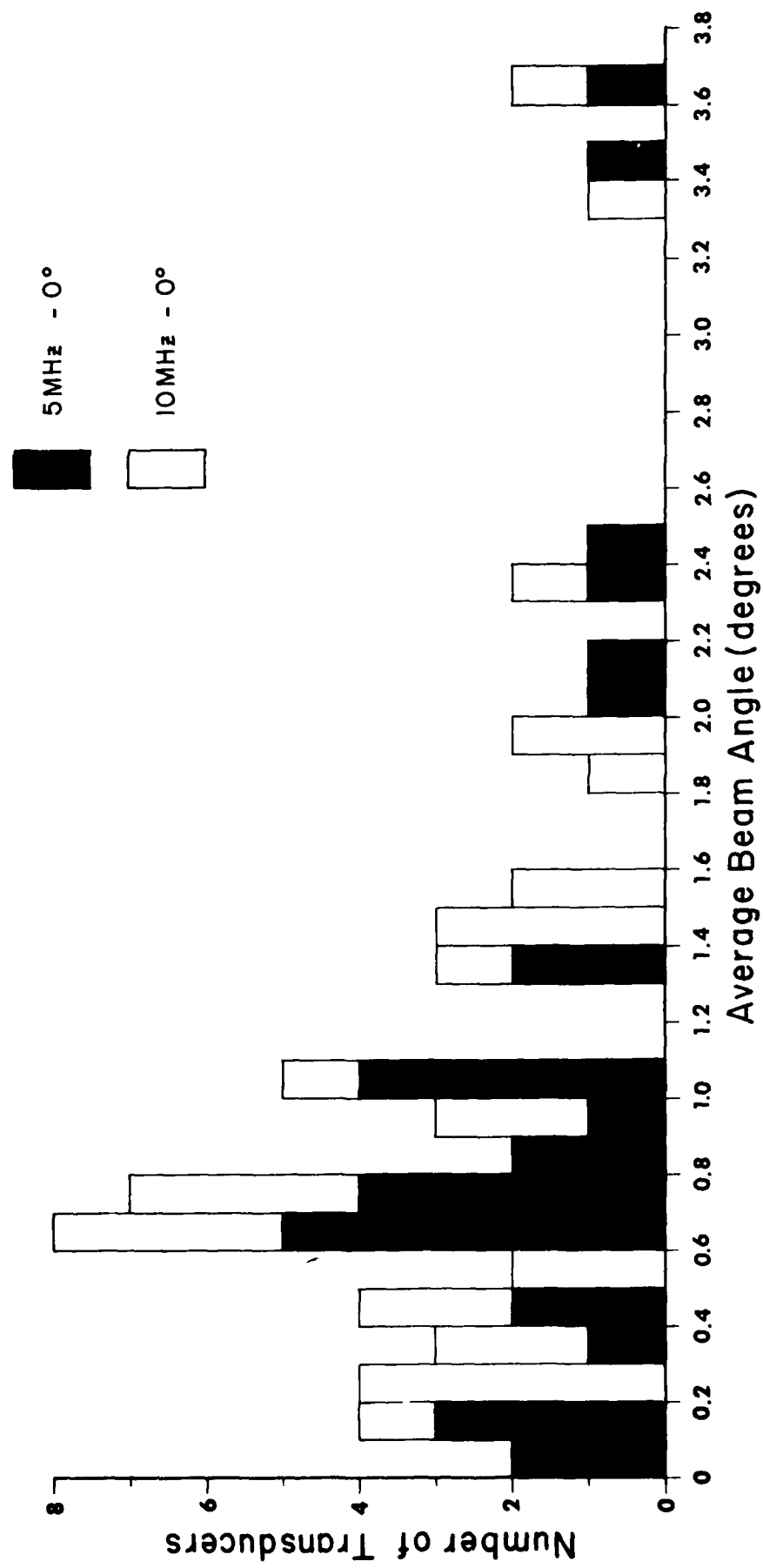


FIGURE 12. NUMBER OF TRANSDUCERS VS. BEAM ANGLE  
(FOR STRAIGHT BEAM TRANSDUCERS)

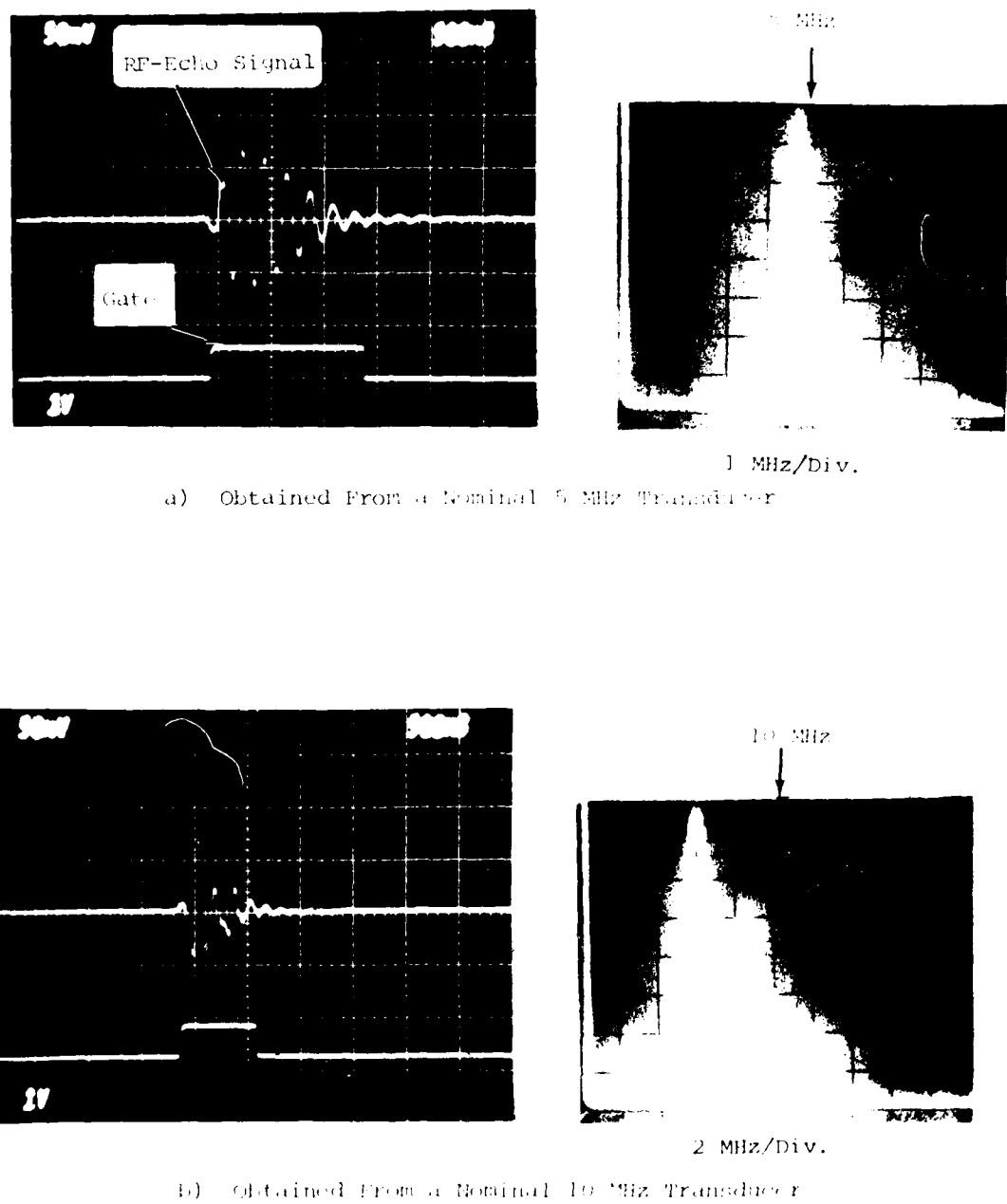


FIGURE 10. EXAMPLES OF RF-ECHO AND FREQUENCY RECORDING (REFLECTION FREQUENCY SPECTRUM).

Figures 21 and 22 show the distributions of the numbers of 5 and 10 MHz transducers, respectively, as a function of center frequency. In the figure, the frequency axis is subdivided for every 0.25 MHz interval for 5 MHz transducers and every 0.5 MHz interval for 10 MHz transducers. The height of each column represents the number of transducers which have a center frequency within the corresponding interval for a given category of transducers. As illustrated, a wide variation exists in the distribution of the center frequency for nominally equivalent transducers. The distribution is centered around a frequency lower than the nominal value (especially for 10 MHz transducers). Only 33% of the nominally 10 MHz transducers (of both 0° and 45° beam angles) had a center frequency within 10% of the nominal frequency. About 70% of the nominal 5 MHz transducers (of 0°, 45° and 60° beam angles) had a center frequency within 10% of the nominal value (for 5 MHz-0° transducers, only 40% of those investigated were within 10% of the nominal value). Therefore, the higher the nominal frequency, the higher the probability for deviation from the nominal value. These trends in distribution agree with the results of other works.<sup>20,21</sup>

Similar variations were also seen in the data of other parameters such as DMP, BWR, etc.

#### C. Loop Sensitivity, Flaw Response and Signal-to-Noise Ratio Parameters

The values of loop sensitivity, flaw response ratio and flaw signal-to-noise ratios of each transducer evaluated in this project are listed in Appendix C. As in the case of other characteristic parameters, there exists a wide variation in the loop sensitivity, flaw responses, and signal-to-noise ratios of nominally equivalent transducers.

Before going further into a discussion of the results, it is useful to examine the variations in the applied initial excitation pulse for different transducers. Figure 23 shows two different types of initial excitation pulses commonly encountered in the measurements throughout which the control settings of the pulser as well as the connecting cables remained unchanged. With few exceptions, type (a) is common to transducers having a negative impedance phase angle and type (b) is common to transducers having a positive impedance phase angle measured at the nominal center frequency. The degree of damping as well as the detailed shape of the initial excitation pulse differs from one transducer to another. Such variations are caused by the differences in the electrical characteristics (such as impedance) of each transducer as well as by the variations in the probe construction<sup>22</sup> (type of backing or bonding material, thickness of the bonding layer or electrode, etc.). Since the ultrasonic waves generated by a transducer are determined by the excitation pulse, non-uniformity in the initial excitation pulse will undoubtedly have an adverse effect on achieving uniform performance of transducers (particularly on the beam characteristics).

In Figs. 24 and 25, the distributions of LSR are shown for 5 and 10 MHz transducers, respectively. LSR is distributed over more than a 40 dB range for both 5 and 10 MHz transducers. Straight beam longitudinal transducers have relatively higher LSR than angle beam shear transducers. This may be due to the fact that angle beam shear waves generated by the mode conversion of the longitudinal waves have considerably smaller amplitude than the original longitudinal wave amplitude.<sup>23</sup>

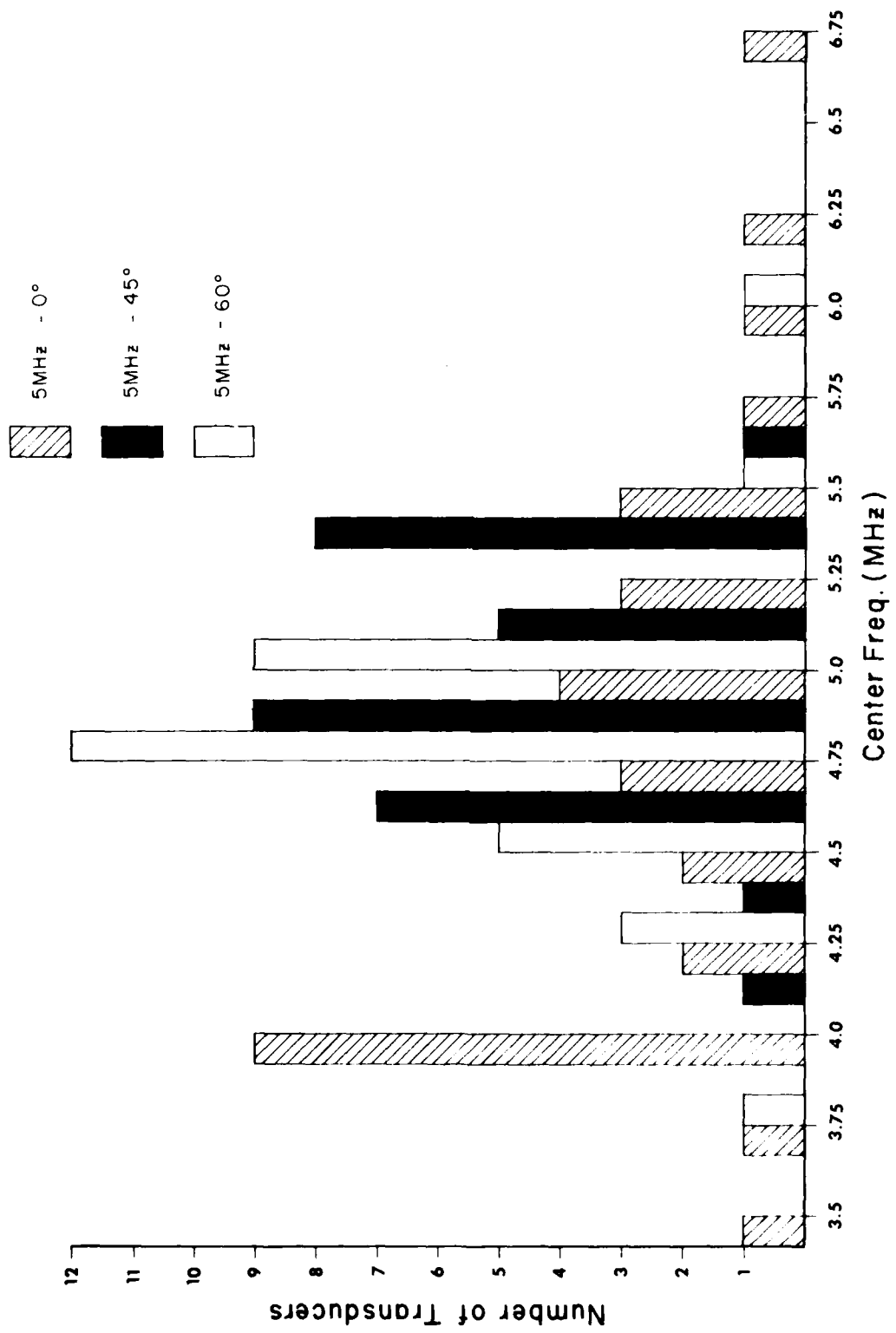


FIGURE 21. NUMBER OF TRANSDUCERS VS. CENTER FREQUENCY (FOR 5 MHz TRANSDUCERS)

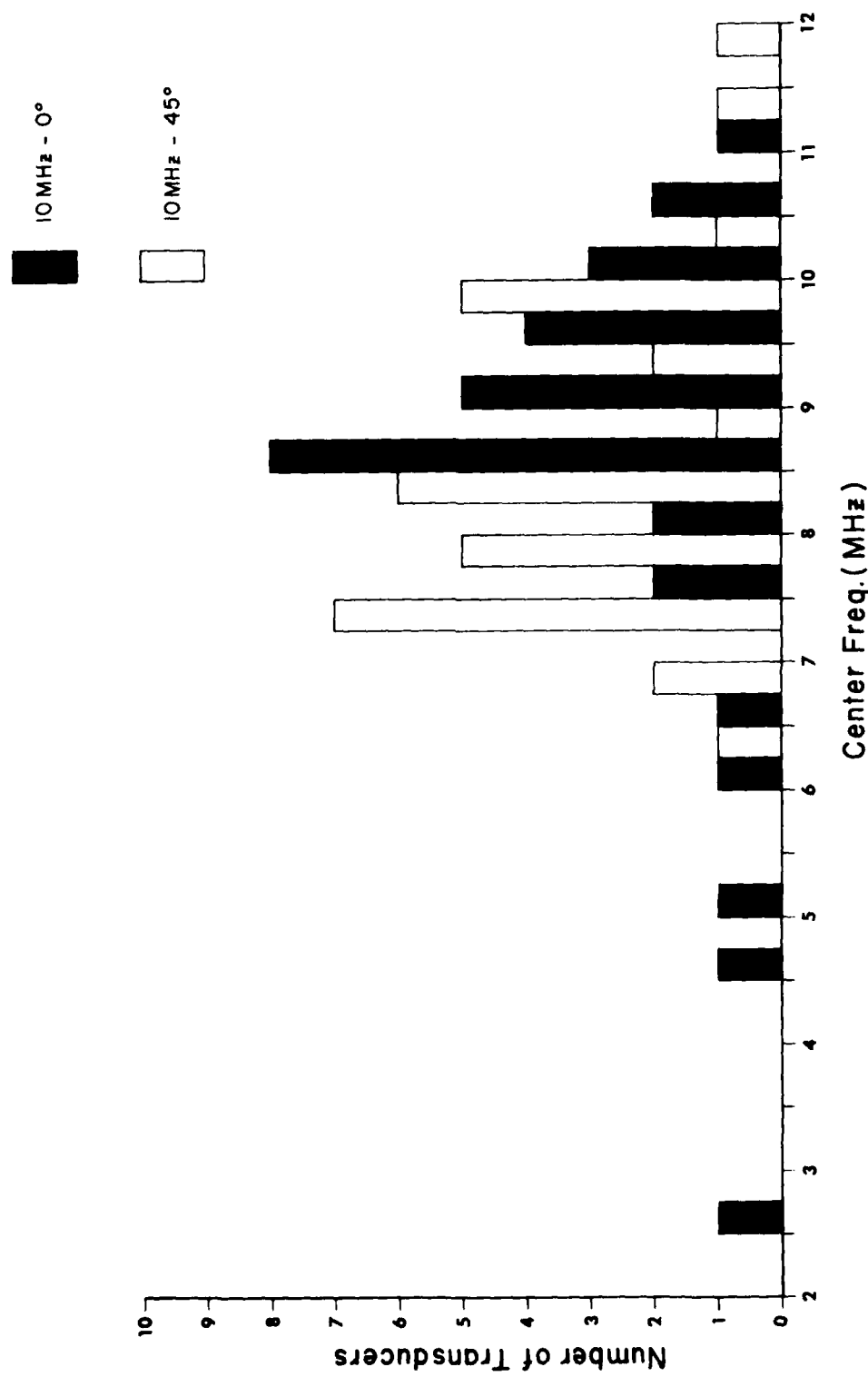
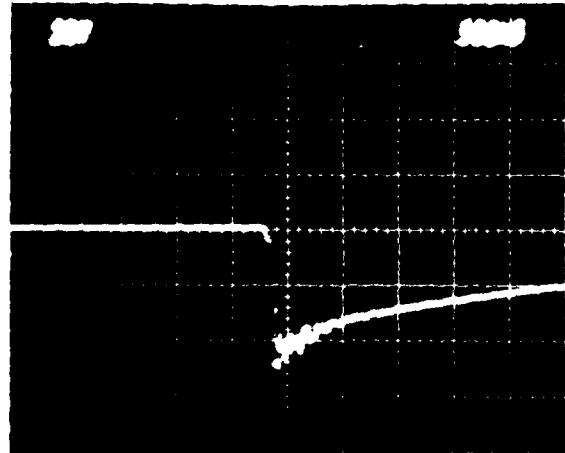


FIGURE 22. NUMBER OF TRANSDUCERS VS. CENTER FREQUENCY (FOR 10 MHZ TRANSDUCERS)

a)

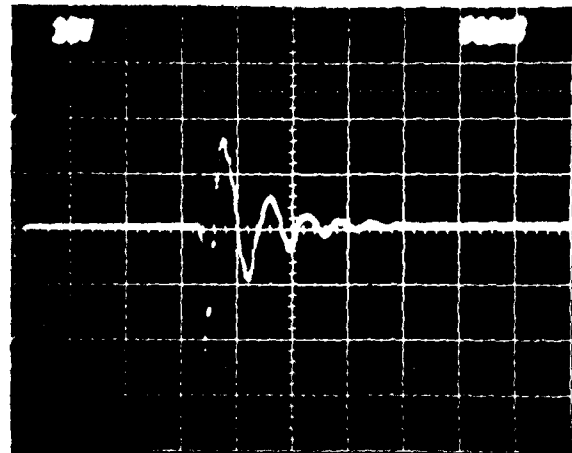
Zero Latitude



10 sec

b)

Zero Latitude



10 sec

Fig. 1. Seismograms of the same event recorded at the same distance but with different filter settings. (a) shows the trace with a low-cut filter of 0.01 Hz and a high-cut filter of 0.5 Hz. (b) shows the trace with a low-cut filter of 0.01 Hz and a high-cut filter of 0.05 Hz.

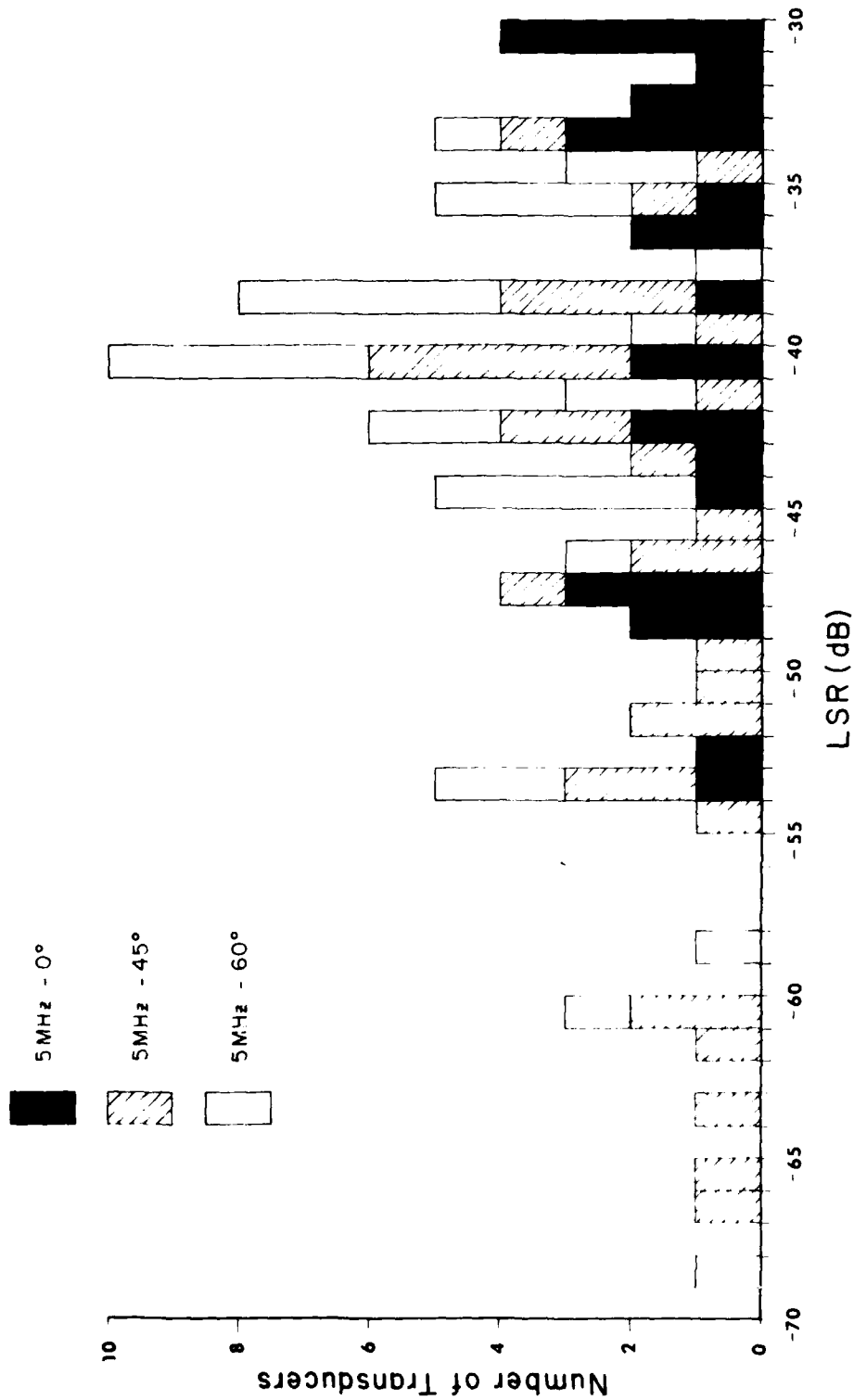


FIGURE 24. NUMBER OF TRANSDUCERS VS. LOOP SENSITIVITY (FOR 5 MHz Transducer)

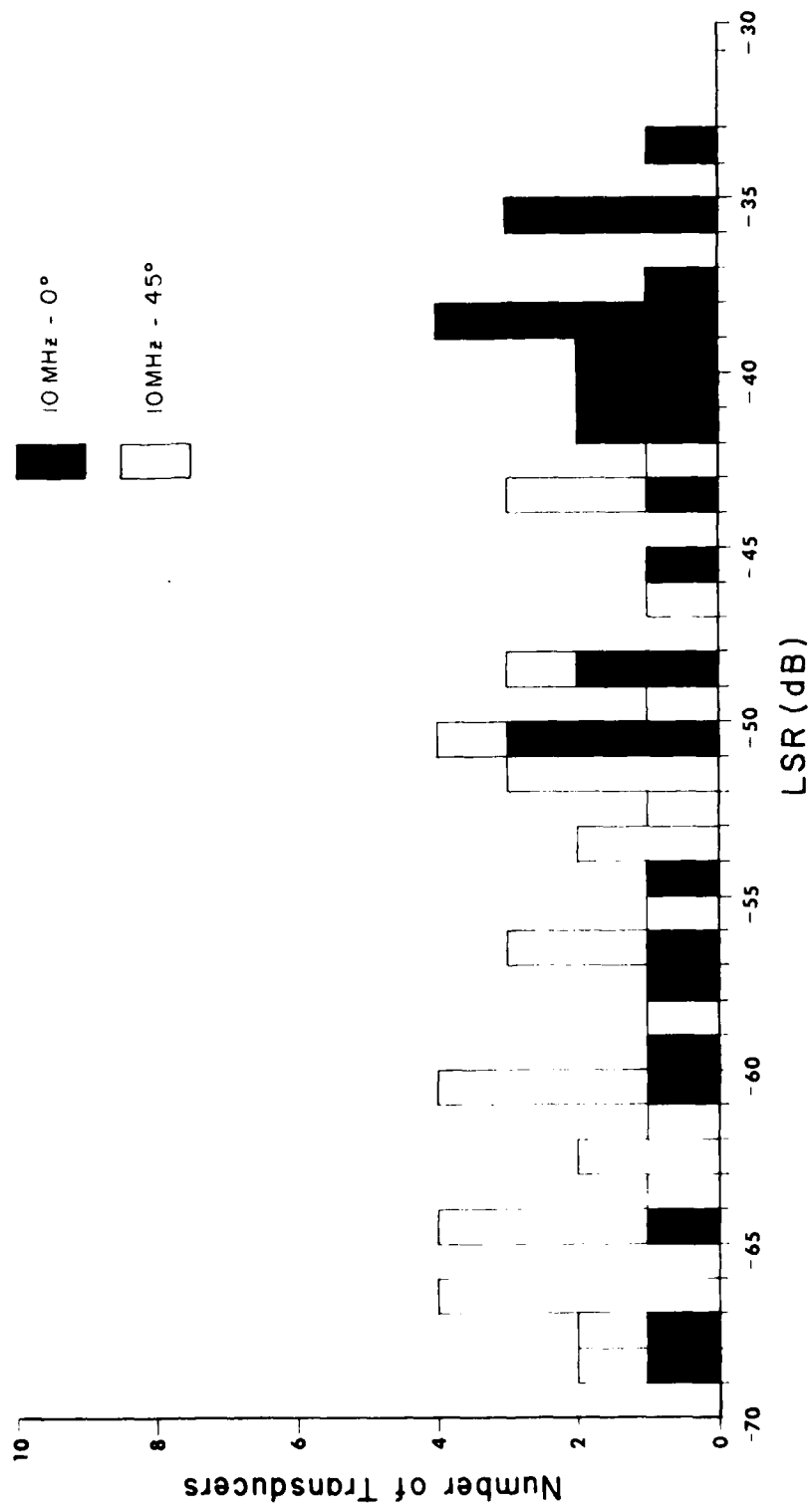


FIGURE 25. NUMBER OF TRANSDUCERS VS. LOOP SENSITIVITY RATIO (For 10 MHz Transducers)

The distributions of the signal-to-noise ratio of the first returned echo in the semi-circle block (SNR) are shown in Figs. 26 and 27 for 5 and 10 MHz transducers, respectively. The distributions cover less than a 30 dB range and have considerably less spread than LSR. The average values of SNR for each category of transducers are shown in Table II. On the average, straight beam longitudinal transducers have approximately 4 dB higher SNR than angle beam shear transducers. Also, on the average, 10 MHz transducers have approximately 5 dB higher SNR than their 5 MHz counterparts. Note that 10 MHz transducers have a relatively lower LSR than 5 MHz transducers (Figs. 24 and 25). This may suggest the lack of any close relationship between the LSR and SNR.

Background noise arises from grain boundary scattering in the material through which the sound is propagated, as well as from reflections in the wedge of the transducer and in the coupling or bonding material. Also, the effects of the different wave modes generated and the side lobes of the sound beam contribute to background noise. It is generally believed that the higher the frequency, the greater the background noise, thus the smaller the signal-to-noise ratio. No such simple trend with frequency exists, however. Depending on the average grain size of the material, the size of a transducer employed, the size of a reflector (or discontinuity) in the material, and the distance between the transducer and the reflector, there exists an optimum frequency which gives the maximum signal-to-noise ratio.<sup>24</sup> For the present measurements, the higher SNR of the 10 MHz transducers may be because they are closer to the optimum frequency than were the 5 MHz transducers.

As seen in Table II, most of the 5 MHz and 10 MHz-45° transducers were able to detect the smallest fatigue crack (#1) without difficulty. Most of the 5 MHz-60° and 10 MHz-0° transducers were not able to detect fatigue crack #1. The echo from fatigue crack #1 was usually indistinguishable from the background noise in these cases. Most of 5 MHz-0° transducers were only able to detect the largest fatigue crack (#3) used in the measurements. The results show that the fatigue cracks used in this project were indeed able to push the transducer to its threshold of detectability as was originally planned. Note that flaw detection in most cases was limited by the background noise rather than by the electrical noise of the flaw detector (which ultimately limits the sensitivity of the flaw detector).

Generally, 10 MHz transducers were superior to 5 MHz transducers in detecting the flaws used in this project. For angle beam 10 MHz shear transducers, this superiority may be attributed partly to a higher SNR within the transducer-to-flaw distance of the present measurements and partly to the higher reflectivity<sup>23</sup> at the fatigue crack boundary (or gap). In addition to these two factors, the superiority of 10 MHz longitudinal wave transducers may also be attributed partly to a higher value of fatigue crack depth-to-wave length ratio than for the 5 MHz counterparts.

For transducers of the same nominal center frequency, straight beam longitudinal transducers were found to be considerably inferior to angle beam shear transducers in detecting surface cracks, despite the fact that the former had higher SNR than the latter. The difference in the wave length between the longitudinal and shear waves might contribute to the difference in the flaw detectability. However, the major reason for longitudinal transducers

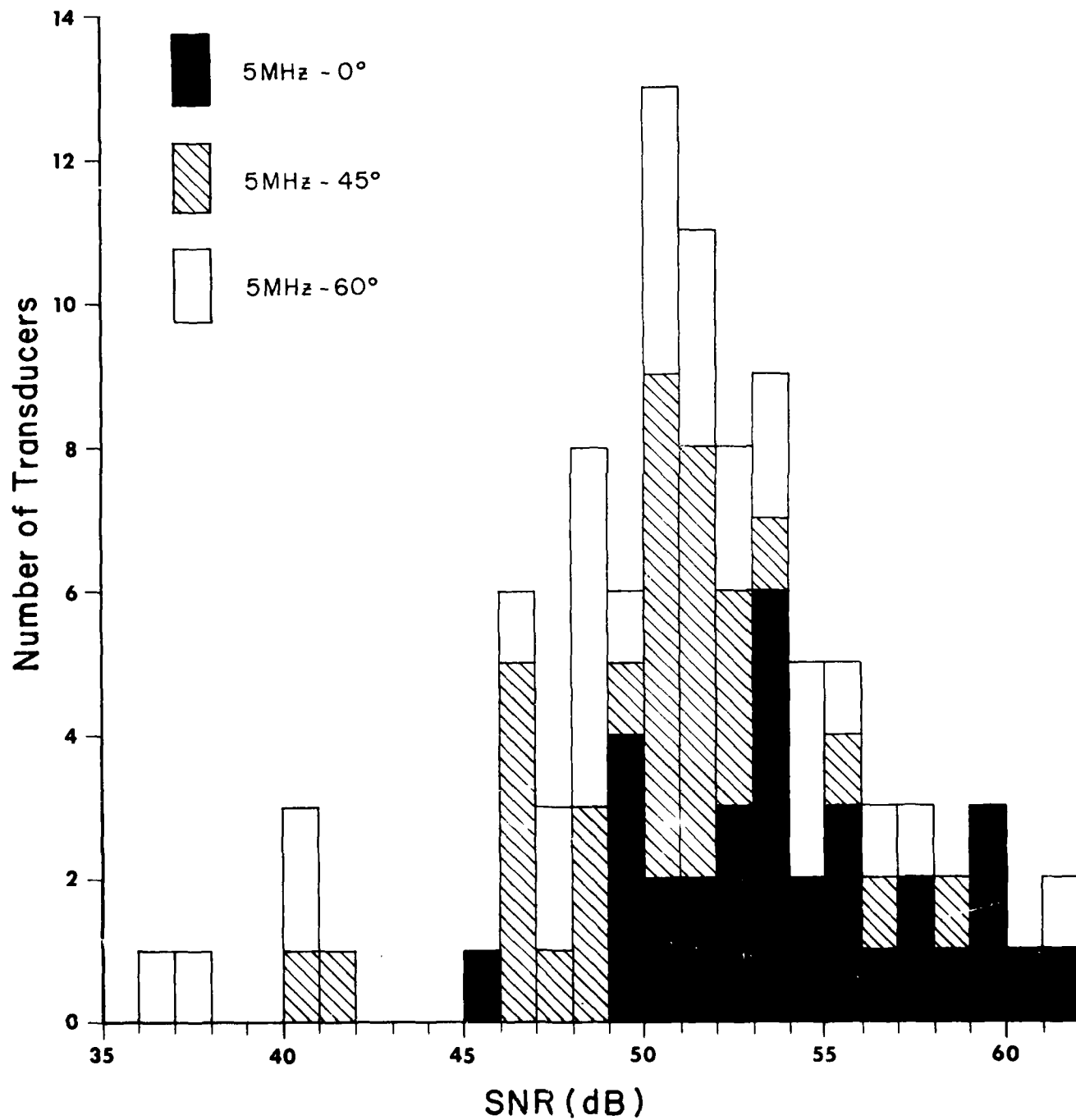


FIGURE 26. NUMBER OF TRANSDUCERS VERSUS SIGNAL-TO-NOISE RATIO (FOR 5 MHz Transducer.)

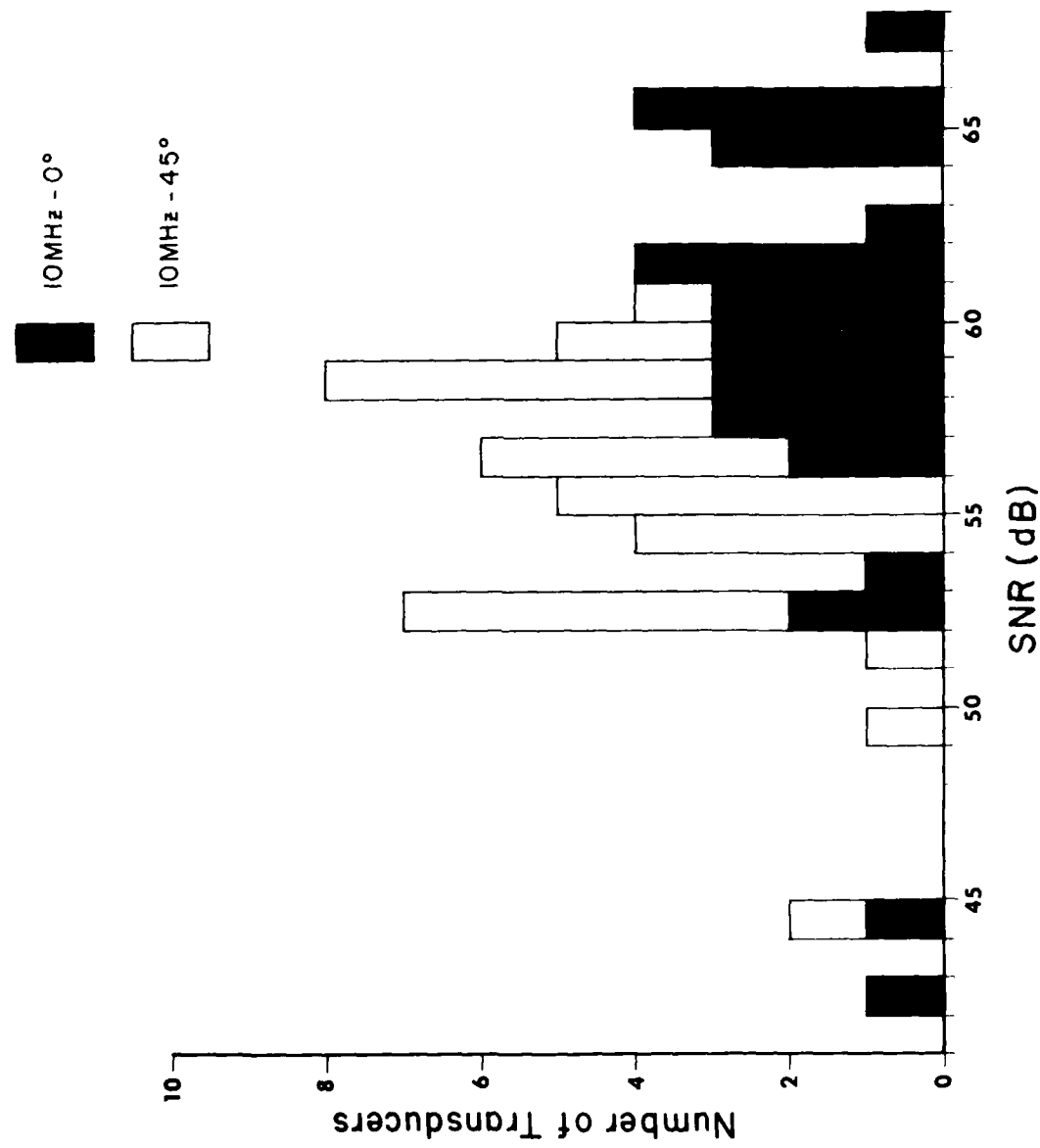


FIGURE 27. NUMBER OF TRANSDUCERS VS. SIGNAL-TO-NOISE RATIO (For 10 MHz Transducers)

TABLE II. AVERAGE VALUES OF SIGNAL TO NOISE RATIO PARAMETERS

	SNR	FN1	FN2	FN3
5 MHz - 0°	53.6±3.73	-	-	20.1±4.02
	49.5±3.66	10.6±3.43	23.8±4.12	40.3±4.30
	49.8±5.56	-	14.4±6.08	33.1±5.54
10 MHz - 0°	58.8±5.56	-	15.1±6.31	39.9±6.17
	54.9±3.76	18.0±4.44	30.2±4.44	46.7±4.02

All values are in dB.

SNR: Signal-to-noise ratio of the first returned echo in semi-circle block.

FN1: Flaw signal-to-noise ratio in specimen #1 which contained fatigue crack of approximately 1.27 mm (0.050 in.) long and 0.31 mm (0.012 in.) deep.

FN2: Flaw signal-to-noise ratio in specimen #2 which contained fatigue crack of approximately 2.54 mm (0.100 in.) long and 0.64 mm (0.025 in.) deep.

FN3: Flaw signal-to-noise ratio in specimen #3 which contained fatigue crack of approximately 3.81 mm (0.150 in.) long and 1.91 mm (0.075 in.) deep.

being inferior is basically due to the way the measurements were made. The placement of longitudinal transducers as shown in Fig. 10 cannot avoid the interference<sup>25</sup> from the reflected wave off the lateral wall which significantly reduces the flaw signal.

It was found also that 5 MHz-60° shear transducers have about 10 dB smaller flaw signal-to-noise ratio than 5 MHz-45° shear transducers. This is caused by the mode conversion of the 60° shear wave beam upon the reflection at the right-angled corner (formed by the fatigue crack and specimen surface) which results in an amplitude decrease of the reflected echo.<sup>23</sup> Since the fatigue cracks used in the measurements were grown at right-angles to the surface of the specimen, 5 MHz-60° shear transducers were less effective in detecting these flaws than 45° transducers. (No mode conversion takes place for shear waves of 45° incident angle.) This explains why 5 MHz-60° shear transducers were not able to detect fatigue crack #1.

If other types of flaws had been used in the measurement of flaw detectability, e.g. side-drilled holes or flat bottomed holes (which have been frequently used as reference flaws in NDI), the above differences in flaw detectability among the different categories of transducers would not have been observed. This is evidenced by the fact that the average values of the amplitude ratio between the first reflected echo in the semi-circle block and the echo from the side-drilled hole near the far-field transition (which is equal to LSR-SDH in dB) are approximately the same for all the categories of transducers investigated in this project (see Table III). Note that taking the amplitude ratio between the two echoes is essentially the same as normalizing the sensitivity of the transducers involved. On the other hand, the amplitude ratios between the first returned echo in the semi-circle block and the flaw echo (designated as  $LF_j$ , where  $j = 1, 2, 3$  in Table III) show the characteristic differences between each category of transducers, as in the case of flaw signal-to-noise ratios (Table II). [If the noise level were the same in both the semi-circle block and the fatigue crack specimen,  $LF_j$  would be equal to  $SNR - FN_j$  (in dB), where  $j = 1, 2, 3$ .]

The right-angled corner of the fatigue crack and the surface of the specimen reflects back an incident beam parallel to itself, thus effectively acting like a plane reflector oriented perpendicular to the direction of the sound propagation. When the surface area of the plane reflector is smaller than the cross section of a sound beam, the amplitude of the reflected echo is linearly proportional<sup>26</sup> to the area of the reflector if the distance between the reflector and the transducer is greater than the near-to-far field transition distance of the transducer. The amplitude ratios of the echoes from fatigue cracks #1, #2, and #3, therefore, are expected to be 12 dB between fatigue cracks #1 and #2 and 13 dB between fatigue cracks #2 and #3. These values are readily calculated from the known sizes of these cracks. The average experimental values of the amplitude ratios between the flaw echoes, obtained from the flaw response ratio data of all the angle beam shear transducers (Appendix C), were  $14.4 \pm 3.8$  dB between fatigue cracks #1 and #2 and  $14.0 \pm 4.4$  dB between fatigue cracks #2 and #3. As anticipated, experimental values and calculated values show good agreement.

TABLE III. AVERAGE AMPLITUDE RATIOS BETWEEN THE REFLECTED ECHOES

	LF1	LF2	LF3	LS
5 MHz - 0°	-	-	26.5±4.78	27.9±8.49
	- 45°	38.4±2.67	23.3±4.48	9.91±3.44
	- 60°	-	33.5±4.86	15.07±2.94
10 MHz - 0°	-	37.5±7.81	14.09±7.70	27.7±7.64
	- 45°	32.6±5.85	19.7±6.29	8.16±4.49
31.8±6.54				

All values are in dB.

LF<sub>j</sub>: Amplitude ratio between the first returned echo in the semi-circle block and the echo off the fatigue crack #j, where j = 1, 2, and 3. (This is equal to LSR-FR<sub>j</sub> in dB.)

LS: Amplitude ratio between the first returned echo in the semi-circle block and the echo from a side drilled hole. (This is equal to LSR-SDH in dB.)

Roughness of the surface of the reflector affects the resultant amplitude as well as the signal-to-noise ratio of the echo signal. It has been reported<sup>26</sup> that if the surface irregularities of the reflector are less than one-third of the sound wave length, then the surface can be considered smooth and mirror-like reflection of the wave can be assumed. The surfaces of the fatigue cracks used in this project were regarded as smooth based upon the surface of the fractured fatigue crack (Figure D-1 in Appendix D).

It has been shown that the measured amplitude ratios between the echoes from different size discontinuities agree well with theory when averaged over all the transducers investigated. Also, the characteristic differences between each category of transducers in flaw responses or in flaw signal-to-noise ratios have been shown to be consistent with the theoretically expected behavior. However, the performance of each individual transducer in a given category varies significantly from the average. It was not unusual to find a transducer whose performance is far from that normally expected.

## IV. CORRELATION ANALYSIS

A. Linear Correlation-Background

In this section, a brief discussion of the theoretical background for linear correlation of two parameters is presented.

Consider  $n$  number of samples for the two parameters  $X$  and  $Y$  which are  $(x_1, y_1), (x_2, y_2), \dots, (x_n, y_n)$ . The linear correlation coefficient  $R$  between the two parameters is defined by

$$R = \frac{\sum x_i y_i}{(\sum x_i^2 \sum y_i^2)}^{1/2}$$

where  $\sum$  is the summation over  $i = 1$  to  $n$ , and  $x_i$  and  $y_i$  represent the deviations of the  $i$ th sample  $(x_i, y_i)$  from the sample mean of the two parameters  $(\bar{X}, \bar{Y})$ , i.e.

$$x_i = x_i - \bar{X}, \text{ where } \bar{X} = \frac{\sum x_i}{n}, \text{ and}$$

$$y_i = y_i - \bar{Y}, \text{ where } \bar{Y} = \frac{\sum y_i}{n}. \quad (2)$$

The linear correlation coefficient  $R$  varies between -1 and +1 depending on the closeness of the relationship between the samples. Positive values of  $R$  indicate a tendency to have linear relationship with positive slope. Conversely, negative values of  $R$  indicate a tendency to have a linear relationship with a negative slope. When  $|R| = 1$ , the two parameters are said to be perfectly related. In this case, any change in one parameter is always accompanied by a proportional change in the other. When  $R = 0$ , two parameters are said to be unrelated. In this case, two parameters vary randomly.

Figures 28-30 shows examples of scatter diagrams of two parameters with a range of linear correlation coefficients. In these figures, the actual data obtained in this project (Appendix C) are used. It can be seen that the higher  $|R|$ , the smaller the degree of scatter from the lines drawn in the figure. The two lines in each diagram represent a least square fit of the linear relationship between the two parameters. One of the lines (indicated by A) is obtained by assuming the parameter on the  $Y$  axis is dependent on the parameter on the  $X$  axis, and the other line (indicated by B) by assuming the parameter on the  $X$  axis is dependent on the parameter on the  $Y$  axis.

Equation (1) can be rewritten as:

$$\begin{aligned} R &= \frac{(\sum x_i y_i)^2 / (\sum x_i^2 \sum y_i^2)}{1/2} \\ &= \frac{[(\sum x_i y_i / \sum x_i^2) (\sum x_i y_i / \sum y_i^2)]^{1/2}}{1/2} \end{aligned}$$

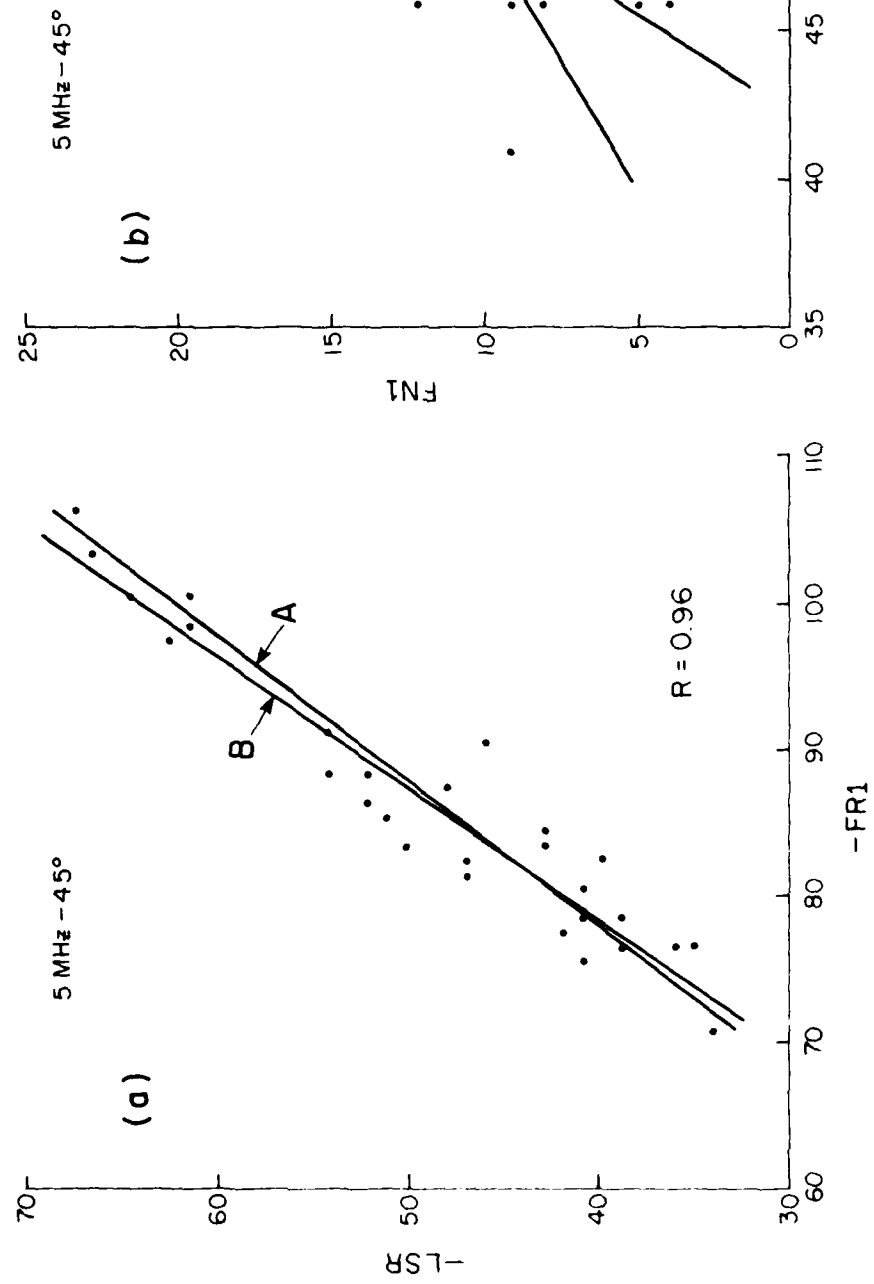


FIGURE 1. SCATTER DIAGRAMS FOR DATA HAVING HIGH AND MODERATE CORRELATION COEFFICIENTS

Legend: 1.  $\downarrow$  indicates linear correlation coefficient. A represents the least square fit line obtained by assuming parameter on Y axis to be independent of parameter on X axis. B represents the same by assuming parameter on X axis to be independent of parameter on Y axis.)

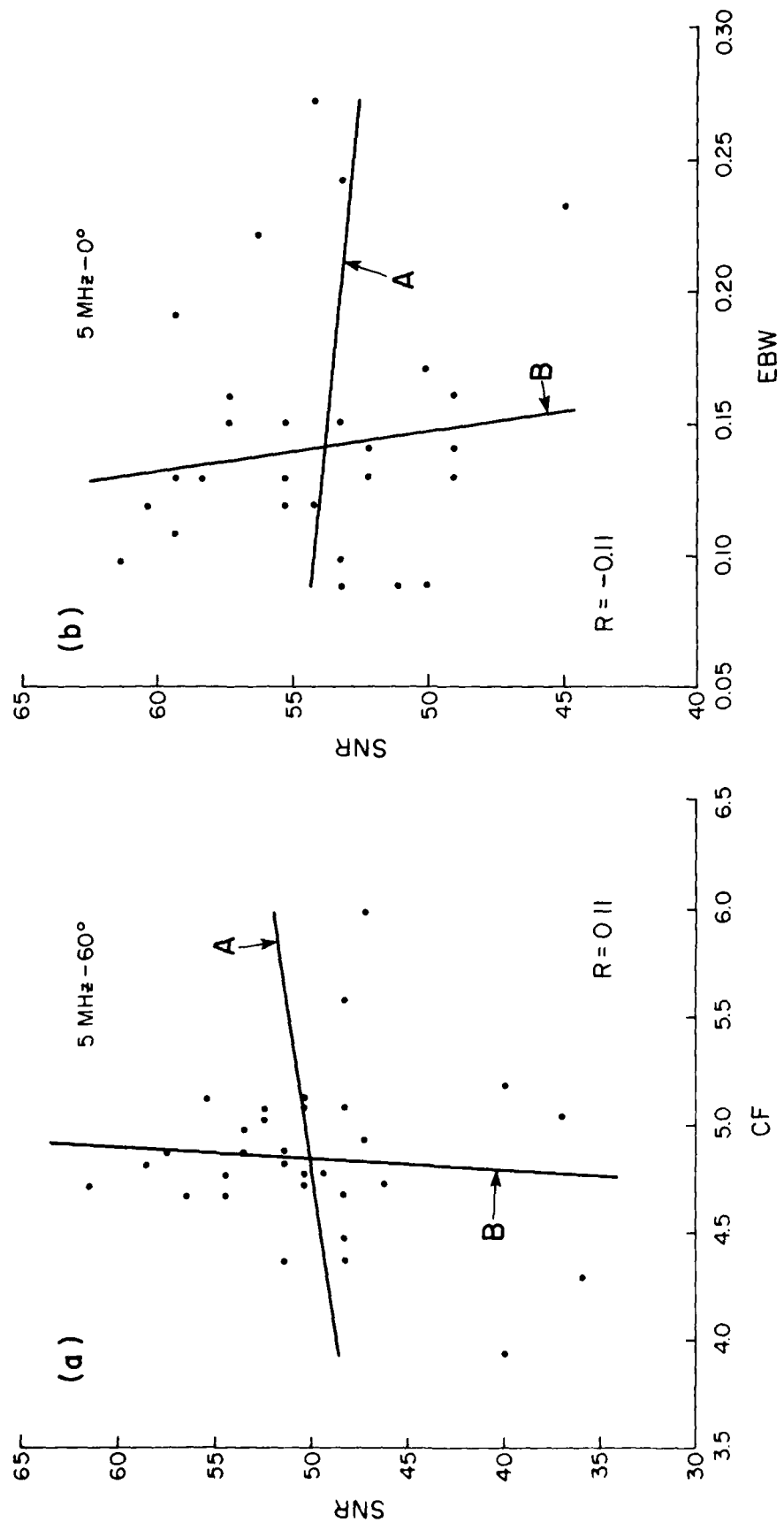


FIGURE 2. EXAMPLES OF SCATTER DIAGRAMS FOR DATA HAVING  
LOW POSITIVE AND NEGATIVE CORRELATION COEFFICIENTS  
( $R$  is linear correlation coefficient. A represents  
the least square fit line obtained by assuming  
parameter on Y axis is dependent on parameter on X  
axis. B by assuming parameter on X axis is dependent  
on parameter on Y axis)

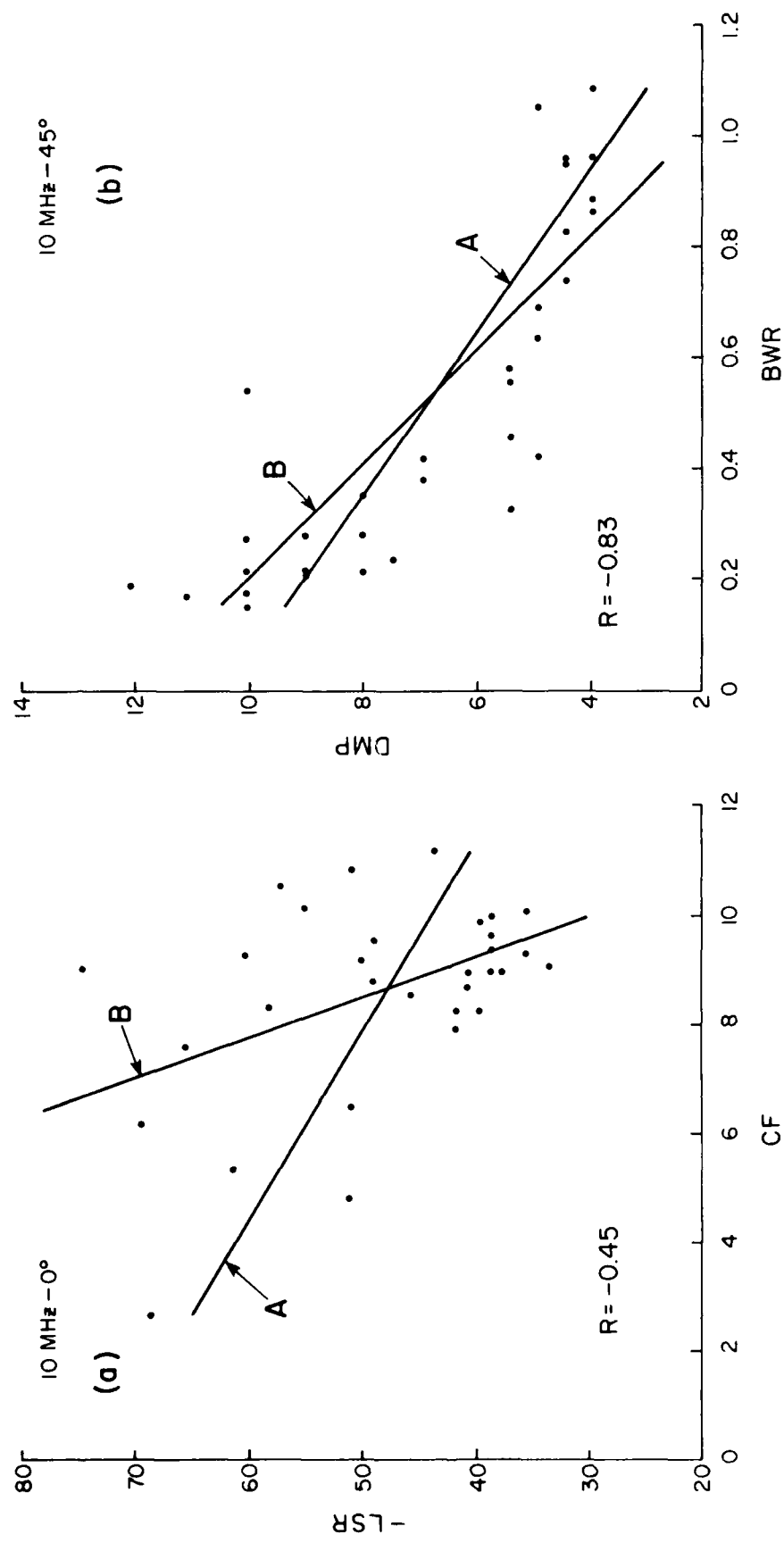


FIGURE 35. EXAMPLES OF SCATTER DIAGRAMS FOR DATA HAVING BOTH HIGH AND HIGH NEGATIVE CORRELATION COEFFICIENTS ( $R$  is linear correlation coefficient. A represents the least square fit line obtained by assuming parameter on Y axis is dependent on parameter on X axis. B by assuming parameter on Y axis is dependent on parameter on X axis)

$$= (b_{xy} b_{yx})^{1/2} \quad (3)$$

where  $b_{xy} = \frac{\sum x_i y_i}{\sum x_i^2}$  and

$$b_{yx} = \frac{\sum x_i y_i}{\sum y_i^2}.$$

Note that  $b_{xy}$  is the slope of the least square fitted line obtained by assuming parameter X is a function of parameter Y. Similarly,  $b_{yx}$  is the slope of the least square fitted line obtained by assuming parameter Y is a function of parameter X. In statistics, this slope is usually called the linear regression coefficient. Therefore, equation (3) states that the correlation coefficient, R, is the geometric mean of the slope of the two least square fitted lines.

It is a well known fact that the linear correlation coefficient is significantly affected by sampling. Table IV shows the confidence limits on a true correlation coefficient (which is not presently known, of course) for the correlation coefficient R determined from thirty-two samples. The 95% confidence limit means that there is 95% probability that the true correlation coefficient lies within the limits given when samples drawn from a normally distributed (Gaussian) population have a measured correlation coefficient of value R. In the table, the correlation is considered high if  $|R|$  is larger than 0.7, moderate if  $|R|$  is larger than 0.4 and smaller than 0.7, and low if  $|R|$  is smaller than 0.4. The above criteria of high or low correlations will be adopted in the following section.

Table V shows the probability of two parameters being randomly correlated (i.e. zero true correlation coefficient) when the correlation coefficient determined from thirty-two samples has a value of R. This table indicates that if R is larger than 0.6, the likelihood that the true correlation coefficient is zero is less than 0.03% for a sample size of 32.

Detailed theory on the correlation analysis, as well as the derivation of confidence limits and probabilities, may be found in the references.<sup>27-30</sup>

#### B. Results and Discussion

The linear correlation analysis between pairs of transducer parameters was carried out using equation (1) and the data shown in Appendix C. The linear correlation coefficients between every pair of parameters were calculated using a computer (Tektronix 4052). This correlation analysis was performed for each category of transducers and the results are shown in Appendix E. To reduce any confusion in reporting the large number of parameters investigated, the correlations of transducer characteristic parameters are divided into three parts in Appendix E. First, correlations among the beam, electrical impedance, rf-echo and frequency spectrum parameters; second, correlations between the above mentioned parameters and the loop sensitivity, flaw responses and signal-to-noise ratios; and third, correlations among the loop sensitivity, flaw responses and signal-to-noise ratios. Accordingly, each table in Appendix E is divided into three parts, e.g. Table E-I-1, E-I-2, and E-I-3, etc.

TABLE IV. CONFIDENCE LIMITS OF LINEAR CORRELATION COEFFICIENT R FOR THIRTY-TWO SAMPLES

Experimental Correlation Coefficient R	99% Confidence Limit		95% Confidence Limit	
	Lower Bound	Upper Bound	Lower Bound	Upper Bound
0.1	-0.36	0.52	-0.26	0.43
0.2	-0.27	0.59	-0.16	0.51
0.3	-0.17	0.66	-0.05	0.59
0.4	-0.05	0.72	0.06	0.66
0.5	0.07	0.77	0.18	0.72
0.6	0.21	0.82	0.32	0.78
0.7	0.37	0.87	0.46	0.84
0.8	0.55	0.92	0.63	0.90
0.9	0.76	0.96	0.80	0.95

TABLE V. PROBABILITY OF RANDOM CORRELATION FOR THIRTY-TWO  
SAMPLES WITH AN EXPERIMENTAL CORRELATION COEFFICIENT  
OF VALUE R

Absolute Value of Experimental Correlation Coefficient R	Probability of Random Correlation (%)
0	100.0
0.05	79.0
0.10	58.6
0.15	41.3
0.20	27.2
0.25	16.8
0.30	9.5
0.35	5.0
0.40	2.3
0.45	1.0
0.50	0.36
0.55	0.11
0.60	0.03
0.65	0.006
<u>&gt;0.70</u>	<u>≤0.0008</u>

1. Correlation Among Beam, Electrical Impedance, Rf-Echo, and Frequency Spectrum Characteristic Parameters.

The inter-relationship between pairs of parameters should be universal for all categories of transducers. This is because there is no theoretical basis for expecting that one category of transducers should behave differently from another. Therefore, the linear correlation coefficients of the five categories of transducers were averaged and the results are shown in Table E-VI in Appendix E.

As expected, there is a very high correlation between Peak Frequency (PF) and Center Frequency (CF). Also, there is a high correlation between Band Width Ratio (BWR) and Damping (DMP). Since the spectral band width ratio is inversely proportional to the number of rf cycles in the wave train,<sup>31</sup> a high negative linear correlation coefficient might be expected in this case. (In fact, the data fit better to the inverse function rather than to the linear function of negative slope, see Fig. 30-b.) Moderate correlations were found between CF (or PF) and BWR, and between CF (or PF) and DMP. These correlations reflect the trend that the higher the center (or peak) frequency, the larger the number of rf cycles in the pulse and thus the narrower the spectral band width. A moderate correlation was also found between Beam Divergence Angle (BDA) and Experimental Beam Width (EBW). Since beam width is directly related to the beam divergence angle, this correlation also is expected.

Except for the foregoing cases, the linear correlations are found to be low among the beam, electrical impedance, rf-echo and frequency spectrum parameters. Since beam angle, skew angle, or frequency of a transducer are independent of each other, no correlations between pairs of these parameters are anticipated. This was confirmed by the experimental results. (If any moderate correlation coefficients had been found between these parameters, one would have wondered about the appropriateness of the sampling as well as the measurements of the present work. Refer to Table V for the probability of random correlation).

Because of the well known theoretical relations between frequency and the near-to-far field transition distance, and between frequency and beam divergence\angle, one may expect to see high correlations between CF and Far Field Ratio (FFR) and between CF and BDA. However, these well known relations are based on the idealized piston sound source which generates a continuous monochromatic sound wave. As previously discussed (Section II-B), there exists no simple relation between these parameters for a pulse generated sound wave. Furthermore, variations in the initial excitation pulse, in the effective area of the transducer, in the spectrum band width, etc. also influence the beam characteristics. Therefore, it is not surprising that this simple linear correlation analysis failed to show high correlations between CF and FFR or between CF and BDA.

The results of the present correlation analysis for the group of parameters discussed in this section do not agree with those of Phase I. This may be due to the small sample size used in Phase I. The low average correlations between Spectrum Inflection Ratio (SIR) and Spectrum Symmetry

Ratio (SSR), or between Beam Inflection Ratio (BIR) and Beam Symmetry Ratio (BSR) indicate that the inflection ratios and the spectrum symmetry ratios have little in common. One might think that inflection points imply asymmetry, but asymmetry can occur with or without inflection points. It is therefore felt that SIR and SSR, or BIR and BSR leave much to be desired in describing the spectrum distribution or beam profile. The area under the envelope of the spectrum distribution or beam profile may serve better in describing these characteristics.

## 2. Correlation Among Sensitivity, Flaw Responses and Signal-to-Noise Ratios

A very high correlation exists among the sensitivity parameters (i.e. LSR, SDH, FR1, FR2, and FR3) as seen in Tables E-I-3, E-II-3, etc. in Appendix E. This is consistent with the results obtained in Phase I. Also, a high correlation exists among the signal-to-noise ratio parameters (i.e. SNR, FN1, FN2, and FN3). The linear correlation coefficients averaged over all the categories of transducers investigated are, respectively,

0.870 ( $\pm 0.007$ ) among the sensitivity parameters, and

0.696 ( $\pm 0.133$ ) among the signal-to-noise ratio parameters,

where the numbers in parentheses are standard deviations.

A moderate correlation was found between the sensitivity and the signal-to-noise ratio parameters. The average linear correlation coefficient between the two groups of parameters is 0.407 ( $\pm 0.316$ ), where the number in parenthesis is the standard deviation.

As discussed in Section II-D, a fixed relationship exists between the amplitudes of the echoes from given reflectors of known size, orientation and location. (In Section II-D, only the relation between the echoes from the fatigue cracks was mentioned. Similar relations exist among the echoes from the side-drilled holes, back surface, etc. These relationships are usually described in terms of a DGS diagram.<sup>3,18,26</sup>) Hence, a high correlation is expected to exist among the sensitivity parameters. The same is true for the case of signal-to-noise ratio parameters provided the background noise level remains fixed in all the specimens. Since the background level varied somewhat in the specimens used in this project, the correlation coefficient among the signal-to-noise ratio parameters was smaller than that among the sensitivity parameters.

It is interesting to note that even with the thirty-two samples of highly correlated parameters there exists a finite probability of experimentally obtaining a low correlation coefficient. One good example is the low correlation coefficient between SNR and FN2 for 5 MHz-45° transducers (0.36, Table E-II-3 in Appendix E), while there is a high average linear correlation coefficient (0.696) among all the signal-to-noise ratio parameters.

The very high linear correlation among sensitivity parameters indicates that the response from a known flaw could be predicted by measuring

the response from a back surface or a corner of the material being inspected. Equivalently, the minimum detectable size of a flaw could be estimated from the signal-to-noise ratio of the echo reflected from a back surface or a corner of the material under inspection.

The moderate correlation between pairs of the sensitivity parameters and the signal-to-noise ratios reflect the following experimental facts: a) a high sensitivity does not enhance the signal-to-noise ratio if the background noise level is higher than the electrical noise level of the system, but b) a low sensitivity does decrease the apparent signal-to-noise ratio because the electrical noise would then limit the flaw detection (in this case the background noise level is lower than the electrical noise of the system). As long as the sensitivity of the system is adequate, such that the flaw detection is not limited by the electrical noise, the sensitivity does not play a major role in detecting flaws.

Recall that flaw responses (as well as signal-to-noise ratio parameters) were calculated from the gain setting and the video output voltage of the signal of the Reflectoscope® receiver. Therefore, the flaw responses were affected by the characteristic frequency response of the receiver employed. The high correlation between loop sensitivity [which was measured at the receiver input (Fig. 9)] and flaw responses indicates that the characteristic frequency response of the Reflectoscope® receiver did not significantly influence the flaw response measurements.

### 3. Correlation Between Beam, Electrical Impedance, Rf-Echo and Frequency Spectrum Parameters and Loop Sensitivity, Flaw Responses and Signal-to-Noise Ratios.

The correlation between these two groups of parameters are shown in Tables E-I-2, E-II-2, etc. in Appendix E. Except for a moderate correlation between IPA and sensitivity parameters, no definitive trends in the correlations can be seen among the different categories of transducers. For example, 5 MHz-0° transducers show moderately high, negative correlations between CF and sensitivity parameters; 10 MHz-0° transducers show moderately high, positive correlations; while all the shear transducers show low correlations. Between EBA and sensitivity parameters, 5 and 10 MHz-45° transducers show moderately high correlations while the rest of the transducer categories show low correlations.

The correlations averaged over all the categories investigated between beam, electrical impedance, rf-echo and frequency spectrum parameters and sensitivity and signal-to-noise parameters are shown in Table E-VII in Appendix E. The moderate correlation between IPA and sensitivity parameters may be due to the trend between the impedance phase angle and the shape of the initial excitation pulse as described in Section II-D.

It was shown in Table II that the average flaw signal-to-noise ratios have distinct differences among the different categories of transducers depending on the nominal frequency and beam angle. Therefore, one might expect a high linear correlation between the flaw signal-to-noise ratio parameters

and CF and EBA parameters. The low correlation between flaw signal-to-noise ratio parameters and CF and EBA parameters obtained in this project seems to contradict this observed dependence of the average flaw signal-to-noise ratios on the nominal frequency and beam angle.

For the case of 45° shear wave transducers, substantial departure from the normal angle (up to  $\pm 10^\circ$ ) would not be expected to influence the response from the fatigue cracks (no mode conversion takes place within the above mentioned angle range).<sup>23</sup> For the case of 60° shear wave transducers, the dependence on the beam angle appears as a moderate negative correlation (Table E-III-2 in Appendix E) between EBA and flaw signal-to-noise ratio parameters (FN2 and FN3). (The relation between mode conversion and beam angle is, however, not linear).<sup>21</sup> Note that the lower the beam angle (i.e. the higher the deviation from the nominal angle), the smaller the effect of mode conversion (i.e. the higher the flaw signal-to-noise ratio) for the case of 60° shear transducers.

For the case of 45° shear transducers, the difference between 5 and 10 MHz transducers for average flaw signal-to-noise ratios was only approximately 6 dB which is comparable to the standard deviation of the measurements. Therefore, even with the wide variation in CF (especially for nominal 10 MHz transducers), CF and flaw signal-to-noise ratio show low correlation.

For the case of 0° longitudinal transducers, the difference between 5 and 10 MHz transducers for average flaw signal-to-noise ratio was substantial (approximately 20 dB). Therefore, 10 MHz transducers which showed the widest variation in CF (Fig. 18-2) have a moderately high correlation between CF and flaw signal-to-noise ratios. For 5 MHz transducers, however, low correlation was obtained between CF and flaw signal-to-noise ratio which might be due to insufficient variation in CF or due to inadequate sampling. It was shown in Table III that the average amplitude ratios between the first returned echo in the semi-circle block and the echo from a side-drilled hole for 5 and 10 MHz-0° transducers are almost identical. This indicates that if other flaws (such as a side-drilled hole or a flat-bottomed hole) had been used, low correlation would have been observed between CF and flaw signal-to-noise ratios for 10 MHz-0° transducers as for the case of angle shear transducers. Therefore, it is apparent that substantial departure from the nominal frequency does not significantly affect flaw detectability.

As mentioned previously, the depth and angular resolution of a transducer are determined by the pulse length (which is roughly proportional to DMP) and the angle of beam divergence, respectively. The low correlation between parameters of DMP and BDA and parameters of sensitivity and signal-to-noise ratio indicates that flaw responses (or flaw signal-to-noise ratios) and resolution are independent of each other, as one would expect.

Thus far, only results of a linear correlation analysis have been discussed. Some of the parameters considered in this study, however, could be interrelated in a more complicated functional form, and these relationships would not be evident from the linear correlation analysis performed in this project. Further study would be required to determine if any more complicated relationships exist.

## V. CONCLUSIONS AND RECOMMENDATIONS

A. Conclusions1. Conclusions on Experimental Findings

As a result of this study, the following conclusions may be drawn.

a) There exists a wide variation in characteristic parameters for individual ultrasonic transducers having the same name-plate size, frequency and angle.

b) Despite the wide variation in performance of individual transducers, the average relationship between the loop sensitivity and the flaw responses for all transducers evaluated agrees well with the theory.

c) It has been shown that the beam characteristics of contacting transducers can be specified in terms of the response from a side-drilled hole.

d) Because of the energy loss due to the mode conversion upon reflection from the right angled corner, 5 MHz-60° transducers are generally less effective than 5 MHz-45° transducers in detecting a fatigue crack grown normal to the surface. Therefore, unless the beam angle is critical, the use of a 45° beam is preferable for inspection purposes.

e) As expected, straight beam (zero degree) longitudinal transducers have significantly poorer performance in detecting small surface fatigue cracks due to the interference effects from the lateral wall.

f) High correlation exists between the loop sensitivity and the flaw responses, between the signal-to-noise ratio of the echo in the reference block and the flaw signal-to-noise ratio, between the spectrum band width and the number of rf cycles in the pulse, and between the peak frequency and the center frequency.

g) Moderate correlation was found between the center frequency (or peak frequency) and the spectrum band width (or the number of rf cycles in the pulse), between the beam divergence angle and the beam width, and between the sensitivity parameters (loop sensitivity or flaw responses) and the signal-to-noise ratios.

h) Except for the above mentioned pairs of parameters, low correlation was found between the other pairs of parameters.

2. Preliminary Specifications for Ultrasonic Transducer Performance Parameters

From the results of the correlation analysis, it was concluded that SNR, LSR, BDA, and DMP are primary performance parameters which should be controlled to assure the good transducer flaw detectability. The reasons for selecting these as primary performance parameters are as follows:

- a) SNR - This parameter has a high correlation with flaw signal-to-noise ratio and is a measure of the transducer flaw detectability.
- b) LSR - The LSR measurement determines if the overall system has adequate sensitivity.
- c) BDA - This parameter is a measure of the transducer angular resolution.
- d) DMP - A close relationship exists between DMP and pulse length which is a measure of the transducer depth resolution.

In Appendix F, preliminary test methods and specifications (acceptance limits) for a total of ten ultrasonic transducer performance parameters are described. Besides the four above mentioned parameters, Dead Zone, Overall Appearance, Beam Exit Point, Beam Angle, Skew Angle and Center Frequency are included in this document. (In this specification, Pulse Length is chosen instead of DMP which is the number of rf cycles in the pulse length.) Underlying reasons for including these additional parameters in the specification are as follows:

- a) Dead Zone - This determines the detectability of a small flaw located near the probe.
- b) Overall Appearance - An uneven face of the transducer, for example, will cause unnecessary complications<sup>32</sup> due to non-uniform coupling to the material or part being inspected.
- c) Beam Exit Point, Beam Angle, and Skew Angle - These parameters generally had a low correlation with flaw detectability; however, they are important for determining flaw location or propagation direction of the sound beam. Controlling these parameters will insure uniformity of test results and reduce unnecessary complications in the measurement procedure and data analysis.
- d) Center Frequency - It was shown in this project that a substantial deviation from the nominal center frequency does not significantly affect flaw detectability. However, controlling the center frequency to the nameplate value would reduce unnecessary variations and thus enhance uniformity of test results.

Except for Dead Zone, these additional parameters are for transducer quality control to improve the uniformity of test results. It is noted that in selecting the above parameters and in developing the preliminary document in Appendix F, reference was also made to other existing standards or handbooks on the subject matter (see references in Appendix F).

Electrical impedance (both magnitude and phase angle) of the transducer affects the sensitivity of the system as well as the shape of the initial excitation pulse. As described in Section III-C, a variety of the initial excitation pulse shapes was observed with the same pulser and receiver. This variation can be attributed partly to the variation in the electrical impedance

of each transducer. Since the characteristics of a sound beam generated by a given transducer are primarily determined by the shape of the initial excitation pulse, specification of the shape of the initial excitation pulse may be essential to achieve uniform testing results. In this connection, specification of the electrical impedance (both magnitude and phase angle) of a transducer may also be important. This parameter is not included in the proposed preliminary specification (Appendix F), however, since its relationship to transducer performance has not been well defined and thus it is difficult to assign acceptance limits.

#### B. Recommendations

It was pointed out that the initial excitation pulse shape varies for different transducers even when the same pulser and receiver are employed. This is associated with transducer electrical impedance and the interaction between the pulser/receiver and transducer. This variation in the initial excitation pulse shape adversely affects the uniform performance of transducers. Further study is therefore necessary to understand transducer impedance effects, the interaction between the transducer and the detection system (pulser and receiver), as well as the effect of the initial excitation pulse on the performance of the transducer.

It has been shown in this study that the beam characteristics of the contacting transducers can be specified in terms of the responses from the side-drilled hole reflectors. However, there is a lack of the theoretical understanding of the expected response from a cylindrical reflector for the continuous or pulsed sound generations. Also lacking is a theoretical and experimental investigation of the beam characteristics of the angle beam shear waves generated by the mode conversion of the longitudinal waves. Such theoretical and experimental investigations will be needed for the better understanding of the fundamentals of the wave propagations and interactions of the procedures most widely utilized in practical NDI.

Several of the parameters considered in this project could have been interrelated in a more complicated manner which would not have been evident from the simple linear correlation analysis conducted in this study. Multi-parameter analysis may be necessary and should be subject of further investigation.

## REFERENCES

1. W. H. Lewis, B. D. Dodd, W. H. Sproat and J. M. Hamilton, Final Report on MME 76-6-38 (Contract No. F41608-76-D-A005), "Reliability of Nondestructive Inspections", December, 1978.
2. V. D. Smith, C. M. Teller, and R. K. Swanson, Final Report on SwRI Project No. 15-5024 (Contract No. F41608-77-C-1381), June, 1978.
3. J. Krautkramer, Brit. J. Appl. Phys. 10, 240 (1959).
4. Technical Manual T.O. 33B-1-1, "Nondestructive Inspection Method", (1979).
5. O. R. Gericke, J. Acoust. Soc. Am. 35, 364 (1963).
6. L. Adler and H. L. Whaley, J. Acoust. Soc. Am. 51, 881 (1972).
7. L. Adler, K. V. Cook, and W. A. Simpson, "Research Techniques in Nondestructive Testing", Vol. III, Chap. 1. Edited by R. S. Sharpe, Academic Press, N.Y. (1977).
8. K. R. Erikson, IEEE Trans Sonics and Ultra. SU-26, 7 (1979).
9. J. P. Weight and A. J. Hayman, J. Acoust. Soc. Am. 63, 396 (1978).
10. D. L. Dekker, R. L. Piziali, and E. Dong, Jr., J. Acoust. Soc. Am. 56, 87 (1974).
11. N. Paton, Proc. ARPA/AFML, Rev. Quantitative NDE, AFML-TR-75-212, p.89 (1976).
12. E. P. Papadakis and K. A. Fowler, J. Acoust. Soc. Am. 50, 729 (1971).
13. W. L. Beaver, J. Acoust. Soc. Am. 56, 1043 (1974).
14. A. Freedman, J. Acoust. Soc. Am. 49, 738 (1971).
15. J. Marini and J. Rivenez, Ultrasonics 12, 251 (1974).
16. A. Weyns, Ultrasonics 18, 183 (1980).
17. G. J. Posakony, NBS Special Pub. 596, "Ultrasonic Materials Characterization", H. Berger and M. Linzer, eds., p. 595, Issued Nov. 1980.
18. H. Wustenberg and E. Mundry, Non-dest. Testing 4, 260 (1971).
19. J. Zemanek, J. Acoust. Soc. Am. 49, 182 (1971).
20. B. H. Lidington and M. G. Silk, Brit. J. NDT, 14, 173 (1972).

21. B. H. Lidington and M. G. Silk, *Non-destruct. Testing* 7, 204 (1974).
22. G. C. Low, *NDT International* 13, 285 (1980).
23. J. Krautkramer and H. Krautkramer, "Ultrasonic Testing of Materials", 2nd Edition, Chap. 2. Springer-Verlag, N.Y. (1977).
24. I. N. Ermolov and O. R. Zaborovskii, *Sov. J. NDT*, No. 5, Sept.-Oct. p. 520, (1970).
25. J. Krautkramer and H. Krautkramer, "Ultrasonic Testing of Materials", 2nd Edition, Chap. 14. Springer-Verlag, N.Y. (1977).
26. Ibid. Chap. 5.
27. R. A. Fisher, "Statistical Methods for Research Workers", Oliver and Boyd, Edinburgh (1925-50).
28. G. W. Snedecor, "Statistical Methods, Applied to Experiments in Agriculture and Biology", Iowa State Univ. Press (1961).
29. R. L. Anderson and T. A. Bancroft, "Statistical Theory in Research", McGraw-Hill, N.Y. (1952).
30. E. E. Lewis, "Methods of Statistical Analysis in Economics and Business", Houghton Mifflin Co., Boston (1963).
31. For example, G. Arfken, "Mathematical Methods for Physicists", Chap. 15, 2nd edition, Academic Press, N.Y. (1971).
32. A. Vary, NASA Tech. Memo. 81489 (1980).

## APPENDIX A

LIST OF PARTICIPATING AIR FORCE BASES  
(In Arbitrary Order)

1. Donnelly Field AL (ANG)
2. Charleston AFB SC (MAC)
3. McGuire AFB NJ (MAC)
4. Tyndall AFB FL (AFSC)
5. Kelly AFB TX (AFLC, ANG, AFRS)
6. Randolph AFB TX (ATC)
7. Grissom AFB IN (SAC)
8. K. I. Sawyer AFB MI (SAC)
9. Wurtsmith AFB MI (SAC)
10. Andersen AB Guam (PACAF)
11. Altus AFB OK (MAC)
12. Kadena AB Okinawa (PACAF)
13. Dover AFB DL (MAC)
14. Cannon AFB NM (TAC)
15. Myrtle Beach AFB SC (TAC)
16. Holloman AFB NM (TAC)
17. Travis AFB CA (MAC)
18. Pope AFB SC (MAC)
19. Tinker AFB OK (AFLC)
20. Norton AFB CA (MAC)
21. McChord AFB WN (MAC)
22. Luke AFB AZ (TAC)
23. Eglin AFB FL (AFCS)
24. Kirtland AFT NM (TAC)
25. Williams AFB AZ (ATC)
26. McConnell AFB KS (SAC)
27. Nellis AFB NV (TAC)
28. Howard AFB Canal Zone (TAC)
29. Dyess AFB TX (SAC)
30. Ellington AFB TX (ANG)
31. Offutt AFB NE (SAC)
32. Will Rogers Field OK (ANG)

## APPENDIX A (Cont'd)

33. Boise IAP ID (ANG)
34. Cheyenne RAP (ANG)
35. Burlington AP (ANG)
40. Minot AFT ND (SAC)
41. Laughlin AFB TX (ATC)
42. March AFB CA (SAC)
43. Maxwell AFB AL (ATC)
44. Garden City AP GA (ANG)
45. Lincoln AP NE (ANG)
46. Terre Haute AP IN (ANG)
47. Bergstrom AFB TX (TAC)

## APPENDIX B

## DEFINITION OF ULTRASONIC TRANSDUCER PERFORMANCE PARAMETERS

- 1) Electrical Impedance, RF-echo and Frequency Spectrum Parameters,
  - a) Electrical Impedance (IMP); magnitude of the electrical impedance of the transducer at its nominal center frequency,
  - b) Impedance Phase Angle (IPA); phase angle of the electrical impedance of the transducer at its nominal center frequency,
  - c) Damping (DMP); number of rf cycles within the time interval when the amplitude of the echo is greater than approximately 10% of its maximum amplitude (page 109),
  - d) Peak Frequency (PF); frequency at which the spectrum amplitude of the rf-echo is maximum (Fig. B-1-a),
  - e) Center Frequency (CF); the average of the frequencies (upper and lower) at which the spectrum amplitude is half of maximum value (-6 dB), i.e.

$$CF = (F_l + F_u)/2$$

where  $F_l$  and  $F_u$  are respectively the lower and upper -6 dB frequencies (Fig. B-1-a).

- 1) Band Width Ratio (BWR); a measure of the width of the spectrum of the rf-echo defined as  $BWR = (F_u - F_l)/CF$ .
- g) Spectrum Symmetry Ratio (SSR); a measure of the symmetry of the spectrum with respect to CF defined as\*

$$SSR = (4CF - F_1 - F_2 - F_3 - F_4) / (2(F_u - F_l))$$

where  $F_1$ ,  $F_2$ ,  $F_3$ , and  $F_4$  are, respectively, the lower and upper frequencies at -12 dB and -20 dB points of the spectrum with respect to maximum amplitude (Fig. B-1-a). Note that SSR is zero when the spectrum is symmetric with respect to CF.

- h) Spectrum Inflection Ratio (SIR); defined as

$$SIR = P_{in}/P_m$$

where  $P_{in}$  is the lowest inflection amplitude among the inflection points within the frequency range between  $F_3$  and  $F_4$ , and  $P_m$  is the maximum spectrum amplitude (Fig. B-1-b). When there is no inflection point, SIR is taken as one.

\*V. D. Smith, C. M. Teller, and R. K. Swanson, Final Report, Contract No. F41608-77-C-1381, SWRI Project No. 15-5024, June, 1978.

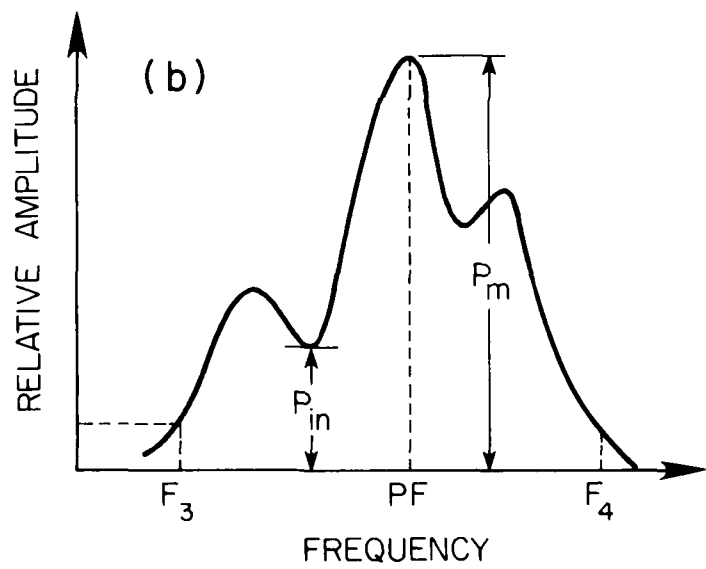
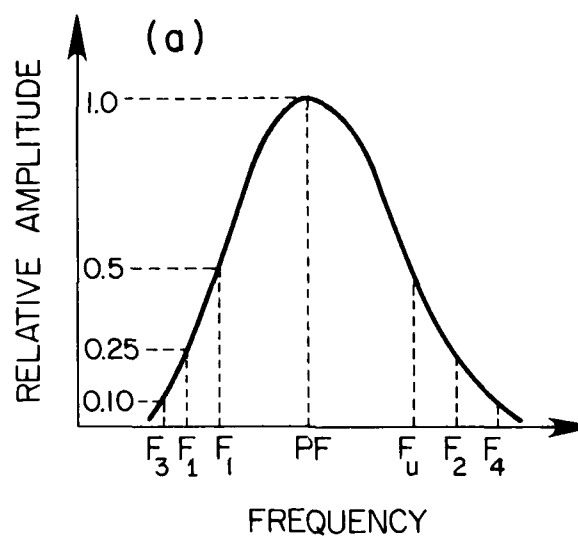


FIGURE B-1. FREQUENCY SPECTRUM PARAMETERS' DETERMINATION

2) Beam Characteristic Parameters

- a) Far Field Ratio (FFR); the ratio between the experimentally determined near-to-far field transition distance and the theoretical value given by  $(D^2 - \lambda^2) / (4\lambda)$  for a monochromatic and continuous sound wave generated by an ideal piston radiator of diameter D, where  $\lambda$  is the wave length of the sound at the nominal center frequency.
- b) Experimental Beam Angle (EBA); experimentally determined angle of the beam with respect to the normal to the contacting surface.
- c) Beam Divergence Angle (BDA); defined as

$$BDA = \tan^{-1}(BW/2R)/\sin^{-1}(0.7 \lambda/D)$$

where BW is the measured beam width between  $\sim 6$  dB amplitude points, R is the distance from the transducer to the point where beam width is measured, and  $\sin^{-1}(0.7 \lambda/D)$  is the theoretical beam divergence angle for the  $\sim 6$  dB beam width for a monochromatic and continuous sound wave generated by an ideal piston radiator of diameter D.

- d) Beam Symmetry Ratio (BSR); defined in the same way as SSR using "beam profile" instead of "spectrum".
- e) Beam Inflection Ratio (BIR); defined in the same way as SIR using the "beam profile" instead of "spectrum".
- f) Experimental Beam Width (EBW); the width of the beam between  $\sim 6$  dB amplitude points.
- g) Skew Angle (SA); an angle of beam misalignment with respect to the probe axis (page 105). This parameter applies only to angle beam transducers.

3) Sensitivity and Signal-to-Noise Ratio Parameters

- a) Loop Sensitivity Ratio (LSR); defined as the logarithmic ratio between the initial excitation pulse peak-to-peak amplitude ( $A_i$ , in volts) and the amplitude of the first returned echo ( $A_e$ , in volts) using a semi-circle test block (page 14), i.e.,

$$LSR = 20 \log_{10}(A_e/A_i)$$

- b) Side Drilled Hole Response (SDH); defined as

$$SDH = 20 \log_{10}(A_{SDH}/A_i)$$

where  $A_{SDH}$  is the side-drilled hole echo amplitude.

c) Flaw Response Ratio (FR1, FR2, FR3); defined as

$$FR1 = 20 \log (A_{F1}/A_i), \text{ etc.},$$

where  $A_{F1}$  is the echo amplitude from the fatigue crack #1, etc. (see page 19).

d) Signal-to-Noise Ratio (SNR); the logarithmic ratio between the noise amplitude and the first returned echo amplitude ( $A_e$ ) using the semi-circle test block.

e) Flaw Signal-to-Noise Ratio (FN1, FN2, FN3); defined as the logarithmic ratio between the noise amplitude and the echo amplitude from the fatigue cracks #1, #2, and #3 (see page 19).

## APPENDIX C

TABLES OF DATA OBTAINED FOR ULTRASONIC TRANSDUCER  
PERFORMANCE PARAMETERS

TABLE C-I . . . . FOR 5 MHz - 0° TRANSDUCERS

TABLE C-II . . . . FOR 5 MHz - 45° TRANSDUCERS

TABLE C-III . . . . FOR 5 MHz - 60° TRANSDUCERS

TABLE C-IV . . . . FOR 10 MHz - 0° TRANSDUCERS

TABLE C-V . . . . FOR 10 MHz - 45° TRANSDUCERS

\*In the tables, PF and CF are in MHz; IMP, in ohms; IPA, EPA, and SA, in degrees; EBW, in inches; LSR, SDH, FR1, FR2, FR3, SNR, FN1, FN2, and FN3, in decibels (dB); and the rest of the parameters have no dimensions.

TABLE C-1. DATA FOR 5 MHz-0° TRANSDUCERS (1)

	1	2	3	4	5	6	7	8	9	10	11	12	13	14	15	16	
PF	6	4.4		4.4	3.9	4.5		3.9	4.9	4.3	5.0	3.8	4.4	6.6	5.8	4.5	3.8
CF	5.5	4.85	3.85	5.4	3.9	5.3	3.95	4.85	4.3	4.75	3.75	5.55	6.65	5.9	4.5	3.8	
BWR	0.475	0.474	0.39	0.889	0.462	0.566	0.532	0.309	0.419	0.611	0.453	0.667	0.256	0.305	0.311	0.421	
SSR	0.135	-0.522	0.2	-0.281	-0.361	0.2	-0.071	0.3	-0.444	-0.586	-0.147	0.014	0.147	0	0.25	-0.344	
SIR	0.725	1.0	1.0	1.0	0.325	1.0	1.0	0.263	0.2	1.0	0.5	1.0	1.0	1.0	1.0	1.0	
DMP	6.5	5	4.5	3.5	4.5	7	4	6.5	4.5	4.5	4.5	6	7	6.5	6.5	5	
IMP	67	100	130	86	115	68	95	182	253	345	220	40	195	250	135	95	
IPA	64	-50	77	-84	74	20	80	46	10	75	62	88	84	68	56	82	
FFR	1.542	1.955	1.954	1.131	1.542	1.953	1.542	1.542	1.957	1.542	1.953	2.331	1.542	1.542	1.132		
EBA	0.1	2.4	0	0.3	0.7	0.1	0.4	0.8	0.9	3.4	0.7	0.1	0.6	0.6	0.6	2.1	
BDL	1.288	1.477	1.191	0.801	0.851	0.801	1.194	0.802	0.802	1.046	0.849	0.753	0.847	0.652	0.802	0.751	
BSP	0	-0.056	0.023	-0.25	0.192	0.125	0.087	0	0.031	0	0.071	0.1	-0.029	0	-0.154	-0.056	
BIR	1.0	0.98	1.0	1.0	1.0	1.0	1.0	1.0	1.0	1.0	1.0	1.0	1.0	1.0	1.0	1.0	
EBW	0.24	0.27	0.22	0.10	0.13	0.12	0.23	0.13	0.16	0.19	0.14	0.15	0.17	0.10	0.13	0.09	
-LSR	31	24	31	49	31	48	34	45	22	37	23	39	48	37	34	31	
-SDR	63	63	64	107	53	70	64	71	52	65	54	62	75	60	59	49	
-FR1																	
-FR2																	
-FR3	51	62	62	79	53	76	60	77	49	62	53	64	75	60	63	56	
SNR	53	54	56	61	55	60	45	58	49	59	52	57	50	53	49	51	
FN1																	
FN2																	
FN3	22	16	18	22	25	20	2	22	19	23	20	26	21	25	18	19	

TABLE C-1: DATA FOR 5 MHz-0° TRANSDUCERS (2)

	17	18	19	20	21	22	23	24	25	26	27	28	29	30	31	32
PF	5.3	3.8	3.4	3.8	4.0	4.7	6	4.5	3.2	3.5	4.2	5	3.8	4.6	5.2	5
CF	5.05	3.75	3.8	3.9	4.0	4.85	6.1	4.45	3.25	3.7	4.1	5.1	3.75	4.7	5.2	4.6
BWR	0.614	0.453	0.421	0.564	0.4	0.68	0.328	0.427	0.462	0.486	0.439	0.588	0.293	0.468	0.385	0.652
SSR	0.032	-0.235	-0.75	-0.636	-0.031	0.045	-0.100	-0.579	-0.267	-0.111	0.306	0.183	-1.045	-0.182	0.5	-0.217
SIR	1.0	1.0	0.375	1.0	1.0	1.0	1.0	1.0	1.0	1.0	1.0	1.0	0.125	1.0	1.0	1.0
DMP	4	5	5	4.5	5	3	7.5	6	5	4.5	5	3.5	6	4.5	5	5.5
IMP	72	125	390	105	145	400	220	280	105	145	530	170	105	180	88	125
IPA	60	24	-38	74	70	32	74	20	75	75	80	18	62	37	-88	-92
FFR	1.133	1.131	1.131	1.131	1.131	1.542	1.542	1.542	1.131	1.131	1.542	1.542	1.543	1.953	1.953	1.543
EBA	.6	1.0	1.3	1.0	0.7	0.6	0.4	0	1.0	0.6	1.3	0.7	2.3	0.8	1.0	2.0
BDA	0.702	0.802	0.802	0.801	0.703	0.751	0.802	0.998	0.751	0.852	0.752	0.851	0.802	0.948	0.850	0.996
BSR	0.111	-0.05	-0.046	-0.05	-0.056	0	0.039	0.1	0	0.125	-0.154	0.192	-0.071	0	0.063	0
BIR	1.0	1.0	1.0	1.0	1.0	1.0	1.0	1.0	1.0	1.0	1.0	1.0	1.0	1.0	1.0	1.0
EBW	0.09	0.10	0.11	0.10	0.09	0.12	0.13	0.15	0.09	0.12	0.13	0.13	0.14	0.16	0.16	0.15
-LSR	32	30	22	33	33	43	44	48	36	27	41	49	41	43	54	53
-SDH	55	57	54	56	51	68	66	76	51	54	70	73	57	70	82	81
-FRI																
NOT DETECTABLE																
-FR2																
-FR3	57	63	59	62	57	74	71	69	53	52	67	76	58	70	80	81
SNR	51	53	59	53	53	54	59	53	50	55	52	52	49	49	57	55
FN1																
FN2																
FN3	18	18	21	18	19	19	22	22	22	21	21	23	20	23	20	17

TABLE C-II. DATA FOR 5 MHz-45° TRANSDUCERS (1)

	1	2	3	4	5	6	7	8	9	10	11	12	13	14	15	16	
PF	4.5	4.7	4.9	4.5	4.6	4.8	5.2	5	4.5	4.8	5	5.3	4.6	5	5	4.8	
CF	4.5	4.7	4.9	4.6	4.75	4.8	5.1	5	4.5	4.75	5.1	5.275	4.7	5.1	4.9	4.9	
BWR	0.311	0.298	0.286	0.435	0.232	0.417	0.588	0.48	0.489	0.316	0.431	0.256	0.383	0.431	0.367	0.531	
SSR	-0.893	-0.929	-0.464	-1.05	-0.182	-0.575	0.2	-0.063	-0.023	-0.267	-0.341	0.148	-0.806	-0.477	-0.389	-0.288	
SIR	1.0	1.0	1.0	1.0	1.0	1.0	1.0	1.0	1.0	1.0	1.0	0.425	1.0	1.0	1.0	0.6	
DMP	5.5	6.5	7	4.5	8	5	4.5	6	6	7	7.5	8	4.5	4.5	5	4	
IMP	34	36	30	92	45	44	120	40	33	47	230	87	54	70	2600	137	
IPA	56	38	33	32	40	54	62	18	70	30	68	62	72	60	-88	-58	
FFR	1.03	1.304	1.53	0.756	1.056	1.021	1.028	1.086	1.023	0.818	1.023	1.274	0.75	1.037	0.972	1.227	
EBA	44	43	43	42	43	43.5	43	44.5*	43.5	47.5*	42	42.5*	42.5*	43*	40.5	40	
BDA	0.690	0.686	0.751	0.747	0.811	0.781	0.71	0.691	0.675	0.787	0.675	0.651	0.781	0.732	0.836	0.748	
BSR	-0.321	-0.25	-0.5	-0.125	-0.3	-0.385	-0.083	-0.346	-0.346	-0.308	-0.346	-0.346	-0.125	-0.077	0.125	0.036	0.208
BIR	1.0	1.0	1.0	1.0	1.0	1.0	1.0	1.0	1.0	1.0	1.0	1.0	1.0	1.0	1.0	1.0	
EBW	0.14	0.12	0.15	0.12	0.15	0.13	0.12	0.13	0.13	0.13	0.13	0.12	0.13	0.12	0.14	0.12	
SA	1.5	0	1.5	0	1	0.5	3.5	1	1.5	2.5	2.5	0.5	0.5	1.5	1.5	1.5	
-LSR	41	40	36	47	35	43	55	41	44	43	48	46	42	39	61	66	
-SDH	72	73	70	79	64	72	87	71	77	71	79	77	71	70	85	96	
-FR1	79	83	77	82	77	84	96	81	82	85	88	91	78	77	99	104	
-FR2	72	75	63	72	63	70	78	71	72	71	73	73	63	61	83	90	
-FR3	57	55	49	51	49	52	66	54	50	49	58	58	50	48	69	81	
SNR	52	51	51	48	51	53	50	46	58	49	46	48	50	51	52	52	
FN1	14	12	15	9	8	10	10	9	12	6	5	12	13	14	13	14	
FN2	22	20	29	19	21	22	22	20	24	19	18	22	24	23	27	75	
FN3	41	41	42	39	43	45	42	44	40	36	40	41	41	43	43	43	

\*Nominal Beam Angle rated in Aluminum, others rated in Steel

TABLE C-II. DATA FOR 5 MHZ-45° TRANSDUCERS (2)

	17	18	19	20	21	22	23	24	25	26	27	28	29	30	31	32
PF	4.2	4.6	5.3	4.9	5.4	5.3	5.4	5.8	5.7	4.0	4.7	5.3	4.7	4.8	5.2	5.1
CF	4.3	4.7	5.25	4.9	5.35	5.3	5.4	5.5	5.4	4.15	4.75	5.4	4.75	4.7	5.25	5.2
BWR	0.512	0.383	0.248	0.286	0.355	0.340	0.296	0.270	0.296	0.795	0.274	0.259	0.316	0.298	0.362	0.385
SSR	-0.295	0.028	-0.115	-0.893	-0.053	-0.056	-0.031	0.2	0.844	-0.302	0	0.143	-0.133	0.071	-0.237	-0.275
SIR	0.438	1.0	1.0	0.125	1.0	1.0	1.0	1.0	0.2	0.25	1.0	0.25	0.188	1.0	1.0	1.0
DMP	4	5	8.5	8	6	6.5	7	7.5	8	5	9	7.5	7.5	8	5	6
IMP	123	110	145	67	190	40	150	190	110	350	28	30	240	24	88	87
IPA	-72	-62	20	66	78	76	37	32	-82	-36	47	-44	70	68	-80	-78
FFR	0.961	0.975	1.277	1.305	1.267	1.815	1.277	1.543	1.019	0.494	0.997	1.309	1.798	1.032	1.297	1.289
EBA	39	40	42.8	43.5	42	42.5	42	42.5	43	45*	42.5	45*	42	45	43.5*	43*
BDA	0.8	0.71	0.682	0.736	0.651	0.68	0.632	0.661	0.653	0.783	0.641	0.567	0.601	0.687	0.573	0.627
BSSR	0.039	-0.107	-0.036	-0.423	-0.385	-0.036	-0.455	0.083	-0.227	-0.202	-0.154	-0.050	-0.583	-0.333	-0.136	-0.250
BIR	1.0	1.0	1.0	1.0	1.0	1.0	0.236	1.0	0.096	0.149	1.0	1.0	0.151	1.0	1.0	1.0
EBW	0.13	0.14	0.14	0.13	0.13	0.14	0.11	0.12	0.11	0.12	0.13	0.10	0.12	0.12	0.11	0.12
SA	2	1	2.5	1	2	1.5	0	2	1	2	1.5	2	3.5	1.5	1.5	1.5
-LSR	61	64	41	39	50	52	47	62	54	67	34	41	54	39	52	51
-SDH	87	87	70	69	77	81	73	94	73	92	66	72	83	73	80	75
-FR1	101	101	79	79	84	89	83	98	89	107	71	76	92	79	87	86
-FR2	86	85	62	68	73	67	79	72	86	52	55	66	58	75	74	
-FR3	75	74	51	52	56	61	56	72	63	78	43	45	56	48	67	59
SNR	50	51	50	56	50	47	50	41	46	55	50	48	51	40	46	
FN1	15	12	15	13	12	10	14	9	12	8	11	12	7	11	0	4
FN2	27	25	26	25	24	23	25	26	28	27	32	29	30	29	14	16
FN3	40	42	43	42	41	43	36	38	39	43	42	41	42	21	32	

TABLE C-III. DATA FOR 5 MHz-60° TRANSDUCERS (1)

	1	2	3	4	5	6	7	8	9	10	11	12	13	14	15	16
PF	4.8	4.8	4.2	5.0	5.0	4.8	4.8	4.5	4.7	5.6	5	4.7	5.1	4.6	5.3	4.3
CF	4.9	4.75	4.3	4.95	5.15	4.85	4.8	4.5	4.7	5.6	5.1	4.7	5.1	4.7	5.15	3.95
BWR	0.286	0.274	0.372	0.424	0.408	0.433	0.25	0.222	0.213	0.179	0.431	0.255	0.275	0.298	0.524	0.684
SSR	-0.357	-0.192	-0.094	0.214	-0.381	-0.024	-0.542	-2.25	-1.15	-0.05	-0.455	-0.417	-0.286	-0.5	0.056	-0.222
SIR	1.0	1.0	1.0	1.0	0.125	1.0	1.0	1.0	1.0	1.0	1.0	1.0	1.0	1.0	0.125	1.0
DMP	7	8.5	9	6	4.5	6	7	9	7	12	4.5	7.5	10	8.5	6	5.5
IMP	50	27	26	37	78	25	28	29	30	1250	40	26	105	34	93	105
IPA	-22	61	70	10	16	60	56	66	60	23	62	87	12	60	-40	12
FFR	0.919	0.893	0.920	0.723	0.621	0.954	0.571	0.916	0.917	0.977	0.604	0.918	0.918	0.282	0.664	
EBA	57	53	53.5	61*	56.5	55*	54.5	51	54	55	54	54	53	55	58*	
BDA	0.876	0.839	0.875	1.018	1.073	1.008	0.911	0.894	0.881	0.754	0.901	0.921	0.878	1.053	1.279	1.042
BSR	-0.423	0	0.107	-0.441	-0.321	0	-0.375	0.042	-0.286	-0.5	-0.107	0	-0.067	-0.130	0	-0.5
BIR	1.0	0.229	0.66	1.0	0.294	1.0	1.0	1.0	1.0	0.242	1.0	1.0	0.216	1.0	1.0	0.281
EBW	0.13	0.13	0.14	0.17	0.14	0.14	0.16	0.12	0.14	0.10	0.14	0.2	0.15	0.23	0.10	0.16
SA	5	1.5	2.5	0.5	2.5	3.5	2.5	1.5	2.5	1.5	2	1.5	0.5	1.5	2.5	2
-LSR	36	39	69	45	45	41	38	46	36	61	47	39	41	34	42	45
-SDH	65	72	107	70	70	69	67	81	67	87	71	66	71	65	63	66
-FRL	-	-	-	-	-	-	67	-	-	-	-	86	85	79	-	-
-FR2	73	77	106	91	83	79	72	83	67	91	82	70	71	65	81	86
-FR3	54	57	84	69	63	60	53	61	50	71	62	54	55	50	61	65
SNR	57	61	36	47	55	58	54	48	56	48	50	54	48	54	50	40
FNL	-	-	-	-	-	-	7	-	-	-	-	6	5	7	-	-
FN2	16	24	0	4	14	12	22	14	19	17	19	20	14	17	9	10
FN3	36	44	28	30	34	34	40	36	39	33	39	34	35	30	30	30

\*Nominal Beam Angle rated in Aluminum, others rated in Steel

TABLE C-III. DATA FOR 5 MHz-60° TRANSDUCERS (2)

	17	18	19	20	21	22	23	24	25	26	27	28	29	30	31	32
PF	4.9	4.9	4.8	5	4.7	6	4.9	4.7	4.5	5.0	4.8	4.4	4.2	4.8	5	5.2
CF	5.05	4.9	4.8	5.1	4.7	6	4.9	4.75	4.75	5.0	4.8	4.4	4.85	4.4	5.05	5.2
BWR	0.297	0.286	0.25	0.275	0.298	0.233	0.286	0.274	0.4	0.320	0.333	0.273	0.68	0.727	0.257	0.308
SSR	-0.567	-0.625	-0.458	-0.5	-0.411	0.071	-0.321	-0.154	-0.342	-0.406	-0.156	-0.125	0.318	-0.141	-0.385	-0.219
SIR	1.0	1.0	1.0	1.0	1.0	1.0	1.0	1.0	0.188	0.125	0.219	1.0	1.0	1.0	1.0	1.0
DMP	7	7	8.5	8.5	9	10	6.5	7.0	5.5	7	6.5	8	4.5	4.5	6.5	7
IMP	30	24	30	85	30	185	28	28	95	38	49	90	91	81	102	90
IPA	44	65	72	54	72	36	53	66	2	0	34	28	0	-1	-74	-78
FFR	0.945	0.915	0.587	0.881	0.592	0.989	0.647	0.630	0.625	0.988	0.973	0.626	0.619	0.650	0.582	0.933
EBA	57*	53	53.5	52	54	56.5*	58*	57.5*	56	56	55.5	55.5	55	58*	56*	57*
BDA	0.979	0.929	0.915	0.744	0.858	0.751	0.845	0.955	1.007	0.890	0.906	0.963	0.922	0.994	0.837	0.840
BSR	-0.469	-0.175	-0.094	-0.458	-0.219	-0.2	-0.179	-0.1	-0.219	-0.20	-0.25	-0.367	-0.393	-0.177	-0.15	-0.179
BIR	0.442	1.0	1.0	0.088	0.074	0.264	0.489	1.0	0.316	0.202	1.0	0.084	0.337	0.222	1.0	0.98
EBW	0.16	0.20	0.16	0.12	0.16	0.15	0.14	0.15	0.16	0.15	0.16	0.15	0.14	0.17	0.1	0.14
SA	1	1.5	1	2	1.5	0.5	2	1	1.5	1.5	1	1	1.5	0	0.5	0
-LSR	45	39	41	36	41	59	39	40	43	35	43	42	46	54	54	54
-SDH	66	66	68	74	71	87	64	65	67	65	61	69	66	71	79	78
-FRL	83	84	-	85	-	-	-	-	-	-	-	-	-	-	-	-
-FR2	69	66	73	68	72	74	73	73	81	62	61	71	71	79	87	88
-FR3	51	51	58	51	50	78	54	54	62	49	48	57	56	60	70	69
SNR	52	53	49	52	48	47	51	50	46	53	50	51	48	37	40	
FN1	5	7	-	5	-	-	-	-	-	-	-	-	-	-	-	-
FN2	18	20	15	19	17	11	12	13	12	22	20	19	17	14	0	2
FN3	37	39	32	37	32	28	31	30	36	34	32	34	31	15	20	78

TABLE C-IV. DATA FOR 10 MHz- $0^\circ$  TRANSDUCERS (1)

	1	2	3	4	5	6	7	8	9	10	11	12	13	14	15	16	
PF	8	7.9	4	8.6	8.4	9.2	5.0	8	8.8	9.9	11.2	8.8	9.2	8.8	9.6	8.8	
CF	8.3	7.9	5.4	8.65	9.15	9.9	4.85	8.2	8.9	9.8	11.1	9.55	9.5	10.8	9.25	6.5	
BWR	0.361	0.27	0.963	0.173	0.536	0.323	0.722	0.146	0.292	0.327	0.306	0.325	0.526	0.778	0.249	1.323	
SSR	-0.367	0.045	-0.183	-0.967	-0.102	0.031	-0.257	-1.333	-0.808	0.062	0.338	-0.097	-0.28	0.173	-0.043	-0.058	
SIR	1.0	0.25	1.0	1.0	1.0	0.60	0.688	0.35	0.225	1.0	1.0	0.688	1.0	0.175	0.125	0.725	
DMP	7	6.5	4	11.5	4.5	8	5	10	7	5.5	5	8	2.5	5.5	9	4	
IMP	92	21	45	60	120	84	76	195	240	77	127	56	22	10	9.5	68	
IPA	-58	30	83	47	66	62	-50	10	30	68	-60	63	-77	54	70	-86	
FPR	1.346	0.947	0.947	0.947	1.146	0.947	1.148	1.146	1.146	0.947	0.947	1.146	1.944	1.546	1.147		
EBA	1.0	1.4	0.3	1.5	0.3	0.9	3.3	0.1	0.9	0.2	0.7	0.5	0.7	0.2	1.4	1.8	
BDA	0.841	0.891	0.991	1.045	0.791	0.896	0.805	0.785	0.796	0.741	1.103	0.691	0.646	0.751	0.846	0.896	
BSS	-0.091	0.071	-0.05	-0.179	0.5	-0.077	0.15	0.150	-0.042	0.182	0	0	0	0.125	-0.033	0	-0.125
BIR	1.0	1.0	1.0	1.0	1.0	1.0	1.0	1.0	1.0	1.0	1.0	1.0	1.0	1.0	1.0	1.0	
EBW	0.11	0.14	0.10	0.14	0.10	0.13	0.10	0.10	0.11	0.11	0.16	0.12	0.08	0.15	0.16	0.12	
-LSR	58	42	61	41	50	39	51	42	38	40	44	39	49	51	36	51	
-SDH	96	71	80	67	80	66	90	69	66	71	77	66	77	63	65	76	
-FRL	-	-	-	-	-	86	-	-	-	-	-	-	-	-	-	-	
-FR2	103	90	101	86	94	76	-	75	75	76	83	70	84	75	72	89	
-FR3	77	64	76	64	69	53	80	54	56	49	63	49	55	49	51	66	
SNR	56	64	58	65	58	65	52	59	67	61	56	61	62	57	64	57	
FN1	-	-	-	-	-	6	-	-	-	-	-	-	-	-	-	-	
FN2	6	12	12	14	8	20	-	18	20	20	12	19	20	21	23	18	
FN3	29	36	37	37	38	44	30	39	43	47	36	44	44	45	47	41	

TABLE C-IV. DATA FOR 1.0 MHZ-0° TRANSDUCERS (2)

	17	18	19	20	21	22	23	24	25	26	27	28	29	30	31	32	
PF	10	9.2	9.3	9.8	9.5	10	9	10	8.5	8.6	10.1	9.2	3	8.8	6	8	
CF	10.5	8.9	8.9	9.3	9.25	10	9	10.1	8.75	8.5	9	9.25	2.75	8.2	6.2	7.6	
BWR	0.324	0.427	0.337	0.409	0.249	0.4	0.222	0.218	0.194	0.353	0.667	0.249	0.909	0.415	0.710	0.421	
SSR	-0.147	-0.184	0.033	-0.026	1.0	0.175	0.525	-0.409	1.559	-0.033	0.525	0.261	-0.42	0.338	-0.136	-0.313	
SIR	0.60	1.0	1.0	1.0	0.175	0.1	0.375	1.0	0.188	0.125	0.25	0.25	0.375	0.125	1.0	0.25	
DMP	8	7	8	7	8.5	8	7.5	10	11	7	7	7	3.5	7	6	8	
IMP	68	13	14	21	14.5	48	10.5	74	145	17.5	65	46	29.5	17.5	29	28	
IPA	71	42	-42	-34	-62	60	-30	72	-48	-43	-84	70	-88	-48	-92	-92	
FFR	1.346	0.947	0.748	0.947	1.146	0.947	0.947	1.346	0.748	1.146	1.346	1.546	1.346	0.949	0.748	0.549	
EBA	0.6	0.2	1.0	0.7	0.5	0.4	0.6	0.6	0.2	0.6	0.4	1.9	1.4	1.3	3.6	1.5	2.3
BDA	0.746	0.801	1.034	0.801	0.746	0.841	0.601	0.796	0.850	0.791	0.796	0.609	0.751	0.790	1.421	0.655	
BSR	0.615	0	0.033	0	0.083	-0.05	-0.136	-0.083	-0.046	-0.083	0.125	-0.091	0.046	0.083	0.182	-0.375	
BIR	1.0	1.0	1.0	1.0	1.0	1.0	1.0	1.0	1.0	1.0	0.065	1.0	1.0	1.0	1.0	1.0	
EBW	0.13	0.10	0.15	0.10	0.12	0.10	0.11	0.12	0.11	0.12	0.12	0.11	0.11	0.12	0.11	0.08	
-LSR	57	39	41	39	36	36	34	55	49	46	74	60	68	40	69	65	
-SDH	80	64	66	60	52	69	55	86	71	69	110	81	122	68	102	91	
-FR1	-	-	-	-	-	-	-	-	-	-	-	-	-	-	-	-	
-FR2	95	78	85	77	70	72	72	88	85	69	113	80	-	75	110	94	
-FR3	68	56	59	54	50	53	52	62	62	50	97	60	103	53	92	70	
SNR	57	64	59	61	58	65	60	59	53	42	61	44	60	52	60	60	
FN1	-	-	-	-	-	-	-	-	-	-	-	-	-	-	-	-	
FN2	17	21	15	19	15	22	16	20	20	16	4	19	-	19	4	14	
FN3	44	46	40	42	36	44	39	44	45	42	28	48	29	45	24	44	

TABLE C-V. DATA FOR 10 MHz-45° TRANSDUCERS (1)

	1	2	3	4	5	6	7	8	9	10	11	12	13	14	15	16
PF	8.8	8.2	7.2	6.5	6.4	6.8	8.0	8.0	9.6	6.0	7.4	12	9.2	9.4	9.9	8.4
CF	8.9	8.2	7.2	6.6	6.0	6.9	8.3	7.9	9.55	7.1	8.1	11.4	9.1	7.8	7.8	7.65
BWR	0.427	0.390	0.556	0.333	0.467	0.841	0.361	0.430	0.22	0.592	0.963	0.281	0.154	0.974	0.974	0.876
SSR	-0.434	-0.641	0.250	0.409	-0.714	-0.138	0.167	0.074	0.714	-0.048	-0.064	0.375	0.571	0.053	0.053	0.045
SIR	1.0	0.3	0.338	1.0	1.0	0.45	0.25	1.0	1.0	0.138	0.325	1.0	1.0	0.688	0.588	1.0
DMP	7	7	10	5.5	5.5	4.5	8	5	8	5.5	4.5	10	10	4.5	4	4
IMP	66	12	14	36	66	33	14	14	185	24	30	360	136	92	105	78
IPA	66	31	55	-82	33	-82	65	65	38	-82	-82	62	82	-66	-64	-64
FFR	0.771	1.022	0.903	0.907	0.66	1.017	0.920	0.937	0.933	0.946	1.040	1.305	0.893	0.884	0.890	0.893
EBA	42	43	42.5	42	44	41	43	43.5	42	42	43.5	42	40	40	40	40
BDA	0.782	0.713	0.787	0.672	1.006	0.653	0.773	0.750	1.092	0.950	0.682	0.950	1.081	0.689	0.650	0.697
BSR	0	0.2	-0.154	-0.107	-0.455	-0.773	-0.125	-0.45	-0.294	0.633	-0.273	-0.3	-0.029	0	0	-0.55
BIR	1.0	1.0	1.0	1.0	1.0	1.0	1.0	1.0	1.0	0.462	1.0	1.0	1.0	1.0	1.0	0.208
EBW	0.09	0.1	0.13	0.14	0.11	0.11	0.16	0.10	0.17	0.15	0.11	0.15	0.17	0.09	0.1	0.10
SA	1.5	2.5	2.5	5.5	0	2.5	3	2	1.5	2.5	1.25	1.5	2	1	0.5	0.5
-LSR	63	47	52	69	43	62	54	54	61	61	59	56	65	67	65	65
-SDR	91	83	83	104	72	99	88	87	98	107	101	104	92	86	87	87
-FRI	88	83	88	120	80	96	91	89	96	95	100	92	89	94	96	96
-FR2	83	70	72	100	71	85	77	74	85	84	81	86	79	74	79	76
-FR3	63	58	59	90	59	74	62	62	71	71	72	71	68	69	69	70
SNR	54	50	59	44	59	52	52	56	54	58	55	55	56	58	57	57
FN1	21	23	18	0	23	20	19	20	16	18	19	12	16	18	20	19
FN2	26	35	34	14	32	27	33	22	36	30	26	27	33	36	33	33
FN3	45	48	47	29	44	50	46	47	46	48	47	46	40	50	52	50

TABLE C-V. DATA FOR 10 MHz-45° TRANSDUCERS (2)

	17	18	19	20	21	22	23	24	25	26	27	28	29	30	31	32
PF	9	8	8.4	8.4	11.8	8	8	10.4	10	9.9	9.5	10	9.8	8.8	6.6	5.9
CF	7.85	7.1	8.4	8.4	11.6	7.1	7.1	10.3	9.9	9.9	9.4	9.9	9.85	8.1	7.3	7.45
BWR	0.752	1.099	0.286	0.286	0.241	0.648	0.704	0.175	0.222	0.222	0.213	0.182	0.193	0.568	1.068	0.899
SSR	0.102	0.038	-0.917	-0.979	0.571	-0.348	-0.34	0.083	0.5	0.386	0.175	0.333	0.316	0.217	-0.103	0
SiK	1.0	1.0	0.275	0.263	1.0	0.2	0.35	1.0	1.0	1.0	1.0	0.175	1.0	0.125	0.338	0.463
DMP	4.5	4	9	8	7.5	5	5	11	9	10	9	10	12	5.5	5	4
IMP	60	75	12	8	250	33	36	53	70	43	105	105	175	39	8	10
IPA	-68	-70	44	20	60	-86	-86	20	54	48	50	61	86	-86	-34	-24
FFR	0.747	0.876	1.56	1.045	0.902	1.554	1.02	0.907	1.019	0.912	1.304	0.869	1.038	1.018	0.913	1.055
EBA	41	39.5	43.5	43.5	42.5	41	41	42.5	42	42.5	42.5	42	43	42	42.5*	43*
BRA	0.666	0.766	0.700	0.669	0.524	0.642	0.650	0.873	0.651	0.676	0.600	1.15	0.562	0.754	0.718	0.713
BSR	-0.15	-0.15	-0.308	0.25	-0.833	-0.375	-0.039	0.071	-0.367	0	0.039	0.357	-0.389	-0.179	0.111	0
BIR	1.0	1.0	1.0	1.0	0.154	1.0	1.0	0.329	1.0	1.0	1.0	1.0	1.0	1.0	1.0	1.0
EBW	0.10	0.10	0.13	0.16	0.09	0.12	0.13	0.14	0.15	0.10	0.13	0.21	0.09	0.14	0.09	0.11
SA	1	1.5	2	2.5	2.5	0	1	2	1	0.5	1	2	1.5	1	0	0
-LSR	63	71	44	49	57	64	68	52	53	57	51	67	67	67	52	44
-SDH	84	91	75	80	91	101	100	84	83	95	89	98	92	96	79	78
-FR1	87	96	72	80	96	101	100	85	83	92	81	105	93	90	80	77
-FR2	74	82	59	67	75	89	84	70	70	77	67	89	80	74	75	67
-FR3	69	70	53	56	65	79	77	59	61	64	59	78	70	69	58	55
SNR	58	54	57	56	51	52	55	58	55	55	56	49	52	54	52	57
FN1	24	15	22	19	14	15	18	18	19	16	21	13	19	16	20	25
FN2	30	33	31	29	28	34	31	30	29	31	24	33	33	27	33	82
FN3	50	48	49	48	46	46	50	50	46	45	50	42	46	47	48	46

\*Nominal Beam Angle rated in Aluminum, others rated in Steel

## APPENDIX D

## PREPARATION OF FATIGUE CRACK SPECIMENS

The fatigue crack specimens used in this study were made of 7075-T651 aluminum alloy. The fatigue cracks were grown normal to the specimen surface from EDM (Electric Discharge Machined) starter notches of approximately 0.81 mm (0.032 in.) long, 0.30 mm (0.012 in.) wide, and 0.41 mm (0.016 in.) deep. The specimens were cycled in fatigue until a crack propagated to approximately 0.25 mm (0.010 in.) long on both sides of the starter notches. The starter notches were then machined off leaving the primary fatigue cracks which had surface length to depth ratio of approximately 4 to 1. Fatigue cycling was continued on the primary fatigue cracks until they grew to the desired surface lengths.

To observe the crack growth patterns, one of the specimens was grown to a surface length of 3.81 mm (0.15 in.) with overloading marks at every 1.27 mm (0.05 in.) surface length. This specimen was subsequently fractured. The internal configuration of the crack is shown in Fig. D-1. From this specimen, it was observed that fatigue cracks of surface length up to 2.54 mm (0.1 in.) had surface length to depth ratios of 4 to 1 and the fatigue crack of surface length 3.81 mm (0.15 in.) had a surface length to depth ratio of 3 to 2. The three fatigue crack specimens used in this study had surface lengths of 1.27 mm (0.05 in.), 2.54 mm (0.10 in.) and 3.81 mm (0.15 in.), respectively. According to the fatigue crack growth pattern observed on the fractured specimen, the depth of the crack was estimated to be 1/4 of the surface length for cracks of surface length up to 2.54 mm (0.10 in.). Also, the depth of the 3.81 mm (0.15 mm) surface length would be estimated to be 2/3 of the surface length. In Sections II-D and III-C of the text, however, the depth of the 3.81 mm (0.15 mm) surface length was taken to be 1/2 of the surface length assuming it was grown in half-penny shape.\* Even if the depth were estimated to be 2/3 of the surface length (which would increase the theoretical echo amplitude by 3.5 dB from that for the case of 2 to 1 surface length to depth ratio), the conclusions drawn in Section III-C would still be the same.

In Fig. D-2, crack surface lengths were plotted as a function of stress cycles obtained during the growth of the three fatigue cracks used in this study. The numbers between the data points indicate the stress amplitude (in kpsi units, 1 kpsi =  $6.895 \times 10^7$  dyne/cm<sup>2</sup>) applied during the cycling.

\*J. R. Birchak and C. G. Gardner, Final Report, Cont. No. F41608-73-D-6739, SwRI Project 15-3711-003, Jan. (1975).

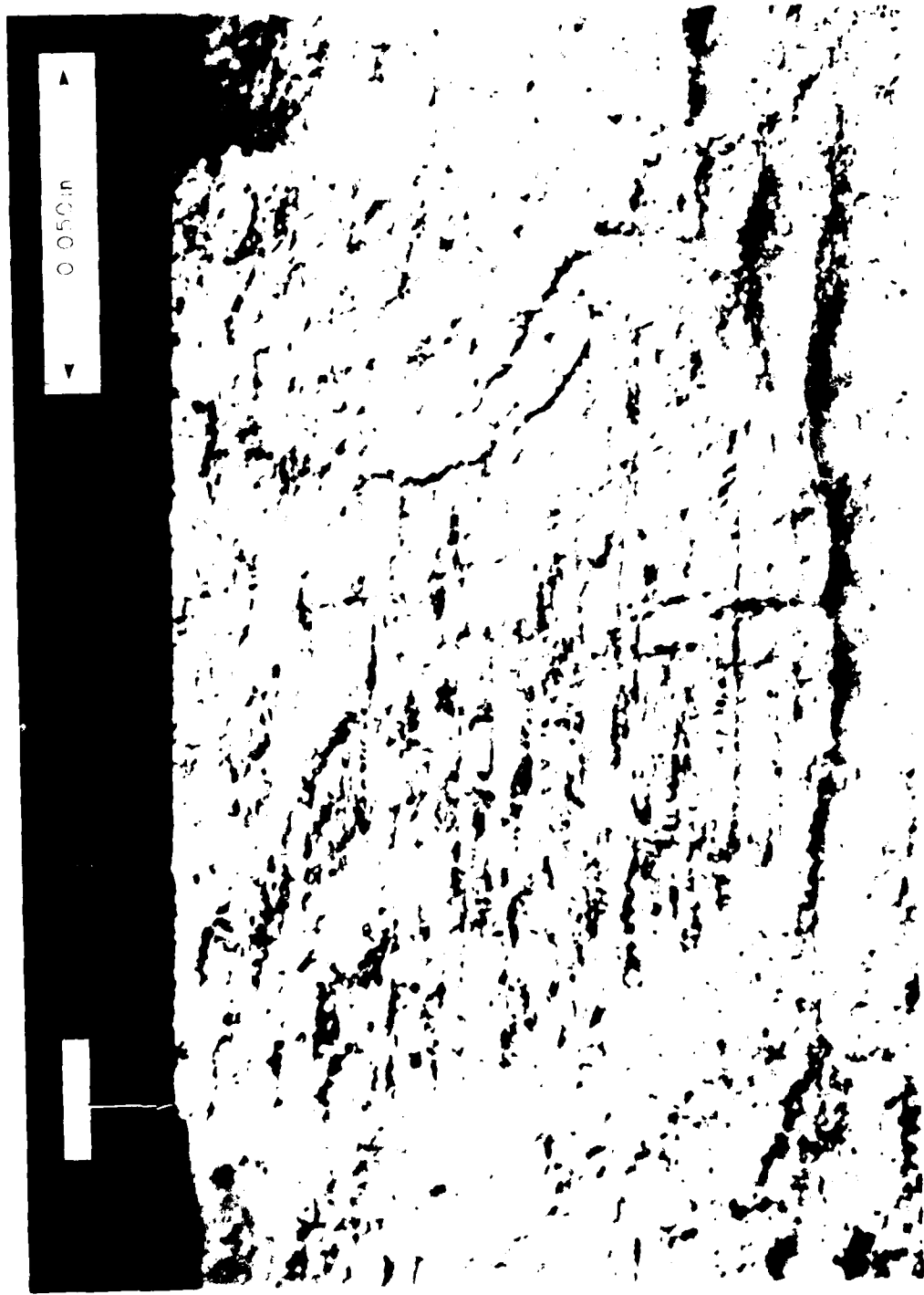


FIGURE D-1. FATIGUE CRACK FRACTURE SURFACE

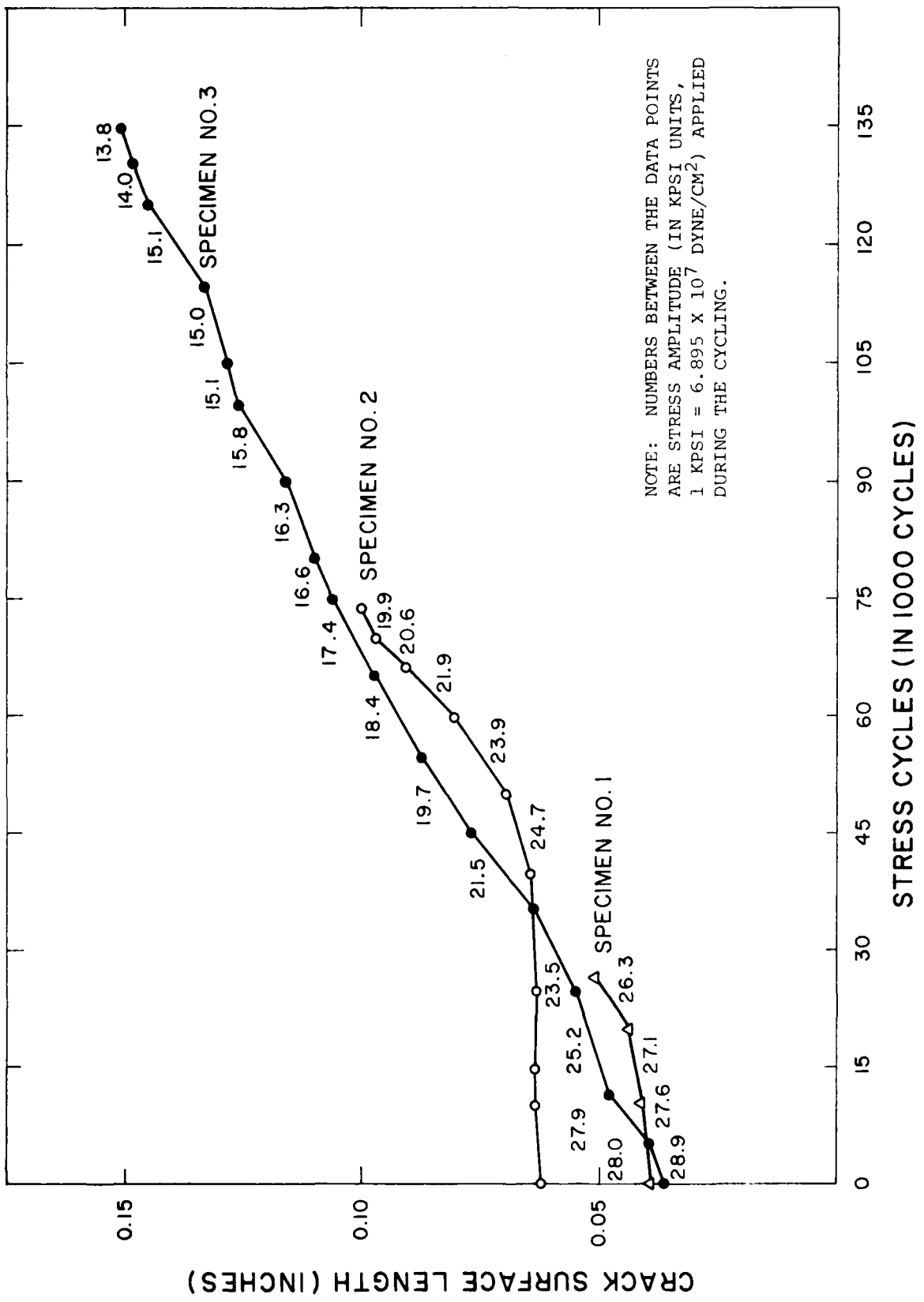


FIGURE D-2. CRACK SURFACE LENGTH VS. NUMBER OF STRESS CYCLES

## APPENDIX E

## TABLES OF LINEAR CORRELATION COEFFICIENTS

TABLE E-I . . . . FOR 5 MHZ - 0° TRANSDUCERS

TABLE E-II . . . . FOR 5 MHZ - 45° TRANSDUCERS

TABLE E-III . . . . FOR 5 MHZ - 60° TRANSDUCERS

TABLE E-IV . . . . FOR 10 MHZ - 0° TRANSDUCERS

TABLE E-V . . . . FOR 10 MHZ - 45° TRANSDUCERS

TABLE E-VI . . . . AVERAGE LINEAR CORRELATION COEFFICIENTS  
AMONG BEAM, ELECTRICAL IMPEDANCE,  
RF-ECHO, AND FREQUENCY SPECTRUM  
PARAMETERSTABLE E-VII . . . . AVERAGE LINEAR CORRELATION COEFFICIENTS  
BETWEEN BEAM, ELECTRICAL IMPEDANCE,  
RF-ECHO, AND FREQUENCY SPECTRUM  
PARAMETERS AND SENSITIVITY AND  
SIGNAL-TO-NOISE RATIO PARAMETERS

\*Each table from Table E-I to Table E-V is divided  
into three parts:

- 1 is for correlation coefficients among beam,  
electrical impedance, rf-echo, and frequency  
spectrum parameters;
- 2 is for correlation coefficients between beam,  
electrical impedance, rf-echo, and frequency  
spectrum parameters and sensitivity and signal-  
to-noise ratio parameters;
- 3 is for correlation coefficients among sensitivity  
and signal-to-noise ratio parameters.

AD-A101 169

SOUTHWEST RESEARCH INST SAN ANTONIO TEX  
ULTRASONIC TRANSDUCER PERFORMANCE REQUIREMENTS. (U)

JUN 81 H KWUN, G L BURKHARDT, C M TELLER

F/G 14/2

F41609-78-C-1823

NL

UNCLASSIFIED

2 of 2

4D A  
101169

END  
DATE  
FILED  
7-8-1  
DTIC

TABLE E-I. LINEAR CORRELATION COEFFICIENTS FOR 5 MHz-0° TRANSDUCERS

TABLE E-I-1

CF	BWR	SSR	SIR	DMP	IMP	IPA	FFR	EBA	BDA	BSR	BIR	EBW
PF	0.91	-0.12	0.35	0.09	0.45	0.03	-0.03	0.44	-0.02	0.07	0.02	0.21
CF	0.04	0.35	0.02	0.44	-0.05	-0.10	0.46	-0.17	0.01	0.04	-0.06	0.17
BWR	-0.07	-0.03	-0.59	-0.12	-0.31	-0.19	0.10	0.04	0.01	0.01	0.00	-0.07
SSR	0.46	0.10	-0.09	0.14	0.25	0.40	-0.40	-0.08	0.26	0.20	0.02	
SIR	-0.17	-0.10	0.02	-0.10	-0.23	0.03	-0.23	0.03	-0.03	-0.09	-0.12	
DMP	-0.12	0.12	0.21	-0.23	-0.05	-0.05	-0.05	-0.05	0.03	0.03	0.06	
IMP		0.06	0.04	0.07	0.19	-0.19	0.12	-0.12	-0.09			
IPA		0.03	-0.10	-0.23	0.27	0.31	-0.09					
FFR			-0.12	0.51	0.18	-0.23	0.73					
EBA				0.03	-0.11	-0.28	-0.03					
BDA					0.07	-0.59	0.93					
BSR						0.12	0.10					
BIR							-0.51					

TABLE E-I-2

	PF	CF	BWR	SSR	SIR	DMP	IMP	IPA	FFR	EBA	BDA	BSR	BIR	EBW
LSR	-0.49	-0.54	-0.18	-0.23	-0.12	-0.22	0.18	0.28	-0.28	0.19	0.10	-0.09	-0.25	0.10
SDH	-0.40	-0.53	-0.39	-0.26	-0.16	0.02	0.03	0.59	-0.33	0.22	-0.15	0.19	-0.02	-0.15
FR3	-0.43	-0.53	-0.23	-0.29	-0.20	-0.12	-0.07	0.46	-0.31	0.17	0.03	0.11	-0.04	0.03
SNR	0.11	0.29	0.32	0.09	-0.18	0.14	0.07	-0.38	-0.09	-0.08	-0.04	-0.01	-0.02	-0.11
FN3	0.21	0.27	-0.10	0.06	-0.22	0.29	0.14	0.03	-0.09	-0.05	-0.40	0.04	0.18	-0.34

TABLE E-I-3

	SDH	FR3	SNR	FN3
LSR	0.75	0.84	-0.26	-0.18
SDH		0.83	-0.41	-0.10
FR3			-0.40	-0.04
SNR				0.48

TABLE E-II. LINEAR CORRELATION COEFFICIENTS FOR 5 MHz-45° TRANSDUCERS

TABLE E-II-1												EBW	SA	
CF	BWR	SSR	SIR	DMP	IMP	IPA	FFR	EBA	BDA	BSR	BIR	EBW	SA	
PF	0.97	-0.48	0.55	0.11	0.39	0.03	0.00	0.54	0.03	-0.53	0.04	-0.02	-0.31	0.07
CF	-0.47	0.49	0.10	0.36	-0.02	-0.01	0.56	0.00	-0.57	0.01	0.01	-0.33	0.05	
BWR	-0.10	-0.19	-0.69	0.07	-0.20	-0.51	-0.08	0.34	-0.02	-0.18	-0.12	0.20		
SSR	-0.13	0.38	-0.04	-0.22	0.19	0.02	-0.42	-0.04	-0.42	-0.33	-0.29	0.33		
SIR	-0.15	0.02	0.25	-0.03	0.03	0.10	0.22	0.53	0.53	0.35	-0.29			
DMP	-0.18	0.29	0.38	0.33	-0.41	-0.27	-0.15	0.03	0.08					
IMP	-0.36	-0.12	-0.30	0.35	0.13	-0.03	0.18	0.07						
IPA	0.18	0.27	-0.03	-0.23	0.16	0.24	0.02							
FFR	-0.15	-0.53	-0.15	0.00	-0.01	0.18	-0.04	-0.17	0.10					
EBA		-0.13	-0.18	0.05	0.19	0.56	-0.14							
BDA				0.36	0.05	0.02								
BSR					0.38	-0.08								
BIR						0.03								
EBW														

TABLE E-III-2

	PF	CF	BWR	SSR	SIR	DMP	IMP	IPA	FFR	EBA	BDA	BSR	BIR	EBW	SA
LSR	0.00	0.04	-0.54	-0.26	0.28	0.48	-0.36	0.56	0.05	0.48	-0.09	-0.20	0.31	0.20	-0.26
SDH	0.05	0.08	-0.57	-0.17	0.20	0.49	-0.28	0.37	0.02	0.46	-0.08	-0.23	0.15	0.19	-0.32
FR1	0.10	0.14	-0.57	-0.22	0.27	0.45	-0.35	0.49	0.08	0.44	-0.22	-0.15	0.27	0.11	-0.27
FR2	0.18	0.22	-0.59	0.00	0.06	0.61	-0.31	0.51	0.17	0.43	-0.31	-0.24	0.08	-0.01	-0.05
FR3	0.05	0.08	-0.53	-0.18	0.22	0.49	-0.29	0.58	0.06	0.50	-0.16	-0.28	0.21	0.10	-0.17
SNR	-0.40	-0.41	-0.06	-0.27	0.04	0.03	0.05	0.30	-0.18	-0.08	0.33	-0.15	0.22	0.35	-0.15
FN1	-0.05	-0.09	-0.12	-0.07	0.01	-0.03	0.09	0.13	-0.01	-0.33	0.28	0.20	0.05	0.23	-0.23
FN2	-0.04	-0.10	-0.09	0.33	-0.38	0.30	-0.01	0.05	0.13	-0.15	-0.04	-0.08	-0.35	-0.03	0.20
FN3	-0.22	-0.26	-0.03	-0.04	0.02	0.11	0.08	0.39	-0.10	-0.07	0.41	-0.13	0.01	0.37	-0.08

TABLE E-III-3

	SDH	FR1	FR2	FR3	SNR	FN1	FN2	FN3
LSR	0.93	0.96	0.86	0.94	0.39	0.12	-0.04	0.23
SDH	0.92	0.83	0.89	0.34	0.10	-0.07	0.19	
FR1	0.90	0.94	0.33	0.10	-0.02	0.15		
FR2		0.91	0.28	0.10	0.26	0.20		
FR3			0.38	0.07	0.03	0.28		
SNR				0.62	0.36	0.75		
FN1					0.60	0.73		
FN2						0.54		

TABLE E-III. LINEAR CORRELATION COEFFICIENTS FOR 5 MHz-60° TRANSDUCERS

TABLE E-III-1

	CF	BWR	SSR	SIR	DMP	IMP	IPA	FFR	EBA	BDA	BSR	BIR	EBW	SA
PF	0.90	-0.33	0.18	-0.11	0.33	0.44	-0.25	0.25	0.14	-0.26	-0.07	-0.16	-0.28	-0.21
CF	-0.37	0.22	-0.12	0.29	0.42	-0.23	0.28	0.04	-0.33	-0.12	-0.04	-0.31	-0.13	
BWR	0.37	-0.16	-0.69	-0.17	-0.30	-0.36	0.40	0.54	-0.11	-0.18	0.07	0.07	0.00	
SSR	-0.06	-0.17	0.16	-0.36	0.01	0.53	0.11	-0.25	-0.19	-0.02	0.07			
SIR	0.33	0.05	0.28	0.15	-0.12	-0.43	-0.43	-0.03	0.11	0.09	-0.09			
DMP		0.49	0.29	0.31	-0.50	-0.55	0.10	-0.19	-0.10	-0.10	-0.13			
IMP			-0.13	0.13	-0.07	-0.30	-0.34	-0.26	-0.26	-0.36	-0.07			
IPA				0.15	-0.46	-0.16	0.22	0.02	0.40	0.17				
FFR					-0.10	-0.56	-0.22	-0.04	0.18	0.00				
EBA						0.26	-0.39	-0.03	0.06	-0.17				
BDA							0.11	0.23	0.22	0.15				
BSR								0.33	0.04	-0.06				
BIR									0.13	0.20				
EBW										-0.21				

TABLE E-III-2

	PF	CF	BWR	SSR	SIR	DMP	IMP	IPA	FFR	EBA	BDA	BSR	BIR	EBW	SA
LSR	-0.25	-0.23	-0.03	-0.15	-0.20	-0.28	-0.45	0.21	-0.05	-0.09	0.24	-0.12	0.11	0.36	0.22
SDH	-0.15	0.19	0.05	-0.27	-0.50	-0.35	-0.02	-0.21	0.23	0.45	-0.24	0.14	0.34	0.11	
FR2	-0.19	-0.13	-0.16	-0.18	-0.15	-0.11	-0.30	0.25	0.11	-0.22	0.05	-0.14	0.02	0.38	0.07
FR3	-0.23	-0.19	-0.12	-0.23	-0.14	-0.18	-0.32	0.26	0.08	-0.19	0.13	-0.15	0.08	0.34	0.15
SNR	0.04	0.11	-0.18	-0.05	-0.09	-0.07	-0.13	0.41	0.12	-0.22	0.10	-0.05	0.03	0.18	0.43
FN2	-0.06	-0.02	-0.20	-0.21	-0.07	0.08	0.02	0.51	0.29	-0.40	-0.12	-0.19	-0.19	0.26	0.18
FN3	-0.16	-0.12	-0.13	-0.25	0.03	0.05	-0.09	0.66	0.31	-0.42	0.00	-0.05	-0.03	0.27	0.39

TABLE E-III-3

	SDH	FR2	FR3	SNR	FN2	FN3
LSR	0.88	0.89	0.93	0.70	0.64	0.55
SDH		0.78	0.82	0.56	0.50	0.35
FR2		0.97	0.63	0.75	0.53	
FR3			0.69	0.75	0.60	
SNR				0.78	0.80	
FN2					0.86	

TABLE E-IV. LINEAR CORRELATION COEFFICIENTS FOR 10 MHz-0° TRANSDUCERS

TABLE E-IV-1

	CF	BWR	SSR	SIR	DMP	IMP	IPA	FFR	EBA	BDA	BSR	BIR	EBW
PF	0.92	-0.52	0.26	-0.04	0.35	0.06	0.19	0.07	-0.26	-0.18	0.01	-0.01	0.32
CF	-0.60	0.23	-0.01	0.36	0.10	0.41	0.16	-0.45	-0.19	0.08	0.01	0.01	0.34
BWR	-0.04	0.15	-0.70	-0.20	-0.31	0.15	0.25	0.18	0.03	0.03	0.06	-0.18	
SSR	-0.31	0.04	-0.27	-0.21	-0.08	0.01	-0.08	0.01	-0.08	0.00	0.00	0.00	0.13
SIR	-0.25	0.02	0.05	-0.22	-0.22	-0.22	0.40	0.40	0.19	0.19	0.23	-0.23	-0.11
DMP		0.17	0.26	-0.17	-0.11	0.02	-0.24	0.00	-0.24	0.00	0.00	0.23	
IMP		0.12	-0.03	-0.17	0.05	0.05	0.15	0.15	0.15	0.14	0.14	-0.05	
IPA		0.30	-0.45	-0.45	-0.15	0.16	0.16	0.12	0.12	0.12	0.21		
FFR		-0.15	-0.35	0.20	-0.20	-0.03	0.29						
EBA			0.08	-0.12	0.13	-0.01							
BDA				0.05	0.04	0.35							
BSR				0.11	0.00								
BIR				-0.03									

TABLE E-IV-2

	PF	CF	BWR	SSR	SIR	DMP	IMP	IPA	FFR	EBA	BDA	BSR	BIR	EBW
LSR	0.46	0.45	-0.50	0.05	-0.08	0.30	0.05	0.33	-0.17	-0.24	-0.14	-0.09	-0.04	0.26
SDH	0.52	0.57	-0.45	0.18	-0.13	0.35	-0.04	0.38	-0.11	-0.33	-0.17	-0.13	-0.08	0.24
FR2	0.63	0.67	-0.53	0.14	-0.25	0.37	0.01	0.38	-0.02	-0.31	-0.29	-0.21	-0.21	0.19
FR3	0.61	0.67	-0.52	0.11	-0.17	0.31	-0.02	0.43	0.01	-0.37	-0.34	-0.17	-0.17	0.18
SNR	0.41	0.48	-0.52	-0.11	0.02	0.35	0.08	0.54	-0.23	-0.25	-0.15	-0.26	0.19	0.05
FN2	0.63	0.66	-0.40	0.10	-0.19	0.36	0.01	0.48	0.05	-0.39	-0.31	-0.22	-0.02	0.13
FN3	0.53	0.57	-0.35	0.10	-0.21	0.25	-0.03	0.53	0.09	-0.27	-0.49	-0.16	-0.06	0.04

TABLE E-IV-3

	SDH	FR2	FR3	SNR	FN2	FN3
LSR	0.89	0.84	0.84	0.74	0.62	0.50
SDH	0.92	0.92	0.76	0.75	0.63	
FR2		0.98	0.72	0.83	0.73	
FR3			0.76	0.87	0.79	
SNR				0.74	0.67	
FN2					0.91	

TABLE E-V. LINEAR CORRELATION COEFFICIENTS FOR 10 MHz-45° TRANSDUCERS

TABLE E-V-1

	CF	BWR	SSR	SIR	DMP	IMP	IPA	FFR	EBA	BDA	BSR	BIR	EBW	SA
PF	0.88	-0.48	0.43	0.42	0.55	0.74	0.46	0.10	-0.02	0.01	-0.17	0.09	0.13	-0.06
CF		-0.64	0.47	0.36	0.71	0.69	0.64	0.14	0.28	0.09	-0.09	0.13	0.23	0.05
BWR			-0.21	-0.27	-0.83	-0.32	-0.76	-0.15	-0.62	-0.28	-0.03	-0.10	0.52	-0.39
SSR				0.43	0.27	0.51	0.17	-0.24	-0.19	0.17	-0.16	0.00	0.22	0.13
SIR					0.19	0.50	0.33	-0.32	-0.04	0.00	-0.38	0.07	-0.26	-0.03
DMP						0.37	0.80	0.17	0.52	0.26	0.11	0.18	0.44	0.23
IMP							0.35	0.06	0.03	0.21	-0.31	0.10	0.11	-0.03
IPA								-0.01	0.66	0.27	-0.05	0.26	0.24	0.12
FFR									0.17	-0.26	-0.11	-0.27	0.13	-0.08
EBA										0.18	0.03	0.31	0.22	0.18
BDA											0.33	0.10	0.65	0.05
BSR												0.11	0.35	0.08
BIR													-0.04	0.24
EBW														0.34

TABLE E-V-2

	PF	CF	BWR	SSR	SIR	DMP	IMP	IPA	FFR	EBA	BDA	BSR	BIR	EBW	SA
LSR	-0.16	0.05	-0.30	-0.37	-0.06	0.27	-0.22	0.50	0.16	0.72	0.07	0.04	0.13	0.03	-0.09
SDH	-0.12	-0.13	0.06	-0.42	0.07	0.02	-0.31	0.30	-0.14	0.29	-0.14	-0.05	0.16	-0.28	-0.30
FRI	-0.09	0.01	-0.01	-0.47	-0.09	0.11	-0.30	0.31	0.11	0.40	-0.12	0.08	0.14	-0.22	-0.43
FR2	0.07	0.12	-0.04	-0.37	-0.07	0.15	-0.22	0.32	0.13	0.34	-0.20	0.00	0.10	-0.20	-0.38
FR3	-0.01	0.14	-0.12	-0.36	-0.03	0.24	-0.22	0.49	0.04	0.51	-0.08	0.08	0.19	-0.18	-0.28
SNR	-0.06	-0.11	0.19	-0.37	-0.06	-0.07	-0.18	0.02	-0.03	0.08	0.05	0.16	-0.03	-0.23	-0.44
FN1	-0.18	-0.15	0.25	-0.47	-0.15	-0.14	-0.31	0.11	-0.03	0.13	-0.14	0.02	0.03	-0.35	-0.57
FN2	-0.10	-0.20	0.34	-0.38	-0.26	-0.19	-0.25	-0.15	0.05	-0.09	-0.29	0.03	-0.10	-0.39	-0.43
FN3	0.18	0.05	0.37	-0.28	-0.18	-0.17	-0.04	-0.14	0.14	-0.23	-0.29	-0.06	-0.07	-0.35	-0.53

TABLE E-V-3

	SDH	FR1	FR2	FR3	SNR	FN1	FN2	FN3
LSR	0.71	0.78	0.73	0.84	0.44	0.51	0.22	0.12
SDH	0.83	0.81	0.81	0.46	0.63	0.38	0.29	
FR1		0.94	0.94	0.64	0.82	0.55	0.52	
FR2		0.91	0.68	0.76	0.65	0.59		
FR3			0.60	0.71	0.49	0.45		
SNR				0.74	0.77	0.64		
FN1					0.74	0.71	0.71	
FN2						0.79		

TABLE E-VI. AVERAGE LINEAR CORRELATION COEFFICIENTS AMONG BEAM,  
ELECTRICAL IMPEDANCE, RF-ECHO, AND FREQUENCY SPECTRUM  
PARAMETERS

	CF	BWR	SSR	SIR	DMP	IMP	IPA	FFR	EBA	BDA	BSR	BIR	EBW	SA
PF	+16 (+0.34)	-0.386 (+0.166)	0.354 (+0.144)	0.094 (+0.204)	0.414 (+0.089)	0.260 (+0.320)	0.074 (+0.266)	0.280 (+0.207)	-0.026 (+0.146)	-0.178 (+0.239)	-0.024 (+0.097)	-0.016 (+0.091)	0.014 (+0.290)	-0.067 (+0.140)
CF	-0.408 (+0.272)	0.352 (+0.128)	0.070 (+0.180)	0.432 (+0.164)	0.228 (+0.318)	0.142 (+0.367)	0.320 (+0.185)	-0.060 (+0.271)	-0.198 (+0.266)	-0.016 (+0.086)	0.010 (+0.074)	0.020 (+0.316)	-0.010 (+0.104)	
BWR	-0.010 (+0.222)	-0.100 (+0.164)	-0.700 (+0.085)	-0.148 (+0.142)	-0.376 (+0.220)	-0.212 (+0.248)	0.010 (+0.395)	0.164 (+0.310)	-0.024 (+0.054)	-0.080 (+0.108)	0.044 (+0.282)	-0.063 (+0.300)		
SSR	0.078 (+0.347)	0.124 (+0.213)	0.054 (+0.297)	-0.096 (+0.237)	0.026 (+0.200)	-0.006 (+0.345)	-0.060 (+0.230)	-0.038 (+0.194)	-0.064 (+0.203)	0.012 (+0.193)	0.012 (+0.193)	0.177 (+0.136)		
SIR	-0.010 (+0.254)	0.098 (+0.232)	0.186 (+0.142)	-0.104 (+0.180)	-0.116 (+0.113)	0.020 (+0.297)	-0.006 (+0.240)	0.170 (+0.232)	-0.010 (+0.237)	-0.010 (+0.237)	-0.010 (+0.136)			
DMP	0.146 (+0.294)	0.352 (+0.260)	0.180 (+0.212)	0.002 (+0.417)	-0.146 (+0.330)	-0.070 (+0.181)	-0.026 (+0.149)	-0.026 (+0.149)	0.132 (+0.209)	0.132 (+0.181)	0.060 (+0.181)			
IMP	0.008 (+0.268)	0.016 (+0.095)	-0.088 (+0.151)	0.024 (+0.270)	-0.112 (+0.237)	0.014 (+0.167)	-0.042 (+0.210)	-0.042 (+0.210)	-0.010 (+0.072)					
IPA	0.130 (+0.124)	-0.016 (+0.483)	0.002 (+0.198)	-0.060 (+0.209)	0.074 (+0.115)	0.174 (+0.115)	0.200 (+0.179)	0.200 (+0.179)	0.103 (+0.076)					
FFR	-0.070 (+0.136)	-0.248 (+0.436)	-0.020 (+0.196)	-0.114 (+0.126)	-0.114 (+0.282)	0.264 (+0.282)	0.033 (+0.133)	0.033 (+0.133)						
EBA	0.084 (+0.149)	-0.154 (+0.153)	0.018 (+0.219)	0.014 (+0.142)	0.014 (+0.183)	0.037 (+0.070)								
BDA	0.122 (+0.119)	-0.006 (+0.335)	0.542 (+0.275)	0.020 (+0.127)	0.122 (+0.140)	0.108 (+0.127)	0.013 (+0.183)	0.013 (+0.183)						
BSR	0.206 (+0.127)	0.122 (+0.335)	-0.006 (+0.275)	0.542 (+0.174)	0.206 (+0.140)	0.108 (+0.140)	0.013 (+0.070)	0.013 (+0.070)						
BIR	-0.014 (+0.325)	-0.006 (+0.276)	0.542 (+0.174)	0.206 (+0.140)	0.122 (+0.140)	0.108 (+0.140)	0.120 (+0.174)	0.120 (+0.174)						
EBW	0.053 (+0.276)	0.053 (+0.276)	0.020 (+0.174)	0.013 (+0.183)	0.053 (+0.174)	0.053 (+0.174)	0.020 (+0.174)	0.020 (+0.174)						

\*N.B.: X.F. = Average standard deviations.

TABLE E-VII. AVERAGE LINEAR CORRELATION COEFFICIENTS BETWEEN BEAM, ELECTRICAL IMPEDANCE, RF-ECHO, AND FREQUENCY SPECTRUM PARAMETERS AND SENSITIVITY AND SIGNAL-TO-NOISE RATIO PARAMETERS

	PF	CF	BWF	SSP	SIR	DMF	IMP	IPA	FFR	EBA	BDA	BSR	BIR	EBW	SA
Sensitivity Parameters	.3.057 (+.325)	.3.039 (+.354)	-.0.291 (+.247)	-.5.173 (+.191)	-.049 (+.168)	.6.155 (+.302)	-.6.197 (+.171)	.0.380 (+.146)	-.0.029 (+.157)	.0.173 (+.335)	-.0.068 (+.192)	-.0.095 (+.132)	.0.061 (+.151)	0.096 (+.205)	-.0.143 (+.212)
Signal-to-Noise Ratio Parameters	.6.653 (+.286)	.0.061 (+.311)	-.5.544 (+.271)	-.6.114 (+.216)	-.9.117 (+.124)	0.081 (+.187)	-.0.031 (+.130)	.6.218 (+.302)	.6.026 (+.152)	-.0.176 (+.166)	-.0.069 (+.260)	-.0.057 (+.129)	-.0.010 (+.141)	0.005 (+.269)	-.0.112 (+.366)

\*Numbers in parenthesis are standard deviations.

## APPENDIX F

PRELIMINARY TEST METHODS AND SPECIFICATIONS (ACCEPTANCE LIMITS)  
FOR ULTRASONIC TRANSDUCER PERFORMANCE PARAMETERS

## 1. Scope

These test methods and specifications provide practical guidance for evaluating ultrasonic transducer parameters which are important in determining overall quality and performance of transducers. Unless otherwise stated, they apply to both angle beam probes (usually shear wave) and straight beam probes (usually longitudinal wave) used in contact with surfaces which are essentially flat. (Thus, these test methods and specifications are not for focused probes). The specifications are primarily intended for procurement of ultrasonic transducers in the 5 and 10 MHz range having piezoelectric elements of 6.35 mm (equivalently 0.25 in.) diameter (or similar area) routinely used in Air Force Nondestructive Inspection (NDI). A glossary of terms used in the specifications is included.

## 2. References

Technical Manual T.O. 33B-1-1, "Nondestructive Inspection Method", (1979).

ASTM E-317, "Standard Recommended Practice for Evaluating Performance Characteristics of Ultrasonic Pulse-Echo Testing Systems Without the Use of Electronic Measurement Instruments", (1979).

Battelle Northwest Specifications 705-7, "Equipment Specification for Portable Pulse-Echo Ultrasonic NDE Equipment", (1980).

British Standards (BS):

BS 2704, "Calibration Blocks for Use in Ultrasonic Flaw Detection", (1978).

BS 3683, "Glossary of Terms Used in Nondestructive Testing"

Part 4, "Ultrasonic Flaw Detection", (1965)

BS 4331, "Methods for Assessing the Performance Characteristics of Ultrasonic Flaw Detection Equipment"

Part 1, "Overall Performance: On-Site Methods", (1978)

Part 2, "Electrical Performance", (1972).

Part 3, "Guidance on the In-Service Monitoring of Probes (Excluding Immersion Probes)", (1974).

International Institute of Welding, "Handbook on the Ultrasonic Examination of Welds", (1977).

Final Report on SwRI Project 15-5468 (Contract No. F41608-78-C-1823),  
"Ultrasonic Transducer Performance Requirements - Phase II", (1981).

### 3. Transducer Quality and Performance Parameters

Overall Appearance  
Beam Exit Point (or Index Point)  
Beam Angle  
Skew Angle (or Beam Alignment)  
Beam Divergence Angle  
Center Frequency  
Pulse Envelope and Pulse Length  
Dead Zone  
Signal-to-Noise Ratio  
Overall System Sensitivity

\* In testing ultrasonic transducer parameters, use is exclusively made of the conventional pulse-echo amplitude measuring method. Since overall performance of the probe is influenced by the flaw detector employed, the use of a standard flaw detector is mandatory. A standard flaw detector is required to have at least following characteristics: a) be capable of generating initial excitation pulse of duration (defined as the time interval over which the pulse amplitude exceeds 10% of its maximum amplitude) less than or equal to 0.5  $\mu$ sec. and unipolar voltage (base to peak) of at least 200 V into 50 ohm external resistive load, b) have either wide band receiver or narrow band receiver operable at 5 and 10 MHz, c) have calibrated receiver gain (or attenuation) of at least 60 dB dynamic range which is adjustable by no more than 2 dB steps, d) have display screen of which vertical and horizontal linearities are within specifications (cf. T.O. 33B-1-1, paragraph 2-78 and 2-79), and e) provide calibrated sweep speeds of at least 100, 50, 20, 10, 5, 2, 1 and 0.5  $\mu$ sec. per division. If a noise suppression control (sometimes called "reject" control) is provided, it shall be set to zero. To ensure that the effects of coupling the probe to the testing block are minimized, it is recommended to repeat the measurement twice.

\*\* The duration of the initial excitation pulse of the standard flaw detector may vary when it is connected to a probe (or transducer). Therefore the duration of the initial excitation pulse must be measured with the transducer connected. In order to do this, connect a "T" connector to the pulser output and, using a 10X or 100X oscilloscope probe, display the initial excitation pulse on an oscilloscope having a bandwidth of 20 MHz or greater. If the duration of the initial excitation pulse exceeds 0.5  $\mu$ sec, then it must be reduced to 0.5  $\mu$ sec or less by either adding an external resistive load (for example 50 ohm) in parallel with the probe or by adjusting the pulse length or damping controls of the pulser. This setup should be maintained throughout the tests described in this specification.

\*\*\* Among the parameters, Overall Appearance, Beam Exit Point, Beam Angle, Skew Angle and Center Frequency primarily determine the quality of workmanship rather than the performance of a probe. Beam Exit Point, Beam Angle, or Skew Angle are very important for locating the position of a flaw. However, as

long as the sound beam directivity is not critical, substantial departure (several degrees) from nominal values of these parameters has little measurable effect on the signal-to-noise ratio of a flaw echo. Minimum detectable flaw size is dependent of Center Frequency of the beam. However, substantial departure of Center Frequency (approximately 10%) from the nominal frequency also has little effect on the flaw detectability of a probe. Nevertheless, controlling these parameters is believed to reduce unnecessary variations in testing results and thus enhances the uniformity of the results.

#### 4. Overall Appearance

##### 4.1 Method

4.1.1 The probe shall be examined visually to check for any signs of mechanical damage (such as dents, pits or severe scratches) and/or misalignment of the probe wedge with respect to the case (Fig. F-1).

4.1.2 The probe wedge contacting surface shall be examined for flatness. Put a straightedge across the center of the probe. Hold the probe and straight edge against a light source while rotating the straightedge successively in two mutually perpendicular directions. Check any bright places with a depth gauge (e.g. feeler gauge, measuring microscope, etc.).

4.1.3 Angle of misalignment with respect to the probe case (Fig. F-1, a, c and d) shall be measured with a protractor. Centering of the wedge with respect to the case (Fig. F-1,b) shall be measured with a graduated scale.

##### 4.2 Specification (or acceptance limit)

4.2.1 There shall be no evidence of mechanical damage.

4.2.2 Except for probe edge chamfer, there shall be no gaps greater than 0.05 mm between the straightedge and the probe face.

\* 0.05 mm is approximately one-fifth the wave length of the 10 MHz longitudinal wave in a plastic wedge or wearplate. Note that the surface can be regarded as smooth if the surface irregularities are less than one-third the wave length.

4.2.3 Angle of misalignment with respect to the case shall not exceed 2°. Center of the probe wedge shall be within 1 mm of that of the case.

#### 5. Beam Exit Point (or Index Point)

5.1 The position of the beam exit (for an angle beam probe) shall be determined before any measurement of beam angle is attempted. The beam exit point shall be engraved on each side of the probe body (or case).

##### 5.2 Method

5.2.1 It is recommended that IIW block, Type 1 or 2, (equivalent to British Standard A2 block) be used (Fig. F-2).

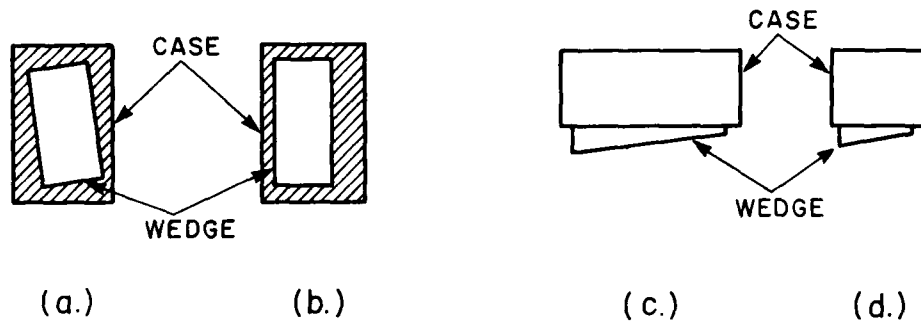
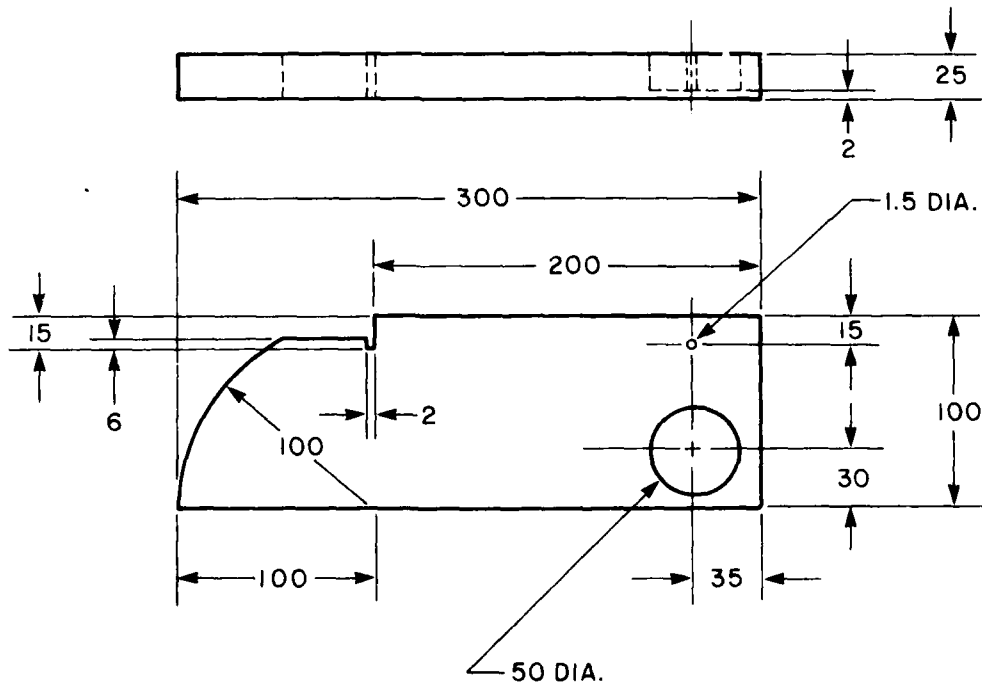


FIGURE F-1. EXAMPLES OF PROBE WEDGE MISALIGNMENT



NOTE: ALL DIMENSIONS IN MILLIMETRES

FIGURE F-2. IIW BLOCK - TYPE 1

5.2.2 Place the probe at the center of the 100 mm radius quadrant of IIW block. Keeping the probe parallel to the edge of the block, adjust the position of the probe until the echo directly from the 100 mm radius quadrant is maximized. The beam exit point of the probe corresponds with the engraved line on the block which marks the center of the 100 mm radius quadrant.

\* Conversely, the quality of a reference IIW block can be checked with a probe of known beam exit point. If the beam exit point measured on a given IIW block is considerably different from the known, it is an indicative of poor quality of the block.

### 5.3 Specification

The measured position of the probe beam exit point shall be repeatable within  $\pm 1$  mm of the engraved mark.

## 6. Beam Angle

### 6.1 Method

#### 6.1.1 Angle Beam Probe

Beam exit point shall be determined prior to this measurement. Place the probe on IIW block so that a direct echo is obtained from the 50 mm diameter hole. By scanning the probe along the side of the block, maximize the echo from the hole. The beam angle is indicated by the position of the beam exit point against the scale engraved on the side of the block.

\* If the maximum echo signal is not obtained with the edge of the probe parallel to the edge of the block, this may indicate significant beam skew (see Clause 7).

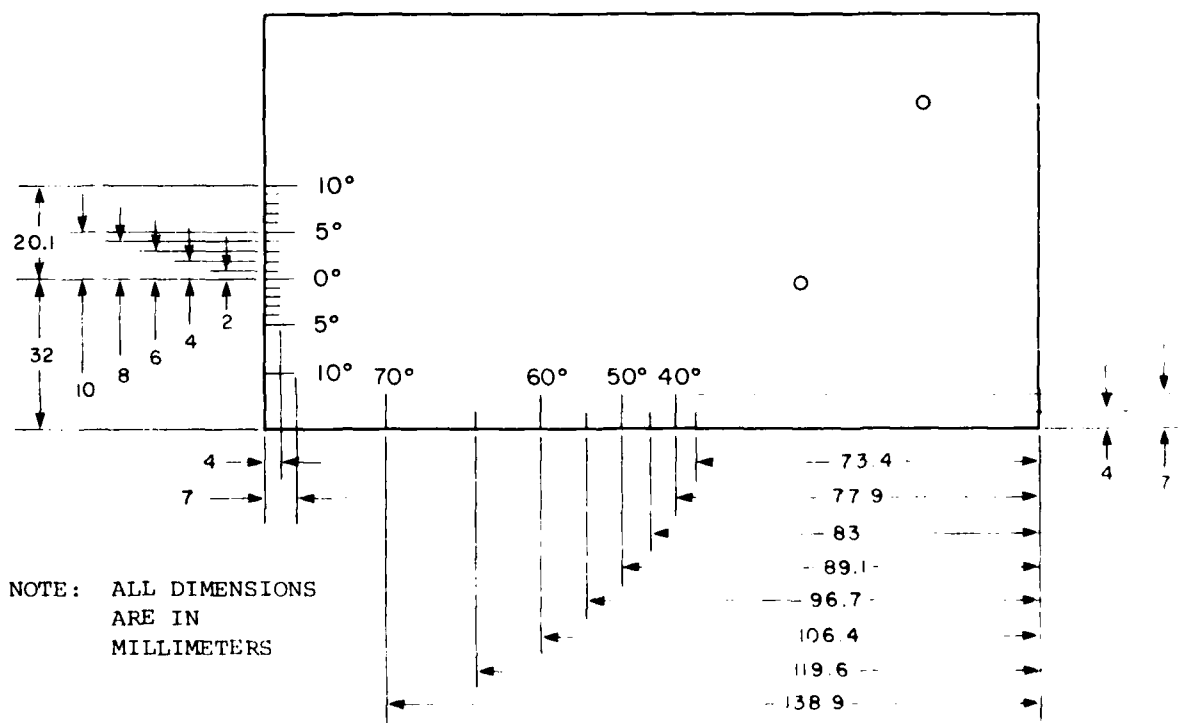
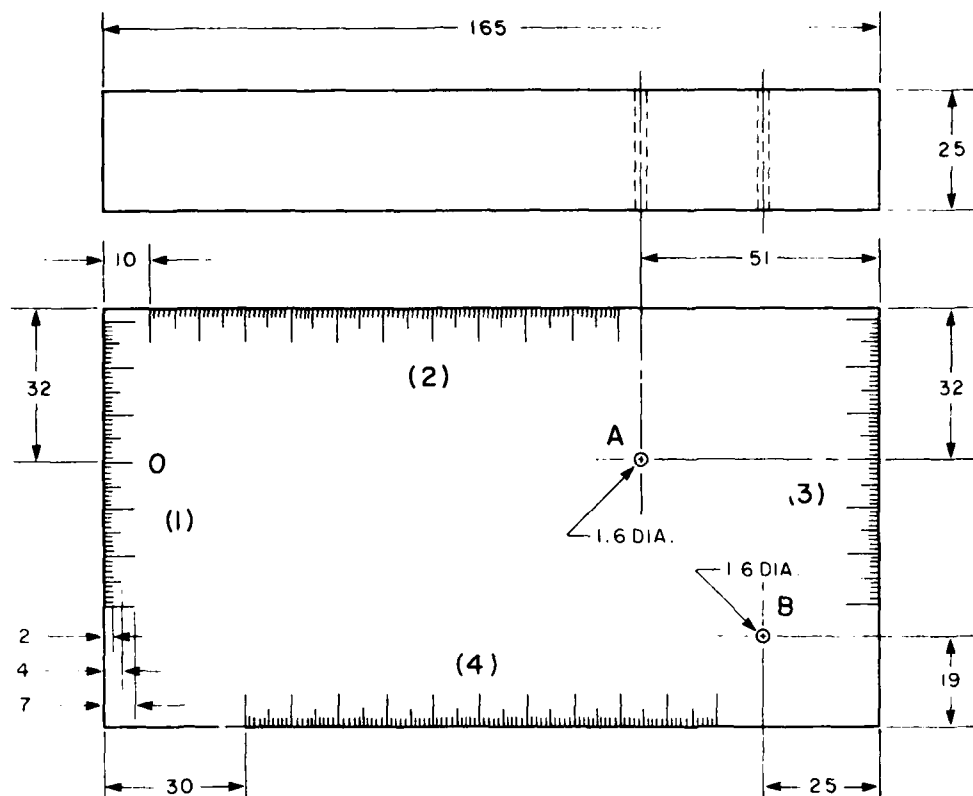
#### 6.1.2 Straight Beam Probe

It is recommended that a block such as shown in Fig. F-3 be used. Place the probe on side (1) of the block which is farthest from the Hole A. Position the probe directly above the hole (reference point 0). Rotate the probe continuously through an angle of 90° and determine the orientation of the probe at which the echo from the hole is minimum (this will direct the sound beam through the center portion of the thickness of the block). While maintaining this orientation, scan the probe across the hole until a maximum echo signal is received from the hole. The beam angle is indicated by the position of the center of the probe against the scale provided on the side of the block.

### 6.2 Specification

#### 6.2.1 Angle Beam Probe

The measured beam angle shall be within  $\pm 2^\circ$  of the nominal beam angle.



NOTE: ALL DIMENSIONS  
ARE IN  
MILLIMETERS

FIGURE F-3. BLOCK FOR MEASURING BEAM ANGLE OF  
STRAIGHT BEAM TRANSDUCER

\* Since beam angle depends on the velocity of sound in the test block, one should either measure the beam angle on the block made of the same material as the probe angle was originally referred to or correct the nominal beam angle in the test block by use of Snell's law (Appendix 1). Also, the beam angle depends on the velocity of sound in the probe wedge which is dependent of ambient temperature (BS4331 Part 3, Appendix C). Thus, the beam angle measurement should be carried out within the temperature range prescribed by the manufacturer. In an actual inspection, the beam angle could be significantly different from the nominal value.

#### 6.2.2 Straight Beam Probe

The angle shall not exceed 2°.

### 7. Skew Angle (angle beam probes only)

7.1 Skew angle represents the degree of beam misalignment with respect to the probe axis (see Fig. F-4).

#### 7.2 Method

Place the IIW block flat on one side and adjust the probe to maximize the echo from the lower corner of the block (Fig. F-5). The part of the corner where there are no scale engravings shall be used. Measure the skew angle using a protractor (Fig. F-5).

#### 7.3 Specifications

Skew angle shall not exceed 2°.

### 8. Beam Divergence Angle

8.1 Beam divergence angle is defined as  $\tan^{-1} (BW/2R)$  where BW represents the -6 dB beam width and R is the path length from the probe to the point where beam width is measured. The beam divergence angle determines the angular resolution of the probe (i.e. the resolution of echoes from reflectors lying side by side at approximately the same distance from the probe).

\* Here the -6 dB beam width is chosen arbitrarily and R is assumed to be in the far field region of the probe.

#### 8.2 Method

##### 8.2.1 Straight Beam Probe

It is recommended that a block having side-drilled hole(s) and providing two different accessible distances to the hole from the sides (such as one shown in Fig. F-3) be used. The distances from the probe to the hole shall be longer than the probe's nominal near-to-far field transition distance (which is approximately given by  $D^2/(4\lambda)$  where D is the nominal diameter of piezoelectric element of the probe and  $\lambda$  is the wave length of the sound beam

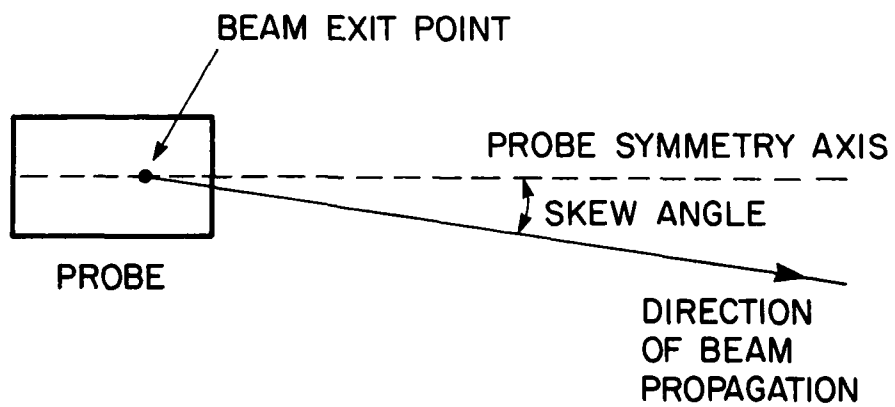


FIGURE F-4. BEAM MISALIGNMENT (SKEW ANGLE)

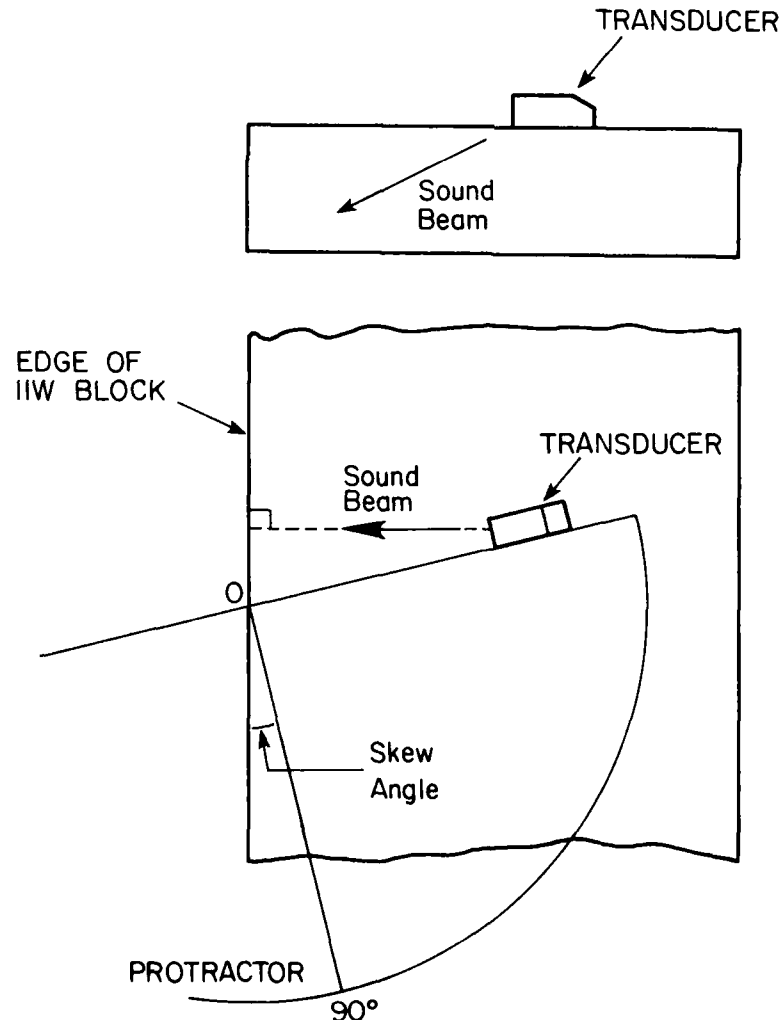


FIGURE F-5. SKEW ANGLE MEASUREMENT

in the block at the nominal frequency of the probe. Wave length  $\lambda$  is equal to  $v/f$  where  $v$  is the velocity of the sound in the block and  $f$  is the nominal frequency of the probe). Place the probe on side (1) of the block and maximize the echo signal from the Hole A as described in Clause 6.1.2. Adjust the gain of flaw detector so that echo height reaches 80% of the full scale of CRT screen. Read (or mark) the position of the center of the probe. Maintaining the orientation of the probe thus obtained, scan the probe across the hole parallel to the edge of the block. When the echo height drops to 40% of the full scale (i.e. -6 dB) on both sides of the maximum, read the respective positions of the center of the probe. The beam divergence angle is determined by the equation given in Clause 8.1 where  $R$  is then the path length from the position of the center of the probe at the maximum echo signal to the side-drilled hole and  $BW$  is the distance between the two -6dB amplitude points. Repeat the same procedures with the probe on side (3) of the block. Average the two values thus obtained.

\* Example:

Suppose the following data are obtained from a straight beam probe.

$R$ (mm)	$x_{max}$ (mm)	$x_{-6dB, left}$ (mm)	$x_{-6dB, right}$ (mm)
113	2	-12	17
50	1	-5	7

where the scale on the left hand side of the reference point is taken as negative (-). Thus, the beam widths are  $17 - (-12) = 29$  (mm) for  $R = 113$  mm and  $7 - (-5) = 12$  (mm) for  $R = 50$  mm. Hence, the beam divergence angle of the probe -  $\theta_D$  is

$$\theta_D = (1/2) (\tan^{-1} (29/(2 \times 113)) + \tan^{-1} (12/(2 \times 50))) = 7.15^\circ.$$

For the value of  $\tan^{-1} x$ , see Table 1.

### 8.2.2 Angle Beam Probe

To perform this measurement, it is recommended that both the beam exit point and the beam angle of the probe be determined first. Place the probe on side (2) of the block and maximize the echo signal from the side-drilled Hole A. Follow the same procedures as described in Clause 8.2.1. and read the position of the beam exit point. The beam divergence angle is determined by the equation  $\tan^{-1} (BW \cos \theta / (2R))$  where  $\theta$  is the measured beam angle of the probe.  $R$  is the path length from the beam exit point of the probe at the maximum echo signal to the side-drilled hole, and  $BW$  is the distance between the two -6dB amplitude points on the block. Repeat the same procedures with the probe on side (4) of the block. (Hole B provides another accessible distance to 60° angle beam probes.) Average the two values thus obtained.

### 8.3 Specification

8.3.1 Beam divergence angle shall not exceed 10% of the theoretical value which is given for the -6 dB beam width by  $\theta_D = \sin^{-1} (0.7 \lambda/D)$ .

\* It should be noted that the beam width measured by utilizing the echo signal from the side-drilled hole is actually different from the beam width obtained if the beam profile is directly measured. This is because the echo height from a side-drilled hole essentially represents an averaged strength of the sound field over a certain fraction of the cross-sectional area of the side-drilled hole, rather than the field strength of a point.

8.3.2 Distances of the left and right -6 dB points from the position of maximum echo signal of the probe shall not differ by more than 10% of the measured beam width.

\* Example: Using the data shown in the previous example, it is determined that the distance between the left -6 dB point and the maximum point is  $2 - (-12) = 14$  (mm) and between the right -6 dB point and the maximum point is  $17 - 2 = 15$  (mm). Thus, the difference between them is  $15 - 14 = 1$  (mm) which is 3.5% of the measured beam width.

### 9. Center Frequency

9.1 It is recommended that the IIW block be used. For angle beam probes the rf-echo from the 100 mm radius quadrant of the block shall be used. For straight beam probes the rf-echo from the opposite face (or back face) of the block, which is also at a distance of 100 mm, shall be used.

\* Small sized reflectors (i.e. smaller than beam cross section) with sharp edges such as flat bottom holes or slots can influence the spectrum of the echo signal via diffraction at the edges. Thus, the use of echoes from these reflectors is not recommended for frequency measurement.

### 9.2 Method

It is recommended that a spectrum analyzer be used with a frequency range of at least 1 to 20 MHz. The reflected rf-echo obtained as described in Clause 9.1 shall be gated with a step-less electronic gating equipment (gating shall not influence the rf-echo). The gate width shall be adjusted to cover the pulse length of the rf-echo (see Fig. F-7 and Clause 10.2). The frequency distribution of this gated rf-echo such as shown in Fig. F-6 shall be displayed on the spectrum analyzer. The center frequency is defined as  $f_c = (f_l + f_u)/2$  where  $f_l$  and  $f_u$  are lower and upper frequencies at which the amplitude drops to one half (-6 dB) the maximum amplitude.

\* Alternately, the tone burst measurement method (Battelle Northwest Specifications 705-7) may be used.

### 9.3 Specification

The center frequency shall be within 10% of the nominal frequency of probe.

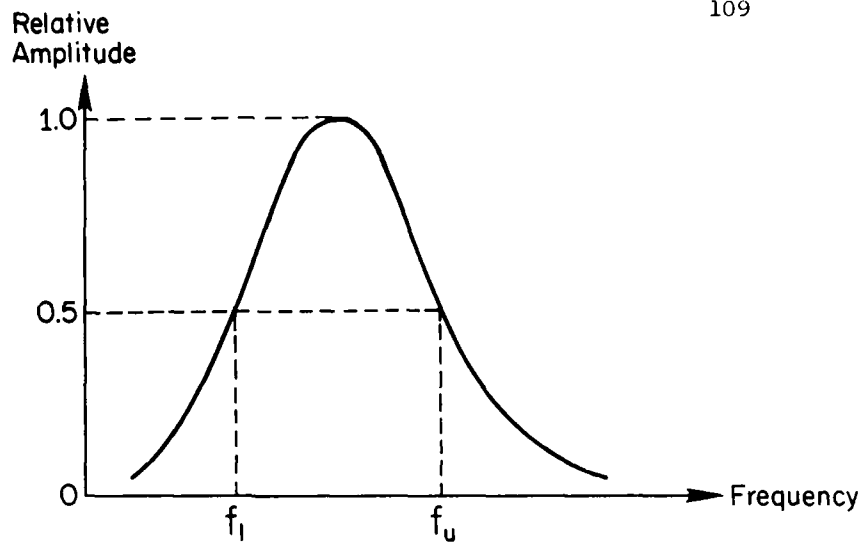


FIGURE F-6. CENTER FREQUENCY MEASUREMENT (EXAMPLE)

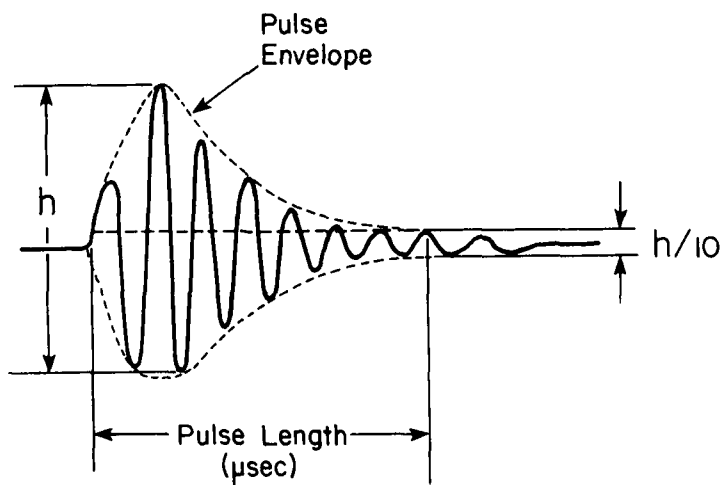


FIGURE F-7. RF-PULSE LENGTH MEASUREMENT (EXAMPLE)

## 10. Pulse Envelope and Pulse Length

10.1 Pulse length determines the depth resolution of the probe.

### 10.2 Method

10.2.1 Display an unrectified rf-echo signal on the screen of a flaw detector as shown in Fig. F-7. It is recommended that the echo obtained by the procedure described in Clauses 9.1 and 9.2.1 be used. The horizontal base of the display screen shall be calibrated against time before the measurement of pulse length. Pulse length is defined as the time interval between the first and last instant at which the amplitude of the pulse reaches 10% of its maximum amplitude. Pulse envelope represents the contour of the envelope of the echo signal.

10.2.2 If the flaw detector does not provide an unrectified echo signal, put a T connector on the pulser output (or receiver input) and connect an oscilloscope probe providing, for example 10X attenuation, 10 megohm, -12 pf loading from 500 kHz to 20 MHz, to the T connector. Display the echo signal on the oscilloscope.

\* A rectified echo signal may be used for the measurement. However, an unrectified echo signal is preferable because a rectified echo signal may conceal potentially important details of the pulse.

\*\* If an actual echo signal exceeds the linear dynamic range of the input of the receiver of a flaw detector, inaccurate measurement of pulse length will result because of nonlinear amplification by the receiver. If this is the case, connect an external attenuator to the receiver so that the echo signal remains within the linear dynamic range of the receiver input.

### 10.3 Specification

10.3.1 Within the pulse length, both the upper and lower pulse envelopes shall increase monotonically to their maximum and then decrease monotonically.

10.3.2 Pulse length shall not exceed 1.5  $\mu$ sec using an initial excitation pulse of up to 0.5  $\mu$ sec duration.

\* As a reference, note that the round trip time of a longitudinal wave over the 6 mm deep slot on IIW block, which is usually used for depth resolution of a straight beam probe (cf. T.O. 33B-1-1), is 2  $\mu$ sec.

## 11. Dead Zone

11.1 The dead zone refers to the region immediately after the time when initial excitation pulse is applied to the probe, in which it is not possible to detect small flaws with certainty. The dead zone is chiefly determined by the damping (or conversely ringing) characteristics of the piezoelectric element of the probe and the internal noises caused by the reflections of the sound within the probe wedge.

## 11.2 Method

### 11.2.1 Straight Beam Probe

To check the duration of the dead zone, it is recommended that the IIW block be used. Place the probe on the block and maximize the echo from the opposite surface 100 mm away. Adjust the gain control so that the echo height is 50% of full scale. Then, increase the gain by 20 dB and measure the time interval between the initial rise of the excitation pulse and the instant at which the amplitude of the excitation pulse tail or internal noises becomes 25% of full scale (Fig. F-8).

### 11.2.2 Angle Beam Probe

Maximize the echo from the 100 mm quadrant of IIW block. The same procedure described in Clause 11.2.1 shall be used with following modification. For 5 MHz probes increase the gain by 20 dB, and for 10 MHz probes increase the gain by 40 dB.

\* Care shall be exercised to keep the echo signal within the linear dynamic range of the receiver input (see \*\* of Clause 10.2).

## 11.3 Specification

### 11.3.1 Straight Beam Probe

The time interval shall not exceed 2.5  $\mu$ sec using an initial excitation pulse of up to 0.5  $\mu$ sec duration.

\* This is roughly equivalent to saying that a longitudinal wave probe which meets this specification would be capable of detecting a perfect planar reflector (whose surface is normal to the incident beam) with a diameter 1/10 that of the probe piezoelectric element, at a depth of 6 mm from the surface of IIW block. The above argument is based on DGS (Distance-Gain-Size) diagram. (Examples of DGS diagram can be found in "Handbook on the Ultrasonic Examination of Welds," International Institute of Welding, 1977.)

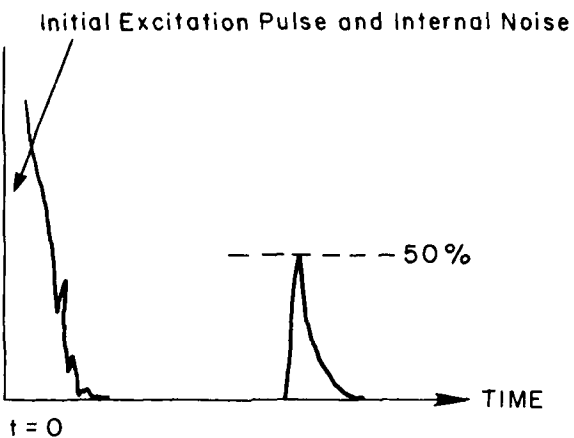
### 11.3.2 Angle Beam Probe

The time interval shall not exceed 8  $\mu$ sec using an initial excitation pulse of up to 0.5  $\mu$ sec duration.

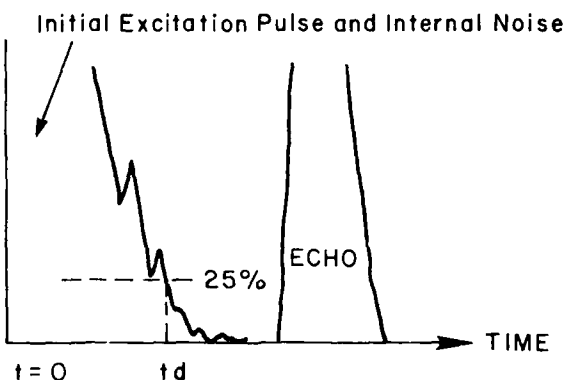
\* This specification takes into account the time elapsed as sound travels through the probe wedge (assumed to be 3  $\mu$ sec.). If one wants to measure the elapsed time in the probe wedge, see Appendix 2. The same statement in \* of Clause 11.3.1 also applies for a shear wave probe to a perfect planar reflector at a distance of 6 mm from the beam exit point.

## 12. Signal-to-Noise Ratio

12.1 This measurement is of particular importance in determining the flaw detectability of the probe.



a) Maximize echo from the opposite surface of the IIW block and adjust the gain control until the echo height reaches 50% of full scale



b) Increase the gain by 20 dB. Then measure  $t_d$  at which excitation pulse tail amplitude becomes 25% of full scale.

FIGURE F-8. DEAD ZONE MEASUREMENT

## 12.2 Method

It is recommended that the IIW block be used. For angle beam probes, the echo from the 100 mm radius quadrant shall be used. For straight beam probes, the echo from the opposite surface 100 mm away shall be used. Maximize the echo signal by adjusting probe position. With the initial excitation pulse positioned at the left edge of the display, position the echo at 60% of full horizontal scale by adjusting the sweep control. Then increase the gain of the receiver until the maximum noise level within the range of 10% to 60% of the horizontal scale reaches 25% of the full vertical scale. Take the gain reading. If the noise height does not reach 25% of the full scale at the maximum receiver gain, then note the height of the noise. Readjust the gain so that the echo reaches either 25% of the full scale or the noise height at the maximum receiver gain. The difference in gain between the two cases is the signal-to-noise ratio of the probe. It is recommended that the signal-to-noise ratio be expressed in dB (decibel) units.

## 12.3 Specifications

The signal-to-noise ratio shall be at least 50 dB.

\* Noises arise from grain boundary scattering of the testing material, internal reflections in the probe wedge and in the coupling or bonding material, the effect of the different wave mode generated, the effect of the side lobes.

\*\* Care shall be exercised to keep the echo signal within the linear dynamic range of the receiver input (see \*\* of Clause 10.2.).

# 13. Overall System Sensitivity

13.1 The overall system includes the pulser and receiver as well as the probe.

## 13.2 Method

It is recommended that the IIW block be used. For angle beam probes, the echo from the 100 mm radius quadrant shall be used. For straight beam probes, the echo from the opposite surface 100 mm away shall be used. Maximize the echo signal. Set the echo height to 25% of the full scale by adjusting the gain of the receiver. Read the remaining gain of the system still available.

## 13.3 Specification

The remaining gain shall be at least 40 dB.

TABLE 1. TABLE OF  $\tan^{-1}x$ 

x	$\tan^{-1}x$ (degrees)	x	$\tan^{-1}x$ (degrees)
0	0	0.16	9.090
0.01	0.573	0.17	9.648
0.02	1.146	0.18	10.20
0.03	1.718	0.19	10.76
0.04	2.291	0.20	11.31
0.05	2.862	0.21	11.86
0.06	3.434	0.22	12.41
0.07	4.004	0.23	12.95
0.08	4.574	0.24	13.50
0.09	5.143	0.25	14.04
0.10	5.711	0.26	14.57
0.11	6.277	0.27	15.11
0.12	6.843	0.28	15.64
0.13	7.407	0.29	16.17
0.14	7.970	0.30	16.70
0.15	8.531		

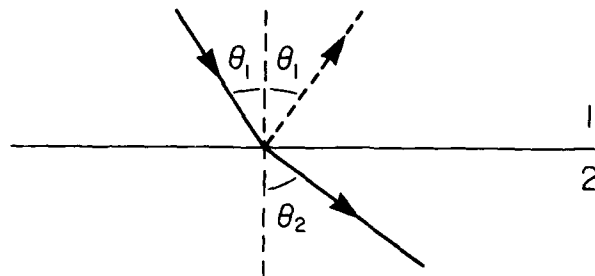
## APPENDIX 1

## SNELL'S LAW

When a sound beam passes from one medium to another of a different velocity at an angle not normal to the interface of the two, refraction as well as reflection occur. Snell's law for the refracted beam is as follows:

$$\sin \theta_1 / \sin \theta_2 = v_1 / v_2$$

where  $v_1$  and  $v_2$  are velocity of sound in medium 1 and 2, respectively, and  $\theta_1$  and  $\theta_2$  are incident and refracted angles respectively (Fig.).



Example: What will be the angle of refraction of a shear probe in aluminum which provides 45° shear wave in steel? From the Snell's law, it can be written:

$$\sin \theta_{2Al} = v_{Al} \sin \theta_1 / v_1 = v_{Al} \sin 45^\circ / v_{steel}$$

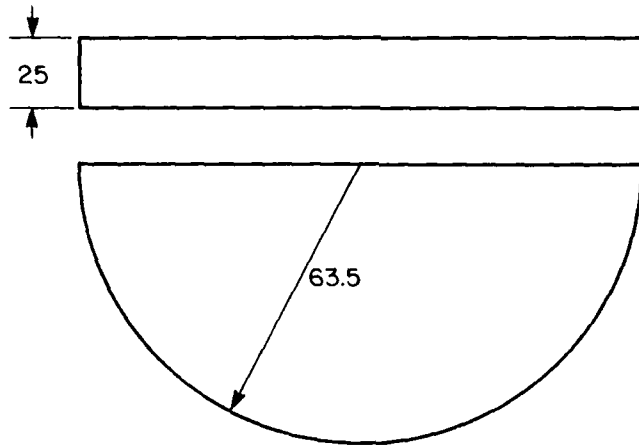
Taking  $v_{Al} = 3.10 \times 10^5$  cm/sec and  $v_{steel} = 3.23 \times 10^5$  cm/sec,  $\theta_{2Al} = 42.7^\circ$ . Thus, the probe has refracted angle of 42.7° in aluminum. Note that no information on the incident angle or the sound velocity in the plastic wedge (medium 1) is needed in calculation.

## APPENDIX 2

METHOD OF ELAPSED TIME MEASUREMENT IN THE  
PROBE WEDGE (FOR ANGLE BEAM PROBES)

It is recommended that a semi-circle block as shown in Fig. A, which is similar to AWS type DC (Distance Calibration) Block, be used. Place the probe near the center of the circle. Adjust the probe position until the echo from the radius is maximized. Figure B shows an echo pattern thus obtained. Measure  $T_1$ ,  $T_2 - T_1$ ,  $T_4 - T_3$ , and then take the average (this average is denoted by  $T_a$ ). Measure  $T_3 - T_1$ ,  $T_5 - T_3$ , and then take the average (of which value is denoted by  $T_b$ ). The elapsed time in the probe wedge is given by  $(T_a - T_b)/2$ .

\* Equivalently, a miniature angle beam block (Fig. C) can also be used.



NOTE: All Dimensions in Millimeters

FIGURE A. SEMI-CIRCLE BLOCK

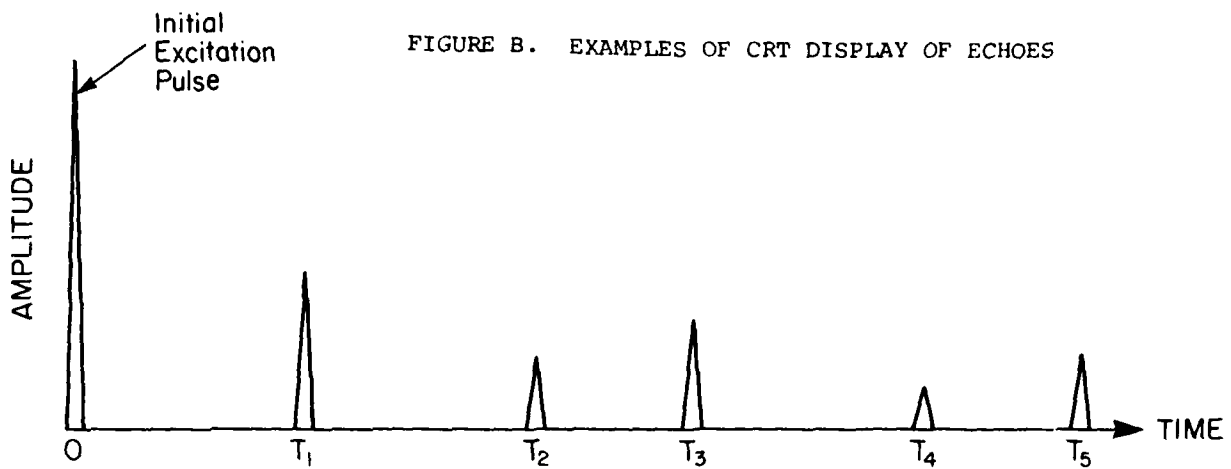
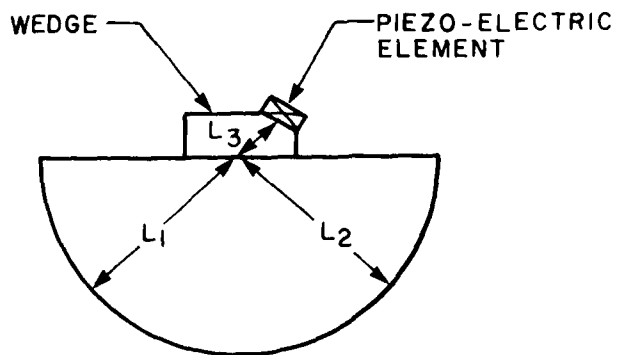
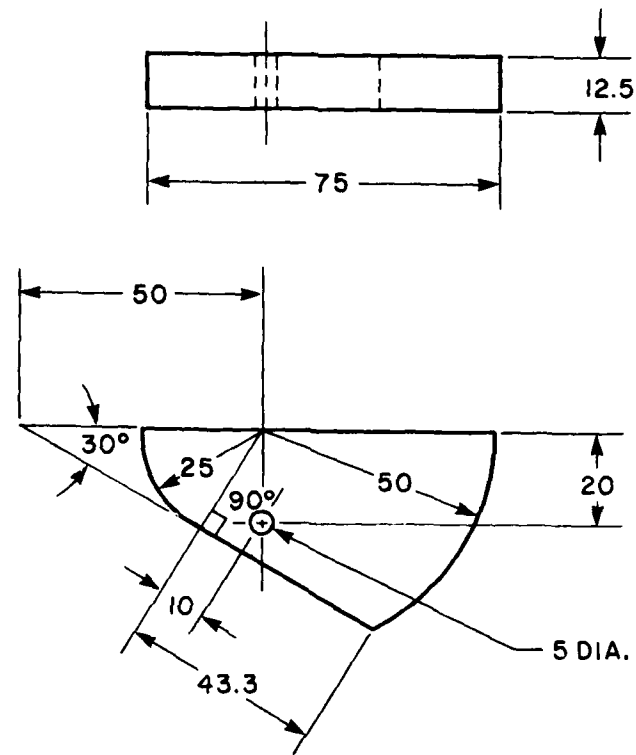


FIGURE B. EXAMPLES OF CRT DISPLAY OF ECHOES

\*\* The echoes shown in Fig. B travel the following paths:

ECHO AT TIME	PATH
$T_1$	$L_3 + 2L_1 + L_3$
$T_2$	$2(L_3 + 2L_1 + L_3)$
$T_3$	$L_3 + 2L_1 + 2L_2 + 2L_1 + L_3$
$T_4$	$L_3 + 2L_1 + 2L_2 + 2L_1 + 2L_3 + 2L_1 + L_3$
$T_5$	$L_3 + 2L_1 + 2L_2 + 2L_1 + 2L_2 + 2L_1 + L_3$





Note: All Dimensions are in Millimeters

FIGURE C. MINIATURE ANGLE BEAM BLOCK

## GLOSSARY

Amplitude: The magnitude of mechanical vibratory movement, voltage or current; indicated by vertical height on a CRT display.

Angle Beam: A sound beam travelling at an angle measured from the normal to a tangent plane of the test surface.

ASTM: Abbreviation for American Society for Testing and Materials.

Attenuation: Loss of amplitude or energy.

Attenuation Coefficient: A number which represents the degree of attenuation per unit distance or unit time.

Attenuator: A device for producing attenuation.

Bonding (or Coupling) Material: A substance used between two separated parts of materials to permit or improve transmission of ultrasonic energy from one part to the other.

CRT: Abbreviation for cathode ray tube.

dB (Decibel): Logarithmic expression of a ratio of two amplitudes; dB is defined as  $dB = 20 \log_{10} (A_2/A_1)$ , where  $A_1$  and  $A_2$  are amplitudes.

Echo: Signal of reflected ultrasonic wave.

Echo Height: Amplitude of the echo.

Focused Probe: A probe which produces a convergent sound beam.

Frequency: A number of repetitional (or periodic) motion of vibrations or oscillations per unit time; one repetitional motion per second is called 1 Hz (Hertz).

Gain: An amount of amplification applied to a received signal.

IIW: Abbreviation for International Institute of Welding.

Impedance Matching: The balancing of two media (electrical or mechanical) to provide optimum transference of energy between them.

KHz: Abbreviation for Kiloherz ( $=10^3$  Hertz).

$\lambda$ : Symbol for wave length.

Linear Dynamic Range: The range within which two quantities have a linear relationship.

Longitudinal Wave: A type of wave in which the displacement of the particle in a material is parallel to the direction of wave propagation.

Initial Excitation Pulse: Electrical pulse applied to a probe to produce an ultrasonic sound beam.

MHz: Abbreviation for megahertz ( $=10^6$  Hertz).

usec: Unit of time equal to  $10^{-6}$  second.

NDT: Abbreviation for Nondestructive Testing.

Piezoelectric: Ability of a material to convert electrical energy into mechanical energy and vice versa.

Probe: A device for generating and/or receiving ultrasonic energy.

Pulse: A series of vibrations or oscillations having a brief duration.

Pulse-Echo Method: A method in which the presence of a discontinuity in a material is indicated by the reflection of pulses from it.

Shear Wave: A type of wave in which the displacement of the particle in a material is perpendicular to the direction of wave propagation.

Side Lobe: Ultrasonic beam emitted from a transducer to the sides of the main sound beam.

Straight Beam: A sound beam travelling normal to a tangent plane of the test surface.

Transducer: A device for converting electrical energy into acoustic energy and vice versa.

Ultrasonic: Mechanical vibrations having a frequency greater than approximately 20 KHz which is generally considered as the upper limit of audible sound of the human ear.

Wave Length: The shortest distance between two corresponding points of the periodic motion.

Wave Mode: Type of wave motion; e.g. longitudinal, shear, etc.

Wedge: A device used to direct ultrasonic beam into a test part at an angle.

